The role of Fluoxetine against preneoplastic lesions and tumors in colon tissue

"Die Rolle von Fluoxetin gegen präneoplastische Läsionen und Tumoren im Darmgewebe"

Doctoral thesis for a doctoral degree

at the Graduate School of Life Sciences,

Julius-Maximilians-Universität Würzburg,

Section Biomedicine

submitted by

Vinicius Kannen Cardoso

Würzburg

2013

Submitted on: ………………………………………………………......

Members of the Supervisory Committee:

Chairperson: ………………………………………………………......

Primary Supervisor: ………..……………..…… Prof. Dr. Helga Stopper

Supervisor (Second): ………………… Prof. Dr. Med. Sérgio Britto Garcia

Supervisor (Third): ……..………. Prof. Dr. Med. Ana Maria Waaga-Gasser

Supervisor (Fourth): …………..………. Prof. Dr. Med. Ricardo Benavente

Date of Public Defence: …………………………………………………

Date of Receipt of Certificates: ………………………………………….

Index

Abbreviations

5-HT – Serotonin
AC – Aberrant crypts
Acetyl-CoA – Acetyl coenzyme A
ACF – Aberrant crypt foci
Akt – Protein kinase B
AntiM – Antimycin A
ATP – Adenosine-5'-triphosphate
Bax – Bcl-2–associated X protein
BCECF-AM – 2′,7′‑bis‑(2‑carboxyethyl)‑5‑(and‑6)‑carboxyfluorescein acetoxymethyl ester
Bcl-2 – B-cell lymphoma 2
Bid – BH3 interacting-domain death agonist
BSA – Bovine serum albumin
CA – Carbonic anhydrase
Ca2+ – Calcium
CAT – Catalase
CO2 – Carbon dioxide
CSC – Cancer stem cell
CTRL – Control
DHE – Dihydroethidium
DMEM – Dulbecco's modified eagle media
DMH – Dimethylhydrazine
DMSO – Dimethyl sulfoxide
EBSS – Earl's balanced salt solution
EDTA – Ethylenediaminetetraacetic acid
EGFR – Epidermal growth factor receptor
FBS – Fetal bovine serum
FCS – Fetal calf serum
FLX – Fluoxetine
FRAP – Ferric reducing antioxidant power
G6Pase – Glucose-6-phosphate
G6PDH – 6-phosphate dehydrogenase
G6PDH – Glucose 6-phosphate dehydrogenase
GLT1 – Glucose transporter 1
GR – Glutathione reductase
GSH – Glutathione
GST – Glutathione S-transferase
H&E – Hematoxylin and eosin
H2DCF-DA – 2′, 7′-dichlorodihydrofluorescein diacetate
H2O2 – Hydrogen peroxide
HCl – Hydrochloric acid
HIF-1 – Hypoxia-inducible factor 1
IkB-α or β – Nuclear factor of kappa light polypeptide gene enhancer in B-cells inhibitor, alpha or beta
iNOS – Inducible nitric oxide synthase

ipH – Intracellular pH
KH2PO4 – Monopotassium phosphate
LDH-A – Lactate dehydrogenase A
MAO – L-Monoamine oxidases
MCT4 – Lactate transporter 4
MDA – Malondialdehyde
MEM – Minimal essential media
MFI – Median fluorescence intensity
MNNG – Methylnitronitrosoguanidine
MSCs – Mesenchymal stem cells
MV - Microvessels
MW – Mean weight
Na2HPO4 – Disodium phosphate
NaASO2 – Sodium arsenite
NaCl – Sodium chloride
NADPH – Reduced-nicotinamide adenine dinucleotide phosphate
NaOH – Sodium hydroxide
NF-kB – Nuclear factor kappa-light-chain-enhancer of activated B cells
NOD/SCID – Nonobese diabetic severe combined immunodeficient
NOX-1 – NADPH oxidase1
O2 – Oxygen
O2- – Superoxide
OS – Oxidative stress
OXPHOS – Human oxidative phosphorylation
PBS – Phosphate buffered saline
PCNA – Proliferating cell nuclear antigen
PDGF – Platelet-derived growth factor
PI – Propidium iodide
R5P – Ribose-5-phosphate
Res – Resveratrol
RIPA – Radioimmunoprecipitation assay buffer
ROS – Reactive oxygen species
RTG – Relative tumor growth
SERT – Serotonin reuptake transporter
SOD – Superoxide dismutase
SSRI – Selective serotonin reuptake inhibitor
TGF-α – Transforming growth factor-alpha
TOMM20 – Translocase of outer mitochondrial membrane 20 homolog
TPTZ – 2,4,6-tripyridyl-s-triazine
Tris – Tris(hydroxymethyl)aminomethane
USA – United States of America
VEGF – Vascular endothelial growth factor
WB – Western blotting
ΔΨm – Mitochondrial membrane potential

Abstract

Introduction: Colon cancer is one of the major human malignancies worldwide, and much effort has been applied to understand the process of colon carcinogenesis, as well as the role of potential treatments and co-therapeutical agents against it. A growing body of evidence suggests that the use of fluoxetine (FLX), an antidepressant belonging to the selective serotonin reuptake inhibitors (SSRIs), may be associated with a reduced colon cancer risk. However, controversial opinions have been published and an identification of the mechanisms of the activity of FLX on colon cells would help in the clarification of this controversy. **Objectives:** Using several *in vitro* and *in vivo*-based methods and analyses, we aimed to verify whether FLX has antioxidant, pro-oxidant or DNA-damaging potential in standard toxicological assays; to check whether and how FLX could prevent and reduce colon preneoplastic lesions; to ascertain whether FLX has any oncostatic potential against colon tumors; and, to investigate whether FLX activity could be comparable with a known and current applied chemotherapeutic agent against colon cancer. **Results:** FLX did not have any antioxidant potential in our experiments. Although it did not induce reactive oxygen species (ROS) generation or DNA-damage in fibroblast and colon tumor cell lines, FLX reduced dysplasia and proliferation in two different carcinogen models. Further, a significant decrease in colon stromal reactivity and angiogenesis was found in both carcinogen-induced preneoplasia models. In a xenograft model of colon cancer, FLX shrank tumors, reduced tumor proliferation, arrested cancer cells at the G_0/G_1 cell-cycle phase, and took ROS generation under control. Such effects were detected together with an intracellular acidification and loss of mitochondrial membrane potential in FLX-treated cells. Modulating mitochondrial respiratory chain, HIF-1 expression and Akt/mTOR signaling pathway, FLX was found to reduce colon tumors similar to the widely used chemotherapeutic agent 5-Fluoracil activity. **Conclusion**: Our collective data suggest that FLX is a remarkable chemopreventive and oncostatic agent against colon preneoplastic lesions and tumors, acting without DNA-damage or ROS generation.

Zusammenfassung

Einleitung: Darmkrebs ist eine der wichtigsten menschlichen Tumorarten weltweit und viel Aufwand wurde unternommen, um den Prozess der Colonkarzinogenese, sowie die Rolle der möglichen Behandlungen und Co-therapeutische Mittel zu verstehen. Eine wachsende Zahl von Hinweisen deuted darauf hin, dass die Verwendung von Fluoxetin (FLX), einem Antidepressivum aus der Klasse der selektiven Serotonin-Wiederaufnahmehemmer (SSRIs), mit einem reduzierten Dickdarmkrebs-Risiko verbunden sein kann. Allerdings sind auch kontroverse Meinungen veröffentlicht worden und eine Identifizierung der Mechanismen der Aktivität von FLX auf Darmzellen würde bei der Klärung dieser Kontroverse helfen. **Ziele:** Mit in vitro-und in vivo-Methoden wollten wir prüfen, ob FLX antioxidatives, prooxidatives oder DNA-schädigendes Potential in Standard-toxikologischen Untersuchungen hat; des weiteren sollte analysiert werden, ob und wie FLX präneoplastischen Läsionen verhindern und reduzieren kann, sowie ob FLX onkostatisches Potenzial gegen Darmtumoren hat. Letzteres sollte im direkten Vergleich mit dem etablierten Chemotherapeutikum 5-Fluoruracil untersucht werden. **Ergebnisse:** FLX zeigte keine direkte antioxidative Kapazität in unseren Testsystemen. Obwohl es keine Bildung reaktiver Sauerstoffspecies (ROS) und keine Induktion von DNA-Schaden in Fibroblasten und Kolon Tumorzellinien verursachte, reduzierte FLX Dysplasien und Proliferation in zwei verschiedenen Kanzerogen-Modellen in vivo. Ferner wurde eine signifikante Abnahme der Reaktivität der Stromazellen und von Angiogenese in beiden Karzinogen-induzierten Präneoplasie-Modellen gefunden. In einem Xenograft Modell des Kolonkarzinoms brachte FLX die Tumoren durch verringerte Proliferation zum Schrumpfen. In vitro wurde in den entsprechenden Zellinien eine Anreicherung der Zellen in der Ga_0/G_1 Zellzyklus-Phase, eine Reduktion Hypoxie-verursachter ROS-Bildung, intrazelluläre Ansäuerung und Velust des mitochondrialen Membranpotentials nach FLX-Behandlung gefunden. Weitere Aktivitäten waren auf die mitochondriale Atmungskette, HIF-1 Expression und den Akt/mTOR-Sinalweg zu beobachten. Die Reduktion der Kolontumoren war der mit 5-Fluoruracil

erzielten vergleichbar. **Schlussfolgerung**: Unsere Daten deuten darauf hin, dass FLX eine bemerkenswerte chemopräventive und onkostatischen Aktivität gegen präneoplastische Läsionen und Tumore im Darm aufweist, die ohne Induktion von DNA-Schäden ROS stattfindet.

1   Introduction

1.1   Fluoxetine

Fluoxetine (FLX) is a selective serotonin reuptake inhibitor (SSRI), and was discovered by a research group from the Eli Lilly Company in 1974 [1]. It is a lipophilic weak base administered orally yielding a direct contact with epithelia from the gastrointestinal tract. Then, FLX is absorbed and induces an increase in serotonin (5-HT) levels by blocking the L-monoamine oxidases (MAO) and serotonin reuptake transporters (SERT). A concentration plateau ranging from 10 to 30 µM was reported in human brain tissue [2-4]

In 1978, FLX was approved for the treatment of patients with depression, anxiety and insomnia, becoming worldwide known as Prozac [5-6]. It exhibits higher safety and less side effects than other antidepressants [3,5-7].

1.2   Fluoxetine and oxidative stress generation

FLX has been found to act upon the cellular oxidative stress (OS) machinery [8-19]. For example, FLX treatment was detected to decrease serum malondialdehyde (MDA), superoxide dismutase (SOD), and ascorbic acid levels in patients with major depression [8]. In stressed rats, FLX treatment reduced MDA and carbonyl levels, whilst it enhanced SOD, catalase (CAT), glutathione S-transferase (GST), glutathione reductase (GR) and glutathione (GSH) contents [9-10]. FLX-induced neuroprotective effects were observed in rats exposed to lipopolysaccharide (LPS), since it decreased the translocation of p67 protein and reactive oxygen species (ROS) generation suppressing the activation of reduced-nicotinamide adenine dinucleotide phosphate (NADPH) oxidase, and inducible nitric oxide synthase (iNOS) [11]. An analysis of blood samples from stressed mice showed that FLX reduced ROS generation

promoting the activity of SOD, GSH, and CAT in leucocytes [12]. In brain tissue of tumor-bearing mice it was found that FLX supported SOD activity [13]. Moreover, FLX was shown to reduce ROS generation reversing the melanoma-induced tissue oxidation in mice [14].

On the other hand, FLX was reported to block voltage-gated ion channels, as observed by calcium (Ca^{2+}) extracellular influx and its release from intracellular stores, which inhibits adenosine-5'-triphosphate (ATP)-induced inward currents [15]. Data from Burkitt lymphoma cells revealed that FLX stimulated Ca^{2+} flux, while it reduced the B-cell lymphoma 2 (bcl-2) expression, and mitochondrial membrane potential ($\Delta\Psi m$) increasing deoxyribonucleic acid (DNA) fragmentation and apoptosis [16-17]. In human ovarian cancer cell lines, FLX induced ROS generation and apoptosis increasing mitochondrial bcl-2-associated X protein (Bax), cytochrome c release, caspase-3 activation and p53 expression levels, whilst it also reduced $\Delta\Psi m$, BH3 interacting-domain death agonist (Bid) and bcl-2 levels [18]. Similar results were found in human neuroblastomas [19]

1.3   Fluoxetine and tumors

In 1982, Tutton and Barkla first reported that FLX has a great potential against colon tumors [20]. However, ten years later, Brandes and colleagues showed that 40% of mice subjected to FLX-treatment for 5 days developed fibrosarcoma, while 95% of rats had breast cancer after 15-weeks [21]. Volpe and colleagues did not support these previous findings regarding the stimulatory effects of FLX treatment upon breast cancer [22]. Jia *et al* showed that FLX did not affect the growth of pancreatic tumors [23]. Moreover, FLX was shown to

reduce lymphoma growth modulating the T-cell-mediated immunity reaction through a 5-HT-dependent activity [7].

Coogan *et al* reported that patients subjected to regular FLX treatment had a 45% decrease in colon cancer risk [24]. These findings were recently supported by data from another research group [25]. Indeed, studies with animals also support this idea of FLX reducing colon cancer [5,26]. From cell culture experiments, FLX was reported not only to inhibit the multidrug resistance and increase the intracellular doxorubicin concentration [27], but also to induce an almost exclusive nuclear distribution of this chemotherapeutic drug [28].

1.4 Incidence of colon tumors

The American Cancer Society estimates the number of new cases and expected deaths for cancer in the United States of America (USA) every year [29]. A projection of 1.5 million cases and 569,490 deaths of cancer was expected in 2010. It ranked colon cancer as the third most common cancer in the country, with almost 50,000 deaths *per* year [29-30]. In 2012, colon cancer was found as the second major malignancy among males, and the third among females. It means that the number of diagnosed people reached over 1.2 million in the USA, and that 143,460 more new patients will be still diagnosed with colon cancer this year [31].

Survival has increased during the 5 years post-diagnosis in those 150,000 new cases of colon cancer *per* year in the USA [30]. Jemal *et al* have nevertheless projected a 60% increase for new cancer diagnosed cases in developing countries until 2030 [32]. It highlights colon cancer as one of the

major human malignancies worldwide, and a great challenge for cancer therapy [33-35].

1.4.1 Adenoma-carcinoma sequence model

The most well accepted theory about colon carcinogenesis was proposed by Fearon and Volgestein. It became known as the adenoma-carcinoma sequence model [36]. This theory was mainly based on Foulds's model, where he proposed that most tumors develop throughout a multi-stepped sequence of changes [37]. This means that during a progressive process genetic and epigenetic mutations in tumor suppressor genes and oncogenes are cumulating [38-39]. The tumor initiation is a relatively fast step, since mutations in one or two gatekeeper genes abrogate tissue homeostasis by disrupting the regular cell turnover [40-41]. Mutated cells seem to automatically undergo clonal outgrowth or promotional stage after being stimulated with endogenous or exogenous factors [40]. All these steps together can take over decades until the full completion of the tumor, since it requires the expansion of mutated cell clones, formation of preneoplastic lesions, tumor growth, invasion, and finally metastasis [42-44].

1.4.1 Colon preneoplastic lesions, aberrant crypt foci, or dysplasia

Understanding the theory of carcinogenic multi-step sequences of changes [37] and the adenoma-carcinoma sequence model [36], researchers had to find early lesions and transitional stages preceding tumors [36-37,45-46]. This means that the concept of first genetic changes (mutations and deletions) inducing tumors had to be translated to detectable histological modifications [46].

Bird therefore identified preneoplastic lesions in the colon of carcinogen treated rodents, and named those as aberrant dysplastic crypts [45]. To clarify this concept, Bird and colleagues argued that carcinogen-induced changes must happen in single crypts, which will show altered structure (as width, height, thickness, and luminal opening) due to genomic instability and aberrant cell growth. It was hypothesized that the more such aberrant crypt areas or foci (ACFs) grow dysplastic, the larger the chances of colon tumor development becomes [47-49].

Furthermore, cells from dysplastic ACFs were found to over-express cytoplasmic/nuclear β-catenin and nuclear cyclin D1 [43-44,50], as well to have a significant apoptosis increase [51]. In humans, dysplastic ACFs were revealed to be hyperproliferative lesions with high gene and protein expression for the proliferating cell nuclear antigen (PCNA), epidermal growth factor receptor (EGFR), transforming growth factor-alpha (TGF-α), and cyclin D1 [52]. Thus, dysplastic ACFs are hyperproliferative preneoplastic lesions with high cell turnover, moving the cryptal proliferation zone from the bottom to the epithelial surface [52-56].

Altogether, ACFs develop into dysplastic form and precede the development of adenomas which give rise to adenocarcinomas or colon tumors [43-44,46,50,57].

1.4.2 Colon preneoplastic lesions and stromal areas

Colon preneoplastic lesions are surrounded by stromal areas besides normal crypts [47]. In general, stromal areas are composed of a large number of fibroblasts and endothelial cells providing epithelia with physiological or pathological signals. During carcinogenesis, stromal cells were suggested to

induce a transition of non-malignant cells towards a malignant state [58-59]. This is normally related to the acquisition of a stromal reactive phenotype, in which stromal cells reorganize the stroma architecture by upregulating the release of growth factors, which enhances the preneoplastic neovascularization process [58,60]. This concept was demonstrated in skin carcinogenesis, where hyperplastic, dysplastic, and invasive lesions were accompanied by the reorganization of stroma architecture and an angiogenic hyperactivation [60].

In colon tumorigenesis stromal areas were observed to acquire a reactive phenotype which enhanced the epithelial transformation from normal to in situ invasive carcinoma [61-62]. Experiments with orthotopic transplantion of mesenchymal stem cells (MSCs) have shown that MSCs cells migrate into stromal areas and differentiate into carcinoma-related fibroblasts, which mainly tumor growth by enhancing angiogenesis [63]. It was also found that a therapy which targeted the platelet-derived growth factor (PDGF)-receptor β therapy reduced tumor growth by controlling stromal reactivity, for example by decreasing the microvessel density   [64]. Thus, this framework involving stroma and tumor components stimulates cancer cells to re-activate cancer stem cell (CSC) features and simultaneously induce the invasion and spread of the malignancy into the surrounding tissue [65-66].

1.4.3 Tumor metabolism

Hyperproliferative growth rates seem to be the main event allowing tumors to grow [52-56,67-68]. However, tumors need high and quick ATP generation to proliferate, besides a tightened maintenance of cell redox status, and enhanced biosynthesis of macromolecules. Basically, tumors shift their energy generation machinery from oxidative phosphorylation to an aerobic-

glycolytic metabolism [69-70]. This strategy allows tumors to keep a high ATP generation avoiding the negative feedback regulation from overusing glycolysis [69].

Specifically, tumors enhance the enzymatic activity of glucose 6-phosphate dehydrogenase (G6PDH) that transforms glucose to glucose-6-phosphate (G6Pase) and then to 6-phosphogluconolactone. This reaction is specifically intermediated by the transition of NADP+ to NADPH. This means that transiting NADP+ to NADPH further transforms 6-phosphogluconolactone to ribose-5-phosphate (R5P), which in turn increases nucleotide synthesis and DNA repair. Besides, G6Pase can be transformed to fructose-6-phosphosphate and glyceraldehyde-3-phosphate, which also enhances glycolysis and NADPH generation [69-70]

Overall, tumor cells thus undergo deep metabolic changes on way to survive in the stressful tumoral microenvironment [70].

1.4.4 Hypoxia, metabolism, and intracellular pH

Hypoxia is a term used to characterize situations of low oxygen levels in tissue, tumors, or cell cultures [71-74]. In tumors, high proliferation enlarges the distance between cells and microvessels reducing the oxygen and nutrient supplies, starting a hypoxic microenvironment. While this promotes the expression of growth factors inducing neovascularization, hypoxic areas are nonetheless present and are enhanced due to the chaotic and malformed structures of tumoral vessels and microvessels [74]. This situation of low oxygen tissue levels stimulates oxygen-dependent and independent mechanisms that alter several molecular signaling pathways [42,56,75].

Moreover, hypoxic tumor cells are known to use glycolysis in order to increase energy generation. This requires an over-activation of glucose transporters (i.e., GLUT1), lactate transporters (i.e., MCT4) and lactate dehydrogenase A (LDH-A) through the hypoxia-inducible factor 1 (HIF-1) transcriptional activity. By inhibiting the degradation of HIF-1, which upregulates the glycolysis-related molecular activities, tumor cells increase the conversion of pyruvate to lactate, thereby enhancing glycolysis [71,74]. However, tumor cells then would suffer from the hypoxia-induced and glycolysis-related acidosis. Therefore, they alkalinize their ipH on way to survive and proliferate. This is achieved via hyperactivation of HIF-1 activity, which enhances the hydration of carbon dioxide (CO_2) to bicarbonate by the catalytic activity of carbonic anhydrase (CA) IX and XII enzymes and promotes the activity of MCT-4 to extrude lactate and H^+ ions, both supporting an intracellular pH (ipH) alkalinization [74,76].

2 Aims

Considering that very little is known about how FLX acts against colon tumor development, we propose herein:

To verify whether FLX has antioxidant, pro-oxidant or DNA-damaging potential in standard toxicological assays;

To check whether and how FLX can prevent and reduce colon preneoplastic lesions; this means that besides dysplasia and epithelial proliferation, preneoplastic angiogenesis will be our target of study;

To ascertain whether FLX has any oncostatic potential against colon tumors; here, we will focus on how the modulation of tumor energy generation-related events could affect tumoral proliferative processes;

To investigate whether FLX activity is comparable with a known and currently applied chemotherapeutic agent against colon cancer.

3 Material and Methods

3.1 Fluoxetine stock solution preparation

FLX was acquired from Sigma-Aldrich (Germany). For a cell culture treatment, for example an amount of 10 mg FLX was dissolved in 646,5 µL dimethylsulfoxide (DMSO; Sigma-Aldrich, Germany). It provided a stock solution of 50 mM. Aliquots of 20 µL were prepared and kept at -20°C. For *in vivo* experiments, FLX solutions were prepared daily. Thus, the mean weight (MW) of each group was calculated and the FLX amount adjusted to 30mg/Kg (30xMW/1000). Around 200 µL were calculated for treating each animal (gavage or injection). From the final volume, 10% were used for solvent [100% ethanol (rats) or DMSO (mice)] and another 90% for vehicle (standard saline solution, 0,9% sodium chloride).

3.2 Ferric reducing antioxidant power assay

The reducing reaction of a ferric-tripyridyltriazine complex to its ferrous form was used to test the antioxidant potential of FLX, according to the standard method of our laboratory [77]. Briefly, FLX stock solutions were adjusted in 20 µL to final concentrations of 1, 10, or 100 µM, and mixed afterwards to 180 µL of water. Next, 600 µL of freshly prepared ferric reducing antioxidant power (FRAP) solution [25 mL of 300 mM acetate buffer, pH 3.6, 2.5 mL of 20 mM ferric chloride hexahydrate dissolved in distilled water, and 2.5 mL of 10 mM 2,4,6-tripyridyl-s-triazine (TPTZ) dissolved in 40 mM hydrochloric acid (HCl)] were added to the first 200 µL mixture. Then, the solution was incubated at room temperature for 5 or 30 min. Absorbance was measured at 595 nm with a spectrophotometer (Bio-Tek, Model Uvikon XL, Germany). Results are given as

FRAP in µmol/L. Tempol (50 µM) was used as positive control, and distilled water as blank.

3.3 Cell culture

Cell cultures were kept under standard conditions (normoxia; 5% CO_2; 95% air; 90% humidity), or hypoxia (1% oxygen (O_2); 5% CO_2; 94% NO_2; incubator C42, Labotect GmbH, Göttingen, Germany) at 37 °C. The use of both conditions was according to the experimental designs (I, II, and III). Subculturing cell lines was performed twice a week, and mycoplasma contamination was checked monthly. Cells were seeded into 6-well plates (Sarstedt Inc., Newton, USA) or 25-cm^2 flasks at a suitable initial concentration for each of the three different cell lines, and were left untreated for 20 to 24h before performing experiments.

3.3.1 Cell lines

3.3.1.1   V79 hamster fibroblast cell line

V79 cells were provided by Dr. Alexander Eckhardt/Prof. Helmut Schweikl (University of Regensburg, Germany). After thawing, cultures were initiated by seeding $5x10^5$ cells in 25-cm^2 cell-culture flasks with 5 ml minimal essential media (MEM) with 10% fetal calf serum (FCS; Biochrom AG, Germany), glutamine, and antibiotics. Cell cultures were kept under normoxia at 37 °C. Cells were seeded at an initial concentration of $3x10^5$ cells before experiments.

3.3.1.2   HT29 human colorectal adenocarcinoma cell line

The HT29 cells were obtained from the American Type Culture Collection (ATCC; USA) and cultured under standard conditions and grown in Dulbecco's modified eagle media (DMEM; 4.5 g/L glucose). The culture medium

was supplemented with 10% fetal bovine serum (FBS), 1% L-glutamine, and antibiotics. Cells were seeded at an initial concentration of 5×10^5 cells before experiments.

3.3.1.3   Caco-2 human colorectal adenocarcinoma cell line

Caco-2 cells were obtained from ATCC and grown under standard conditions in Eagle's MEM medium supplemented with 20% FBS, 1% L-glutamine, 1% Na-pyruvate, 1% nonessential amino acids, and antibiotics. Cells were seeded at an initial concentration of 3×10^3 cells before experiments.

3.3.1.3.1   Experimental design I

V79 and HT29 cells were seeded into 6-well plates under normoxic conditions, and left untreated up to 24h before experiments. Then, cells were treated with 1, 10 or 100 µM FLX. According to experimental aims, positive controls were resveratrol (Res; 60 µM), hydrogen peroxide (H_2O_2; 100 or 200 µM), sodium arsenite ($NaASO_2$; 100 µM), or Antimycin A (AntiM; 10 µM). Experiments were performed for 30min, 4h or 24h.

3.3.1.3.2   Experimental design II

HT29 and Caco-2 cells were seeded into 6-well plates under normoxic conditions, and left untreated up to 24h before experiments. Then, cells were exposed to 10 or 20 µM FLX, and/or 10 µM AntiM for 30min.

3.3.1.3.3   Experimental design III

HT29 and Caco-2 cells were seeded into 6-well plates, and underwent normoxia or hypoxia exposure up to 24h before experiments. The same conditions were used to expose cells to 20 µM FLX for 30min or 24h. Hypoxia was used as positive control for oxidative effects.

3.3.2 Analytical methods

3.3.2.1   Flow cytometry

For each experiment, 20,000 cells were analyzed per sample with a Becton Dickinson LSR I^{TM} (BD; Heidelberg, Germany) flow cytometer together with BD CellQuest Pro^{TM} software. At least four independent experiments were carried out for each endpoint.

3.3.2.1.1   Detection of reactive oxygen species generation

Detection of ROS generation was performed by staining cells for 10 minutes with 10 µm 2′, 7′-Dichlorodihydrofluorescein diacetate (H$_2$DCF-DA) in culture medium in 3ml medium/well. After harvesting, cells were washed twice (1000 rpm, 4°C, 5 min) with phosphate buffered saline (PBS) + 1% bovine serum albumin (BSA), and, then analyzed by flow cytometry. An argon laser excited cells at 488 nm (300 – 400 mW power), and emission was detected with a 530 nm (FL1) band pass filter.

3.3.2.1.2   Annexin V/Propidium iodide assay

A viability and apoptosis assay was performed by an Annexin V/PI kit, according to the manufacturer's instructions.

3.3.2.1.3   Detection of superoxide

Detection of superoxide (O$_2^-$) was performed by staining cells for 30 minutes with 10 µM dihydroethidium (DHE) in 3ml PBS or medium without serum/well. A flow cytometer equipped with an argon laser was used for analysis, and emission was detected with a 575 nm (FL2) band pass filter [78].

3.3.2.1.4   Intracellular pH analysis

Manufacturer's instructions were followed to stain cells with 10 µM 2′,7′‑bis‑(2‑carboxyethyl)‑5‑(and‑6)‑carboxyfluorescein   acetoxymethyl   ester

(BCECF-AM, B-1150; Molecular Probes, Invitrogen, Germany) for 20 min at 37°C under constant shaking. Before this, cells were treated with 1%DMSO or FLX for 30 min in complete medium. After harvesting, cells were washed twice (1000 rpm, 4°C, 5 min) with Earl's balanced salt solution (EBSS), then stained with BCECF-AM. Calibration curve was achieved by washing untreated cells with high-[K$^+$] buffers at pH values of 6.6, 7.0, and 7.6. Cells were kept in these buffers during staining procedure. Afterwards, cells were washed and analyzed by flow cytometry with an argon laser (200 mW power), and band pass filters of 530 nm (FL1) and 670 nm (FL3). The FL1/FL3 ratio was considered to reflect ipH alterations.

3.3.2.1.5   Mitochondrial membrane potential analysis

The alteration of the mitochondrial membrane potential (ΔΨm) was detected with the dye JC-1 according to the manufacturer's instructions. Briefly, cells were gently washed and kept in PBS with 3 µM JC-1, and 1% DMSO or 20 µM FLX for 30 min. Then, cells were washed twice and analyzed by flow cytometry as described above. The FL1/FL3 ration was used as ΔΨm.

3.3.2.1.6   Cell-cycle analysis

FLX-treated and control cells were harvested, permeabilized (Cytofix/Cytoperm kit), and stained with 2.5 µM bisbenzimide for 30 min. A HeCd UV laser excited cells at 325 nm, whilst emission was detected with a 424 nm (FL5) band pass filter. Cell cycle phases were determined with the ModFit LT^{TM} software package (Verity Software House, USA).

3.3.2.2   Viability test

A morphological assessment of cell viability was performed. In brief, cells were incubated for 24 h with the desired compounds in 3 ml of complete

medium. After harvesting, cells were applied onto glass slides by cytospin centrifugation, and fixed in cold methanol (-20°C; 2 h). Before counting, cells were stained for 3 minutes with Gel Green (62.5 µl/ml in Sørensen buffer, pH 6.8), washed twice with Sørensen buffer (15 mM disodium phosphate (Na_2HPO_4) and 15 mM monopotassium phosphate (KH_2PO_4), pH 6.8) and mounted for microscopy. From each of two slides, the morphology of 1000 cells was evaluated for occurance of mitosis, apoptosis, or necrosis. Numbers were expressed as percentages of all analyzed cells.

3.3.2.3   Comet Assay

A standard alkaline version of the comet assay was performed. Hence, 20 µl harvested cells were mixed with 180 µl low melting agarose (0.5 %). This mixture was added to SuperFrost slides (covered with a layer of normal melting point agarose [1%]). Slides were incubated at 4°C for 1h in 60 ml lysis buffer [2.5 M sodium chloride (NaCl), 0.1 M ethylenediaminetetraacetic acid (EDTA), 0.01 M tris(hydroxymethyl)aminomethane (Tris) and 1 % Triton X-100, 10 g/l N-lauroylsarcosine sodium adjusted to pH 10 with sodium hydroxide (NaOH)]. Then, slides were washed, and placed within a special electrophoresis reservoir for 20 min in electrophoresis buffer (300 mM NaOH, 1 mM EDTA, pH > 13.0). Afterwards, electrophoresis was performed for 20 min at 25 V (1.1 V/cm) and 300 mA. Slides were neutralized in 0.4 M Tris buffer (pH 7.5), dehydrated in methanol at -20°C for 10 min, and left to dry at 37°C for 1h. Slides were stained with 20 µl of Gel-Red/Dabco-solution (1:3; Biotrend, Germany). During evaluation, 100 cells were selected randomly (50 cells *per* replicate) for each sample, and analyzed at 200-fold magnification with fluorescent microscopy (Labophot 2, Nikon, Germany) connected to Komet 5 software (BFI Optilas,

Germany). The percentage of DNA in the tail was used to quantify DNA migration.

3.3.2.4 Western blotting analysis

Cell cultures were washed and then directly lyse in 1X radioimmunoprecipitation assay (RIPA) buffer (150mM NaCl, 3mL; 20mM Tris, pH7.5, 2mL; 1mM EDTA, 200µL; 1%NP-40, 1mL; 1%DOC, 1g; 0.1%SDS, 1mL; 5mM NaF, 12.5mg; 100mL distilled $H2O$). WB analysis was performed as described in NuPAGE Technical Guide (Invitrogen, USA). Briefly, protein extracts were run on NuPAGE 4-12% Bis-Tris Mini Gels (Invitrogen), and transferred to membranes with iBlot Dry Blotting System (Invitrogen).The membranes were incubated 4°C overnight with anti-p27 (D69C12, Cell Signaling, USA), anti-Cyclin E (HE12, Cell Signaling), and anti-GAPDH (9484, Abcam, UK) or anti-β-Actin (13E5, Cell Signaling) antibodies. Secondary antibodies (goat anti-rabbit and goat anti-mouse IgG HRP antibodies) were incubated for 1h at room temperature. Bands of labeled antibodies were detected by using SuperSignal West Pico Chemiluminescent Substrate (Thermo Scientific, USA). Films were scanned and intensity of bands quantified with ImageJ software (National Institutes of Health, NIH, USA).

3.4 Animal experiments

All experimental protocols were approved by the Animal Care and Use Committee from the Medical School, University of São Paulo. Approvals were numbered subsequently as n° 150/2008 for Wistar rats, n° 068/2012 for C57BL/6 mice, and n° 121/2012 for nonobese diabetic severe combined immunodeficient (NOD/SCID) mice. All animals were acclimated for 1 week before starting the experiment, housed from 4 to 6 per plastic cages with

softwood chips used as bedding at 22 ± 2°C (55% huminity and 12 h light/dark cycle), allocated randomly into their respective groups, and had free access to chow and water.

3.4.1 Wistar rats

Male Wistar rats (150-160 g) were assigned to control (CTRL), DMH treatment (a single dose of dimethylhydrazine [DMH;125 mg/kg; i.p.] in the second week from the beginning of the experiment), FLX treatment (given a daily FLX gavage [30mg/kg] for 6-weeks.) or DMH+FLX treatment groups. All rats were euthanized by CO_2 exposure after 6 weeks from the first FLX gavage. Individual autopsies were performed, and colon tissue samples were fixed in formaldehyde-buffer (4%; 24 h). Rats with fragmented tissue sections were discarded from the analysis.

3.4.2 C57BL/6 mice

Groups of female C57BL/6 mice (25 g) consisted of control (CTRL) animals or received methylnitronitrosoguanidine (MNNG) treatment (four successive doses of MNNG [5mg/ml; intrarectal deposits of 100 μl] twice a week for 2 weeks), FLX treatment (30mg/kg/day; intraperitoneal, i.p.) or MNNG+FLX treatment. FLX treatment was started after 2 weeks from the end of MNNG treatment, and continued for the next 4-weeks. All mice were euthanized by CO_2 exposure at week 8. Individual autopsies were performed, and colon tissue samples were fixed in paraformaldehyde buffer (4%; 24 h).

3.4.2.1   Analytical methods

The following methods were used for analyzing samples from Wistar rats and C57BL/6 mice.

3.4.2.1.1   Histopathological analysis

Colon tissue samples were sectioned from paraffin blocks and stained with hematoxylin and eosin (H&E) according to standard procedures for analysis under light microscopy. A first analysis was carried out at 200x magnification in transversal colonic sections, giving an en face overview of the tissue.   Dysplastic ACFs were detected and enumerated according to pathological features, as ranging from mild to severe dysplasia [43]. Afterwards, a second analysis was carried out at 400x magnification for each detected ACF for confirmation of dysplastic features and counting the number of aberrant crypts (AC). Microvessels (MV) were counted at 400x magnification in horizontal sections from rats, and transversal sections from mice. The whole area of each analyzed section was determined with a graduated lens (100x; Carl Zeiss, Germany; Nikon, Japan), and its area (μm2 or mm2) was calculated as values (V) x 5 for analysis with Carl Zeiss graduated lens (rats), or values (V) x 0.9801/121 for analysis with Nikon graduated lens (mice).

In rats, relative values for dysplasia are shown as total number of lesions per μm2. Microvessels were enumerated in horizontal sections. In mice, relative values for ACF-i (index), AC-i, and MV-i were calculated as their total number per mm2 [79-80]. The vascularization-related dysplasia was determined to be ACF x MV/ AC.

3.4.2.1.2   Immunohistochemistry and immunofluorescence

A standard method for immunohistochemistry (IHC) was performed in tissue samples. In brief, paraffin-embedded tissue sections (4μm) were mounted on SuperFrost slides, and dried at 56°C for 30 min. Sections were deparaffinized in xylene bath (100%), then rehydrated in graded ethanol (100 to

80%) and water baths. Tissue endogenous peroxidases were blocked incubating sections in 3% H2O2 for 20 min. Antigen retrieval was achieved incubating sections in a citrate buffer (pH 6.0) at 98°C for 40min, and cooling at room temperature for 30 min. Prediluted horse serum (1:50) was used for blockage against nonspecific endogenous protein binding.

The primary antibodies against Ki67 (clone MMA), PCNA (clone PC 10), *c-Myc* (clone 9E11), CD34 (clone QBEnd), and CD31 (clone 1A10) were purchased from Novocastra (USA). Anti- nuclear factor kappa-light-chain-enhancer of activated B cells (NF-kB,p50; clone C-19), nuclear factor of kappa light polypeptide gene enhancer in B-cells inhibitor, alpha (IκB-α; clone N-20), IκB-β (clone H-4), and vascular endothelial growth factor (VEGF; clone A-20) antibodies were acquired from Santa Cruz Biotechnology (Heidelberg, Germany). Anti-CD133 antibody was from Biocare Medical (USA). Picture-MAX Polymer Kit was purchased from Invitrogen (USA). These primary antibodies were used for IHC staining.

To perform the immunofluorescence (IHF) staining, mouse anti-human CD133 primary antibody was acquired from Miltenyi Biotec (n°130-090-422; Germany), and secondary anti-mouse FITC conjugated antibody from Dianova (n° 715-095-150; Germany); rabbit anti-mouse VEGF antibody was purchased from Santa Cruz (clone sc-152; Germany), and secondary anti-rabit Cy3 conjugated antibody from Dianova (n° 111-165-144); rat anti-mouse CD34 and rabbit anti-mouse CD31 antibodies were acquired from Applied Biosystems (n° ab 8158 and ab 28365; Germany); secondary anti-rat Texas Red conjugated antibody was purchased from GeneTex (n° GTX 26732; Germany), and secondary anti-rabitt Cy3 conjugated antibody from Dianova (n° 111-165-144).

During IHC staining, sections were incubated (1:100) with anti-Ki67, anti-PCNA, anti-*c-Myc,* anti-NF-kB, anti-IκB-α, anti-IκB-β, anti-CD133, anti-VEGF, anti-CD34, and anti-CD31 primary antibodies overnight. The brown color was displayed by incubating sections with Picture-MAX Polymer Kit for 1h, and DAB for 30sec. Sections were counterstained with hematoxylin. For negative controls, the primary antibody was omitted, and positive tissue controls were used in according to manufacturer's instructions of each antibody.

In positive reactions a brown precipitate at the nucleus was detectable (x200 magnification) for Ki67, PCNA, and NF-κB (analyzed at x1000 magnification), and in the cytoplasm and/or perinuclei for *c-Myc,* IκB-α, IκB-β, CD133, VEGF, CD34, and CD31. Analysis performed in epithelia was expressed as a ratio between positively stained nuclei to total unstained nuclei, whereas analysis in stromal colon areas was performed as a ratio between total positive cells and number of counted areas. Nuclear-transitional activity for NF-κB protein, within stromal areas, was calculated as a ratio between positively stained nuclei to cytoplasmic positive cells.

Double-labeling (IHF) was performed in fixed colon samples labeled with mouse anti-human CD133 (1:100; secondary anti-mouse FITC conjugated antibody; 1:400), rabbit anti-mouse VEGF (1:100; secondary anti-rabitt Cy3 conjugated antibody; 1:400), rat anti-mouse CD34 (1:100; secondary anti-rat Texas Red conjugated antibody; 1:400), and rabbit anti-mouse CD31 (1:100; secondary anti-rabitt Cy3 conjugated antibody; 1:400, Dianova) antibodies. Nuclei were stained with DAPI. Images were acquired with an Olympus BX51 microscopy equipped with anOlympus DP71 camera and a CellSens Dimension software (Olympus, Germany).

Rats or mice with fragmented tissue sections were discarded from the analysis

3.4.2.2 Nonobese diabetic severe combined immunodeficient mice

NOD/SCID mice (20g) were maintained under specific pathogen-free conditions. For colon xenograft-tumors, 1.5×10^6 HT29 or Caco-2 cells (50-60% confluence; $200\mu L$) were injected subcutaneously into shaved areas at the back of the mice. Tumor growth was monitored daily a caliper. Pharmacological treatment was initiated when the tumors achieved a mean volume of around 21.4 cm^3 for Caco-2 xenograft-tumors, and 0.13 cm^3 for HT29 xenograft-tumors.

3.4.2.2.1 First experiment – Caco-2 xenograft-tumors

During the first experiment, mice bearing Caco-2 xenograft-tumors were divided into a ontrol group [CTRL; receiving a daily intraperitoneal (i.p.; 200 µL) injection of saline solution], and an FLX treatment group [daily dose of 30mg/kg/day (i.p.) for 6 days]. On the seventh day, the mice were sacrificed in a CO_2 chamber. Serum was collected by centrifuging blood samples (835g, 10min, 4°C). Tumor tissue samples were fixed in formalin or frozen in liquid nitrogen. All frozen samples were kept at -80°C.

3.4.2.2.2 Second experiment – HT29 xenograft-tumors

The second experiment was performed with mice bearing HT29 xenograft-tumors. Mice were divided into control group (CTRL), and an FLX treatment group. The treatment group received the same daily FLX dose as described above for 3 days. On the fourth day mice were sacrificed as described above.

3.4.2.2.3 *Third experiment – HT29 xenograft-tumors*

A third experiment was performed with mice bearing HT29 xenograft-tumors to compare FLX induced effects with those of a known chemotherapeutic agent (5-Fluorouracil, 5-FU; 50 mg/kg/day). FLX treatment was applied as described above. During sacrifice, the mice underwent general anesthesia [1,5% isoflurane (Forane® Abbott GmbH & Co, Germany) in 98,5% oxygen; 2l/min] before receiving a cardiac puncture for blood collection. Serum was prepared as described in section 3.4.2.2.1. Tissue samples for protein extraction were directly frozen in liquid nitrogen. For RNA extraction, tissue samples were frozen in RNAlater RNA stabilization buffer (Qiagen, Germany) with liquid nitrogen, or within Tissue-TEK (Sakura Finetek, Netherlands) for histological preparations.

3.4.2.2.3.1 Monitoring of xenograft-tumors

Tumor volume was monitored by measuring the tumors with a caliper on the first (initial volume, IV) and seventh days (final volume, FV) for NOD/SCID mice bearing Caco-2 xenograft-tumors, or on the first and fourth days for those bearing HT29 xenograft-tumors. Values were calculated according to the formula volume = π x L x W x T/6 (where L is length; W is width; and, T is thickness). The relative tumor growth (RTG) was calculated according to the formula, RTG = FV-IV/number of days.

3.4.2.2.4 Analytical methods

3.4.2.2.4.1 Histopathological analysis

After standard H&E staining, three different areas were classified in each colon xenograft-tumor section: Invasive Front (IF), which was determined as a cell population at the border of the tumors; Tumor Parenchyma (TP), which

was determined as areas composing the inner part of the tumors, as associated with a high-density cell population; Peri-Necrotic (PN) area, which was detected as non-dense areas surrounding the irregular and widespread necrotic foci. PN cells were in close and direct contact with necrotic areas, and clustered in cell sets, which were generally separated between themselves and from TP areas by thin non-proliferative cell layers. Fig. 20 and 31 illustrate this classification in the results section.

3.4.2.2.4.2 Immunohistochemistry and immunofluorescence

Immunehistochemical and -fluorescence detections were performed as described above (section 3.4.2.1.1.2). Positive Ki67 nuclei were manually counted throughout pictures (3.15 mm2) taken at 400x magnification from five randomly chosen microscopic fields. A ratio between stained nuclei and pictured areas was established as tumor proliferation rate. Tumor necrotic areas were excluded from counting.

3.4.2.2.4.3 Western blotting analysis of xenograft-tumor samples

Caco-2 xenograft-tumors (section 3.4.2.2.1) were macerated in liquid nitrogen and lysed directly in 1mL of lysis buffer (1X RIPA) with 1% protease inhibitor cocktail solution (Sigma-Aldrich, USA). The lysates were centrifuged at 14,000 x g for 20min and the supernatant was stored at −80°C. The soluble proteins were then measured following the manufacturer's protocol of bicinchoninic acid (BCA Protein Assay Reagent (Thermo scientific Rockford, IL, USA). Total cellular protein (50 µg) was separated by electrophoresis through a 10% SDS–PAGE resolving gel. For Western blot analysis, the proteins were transferred onto a polyvinylidene fluoride (PVDF) membrane (Gelman Science), and the blotting was performed with a snap identification protein detection

system (Millipore, USA), following the manufacturer's protocol. Briefly, the membranes were blocked for 20min and then incubated for 10 min with anti-NF-KB p-50 (goat polyclonal antibody 1:400, Santa Cruz Biotechnology, USA), washed and then incubated with secondary antibody (anti-rabbit IGg and anti-goat IGg respectively), conjugated to horseradish peroxidase (1:2000, Santa Cruz Biotechnology, USA). ψ-tubulin (rabbit polyclonal antibody 1:3000, Santa Cruz Biotechnology, USA) was used as a loading control. The optical densities of the protein bands were detected using enhanced chemiluminescence ECL (PerkinElmer, USA) and were obtained and measured using the ImageQuant 350 device and software from GE Healthcare (General Electric, USA).

Frozen-tumor tissue samples (section 3.4.2.2.3) were sectioned and put into 2mL eppendorf tubes with lysis buffer (1x RIPA) and a 5 mm stainless steel bead (Qiagen, Germany). Eppendorfs tubes were inserted in a TissueLyser Qiagen system according to the manufacturer's instructions (Qiagen, Germany). The following procedures were performed as described above (section 3.3.2.4). Membranes were incubated with anti-p27, anti-Cyclin E, and anti-β-Actin antibodies.

3.4.2.2.4.4 MILLIPLEX assay for human oxidative phosphorylation and protein kinase B/mammalian target of rapamycin phosphoprotein signaling

Tumor protein extraction was performed as described above (section 3.4.2.2.4.3). MILLIPLEX® human oxidative phosphorylation (OXPHOS; Cat. N° H0XPSMAG-16K) and protein kinase B (Akt)/mammalian target of rapamycin (mTOR) phosphoprotein magnetic bead panel kits (Cat. N° 48-611MAG) were bought from Merck Millipore (Germany). The applied protein concentrations

were 60 µg/mL for OXPHOS assays, and 300 µg/mL for Akt/mTOR analyses. Sample preparations and data collection were performed according to the manufactures' instructions. Values are given as median fluorescence intensity (MFI) collected from replicates during analysis of the tumors samples.

3.4.2.2.4.5 Quantitative real-time reverse transcription-polymerase chain reaction

Frozen tissue samples were thawed and taken out of the RNAlater RNA stabilization buffer (Qiagen, Germany). Samples were put into 2mL eppendorf tubes with lysis buffer (RTL; Qiagen, Germany) and a 5 mm stainless steel bead (Qiagen, Germany). Eppendorfs tubes were inserted in a TissueLyser Qiagen system according to the manufacturer's instructions (Qiagen, Germany). The supernatant was collected and added to sterile 1.5mL eppendorf tubes. Pure RNA was prepared with a fully automated sample preparation QiaCube system (Qiagen, Germany). Pure RNA was used to synthesize cDNA applying an iScript^{TM} cDNA Synthesis Kit (BIORAD, Germany). Primers for translocase of outer mitochondrial membrane 20 homolog (TOMM20; QT00088914), GLUT1 (QT00068957), MCT4 (QT00044044), LDHA (QT00001687), NADPH oxidase 1 (NOX-1; QT00025585), and HIF-1 (QT00083664) were bought from QIAGEN (Germany), and amplified using a with QIAGEN kit for SYBR Green-based qRT-PCR technology according to the manufacturer's instructions (QIAGEN, Germany). Total RNA input was normalized based on Ct values for 18s housekeeping gene, as a reference standard. The 18s primer control was bought from Biomers (Germany; Forward sequence: tca aga acg aaa gtc gga ggt tcg; Reverse sequence: tta ttg ctc aat ctc ggg tgg ctg). All quantitative real-time reverse transcription-polymerase chain reaction (qRT-PCR) reactions were

duplicated, according to the standard procedure. Data were collected and analyzed using a DNA Engine Opticon 2 Real-Time Cycler PCR detection system (MJ Research, USA) together with Opticon Monitor 2 software package. The fold change was calculated using the $2^{-\Delta Ct}$ method.

3.4.2.2.4.6 Biochemical measurements

Serum and tumor samples were prepared as described in the sections 3.4.2.2.1 and 3.4.2.2.4.3, respectively. Then, glucose (mg/dL) and lactate (mmol/L) were determined by standard methods [glucose and lactate monitoring system (Precision Xtra, Abbott Laboratories, Abbott Park, U.S.A.) together with corresponding test strips (Abbott GmbH & Co. KG, Germany)] in a certified clinical chemistry laboratory (Zentrallabor des Universitätsklinikums Würzburg; Gerinnungsambulanz Zentrum Innere Medizin, A4, Oberdürrbacher Strasse 6, Würzburg). To estimate the glycolytic metabolism a ration between glucose and lactate was calculated for each sample.

3.4.2.2.4.7 Statistical analysis

Data were analyzed using the statistical GraphPad Prism 5.0 software package (Graph Pad Software Inc., San Diego, California, USA). Comparison of data from two different groups was performed with a Mann Whitney test. Results from multiple different groups were analyzed with a One-way ANOVA, and post hoc tests were chosen according to sample distributions. Analyzing different categorical independent variables on one dependent variable was performed with a Two-way ANOVA test and Bonferroni post hoc test. A probability of $P<0.05$ was considered to be statistically significant. All values represent means $\pm$ standard deviations.

4 Results

4.1 FLX does not show antioxidant, pro-oxidant or DNA-damaging potential

We first investigated whether FLX has antioxidant properties with a cell-free FRAP-assay. After 5min exposure, all FLX concentrations yielded lower Fe^{3+} reduction values than the control (Figure 1A). After 30min exposure, values were similar to the control (Figure 1B). Tempol was used as positive control, and the difference to that was significant for all tested FLX concentrations.
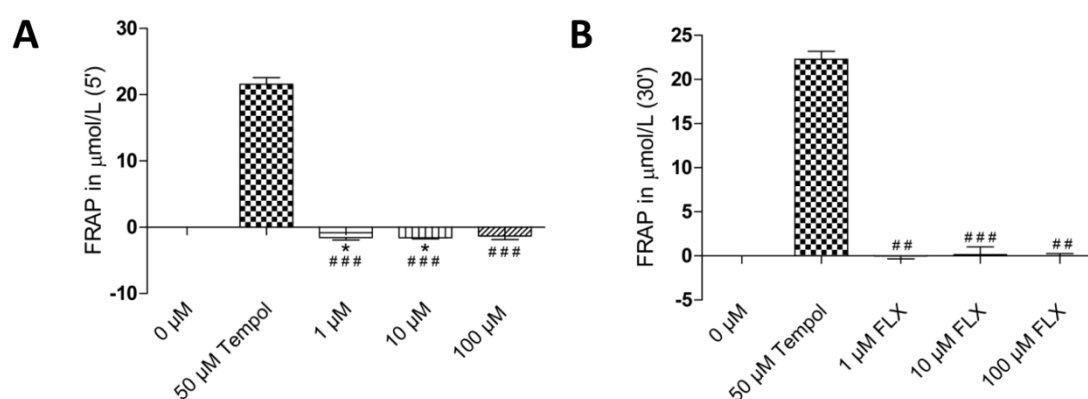
Figure 1 – Cell-free FRAP-assay after 5 min [**A**; *P > 0.05 *vs* 0 µM (blank); $^{###}$P > 0.001 *vs* 50 µM Tempol], and 30 min [**B**; $^{##}$P > 0.01 and $^{###}$P > 0.001 *vs* 50 µM Tempol] treatment with FLX or Tempol (positive control).

Next, we evaluated whether FLX can modulate GSH levels in V79 cells. Flow cytometry analysis showed that 1 or 10 µM FLX treatment for 4h or 24h did not alter GSH intracellular levels (Figure 2A), while 100µM FLX treatment reduced GSH levels significantly in comparison with H_2O_2-exposed cells after 24h (Figure 2B). Resveratrol (Res) was applied as positive control. Cell viability was also checked for FLX treatment in V79 cells after 24h. None of the applied FLX-concentrations induced significant differences in the numbers of mitosis or

apoptosis; while 10 µM FLX treatment decreased necrosis 3-fold compared with

DMSO-exposed cells (Figure 2C).
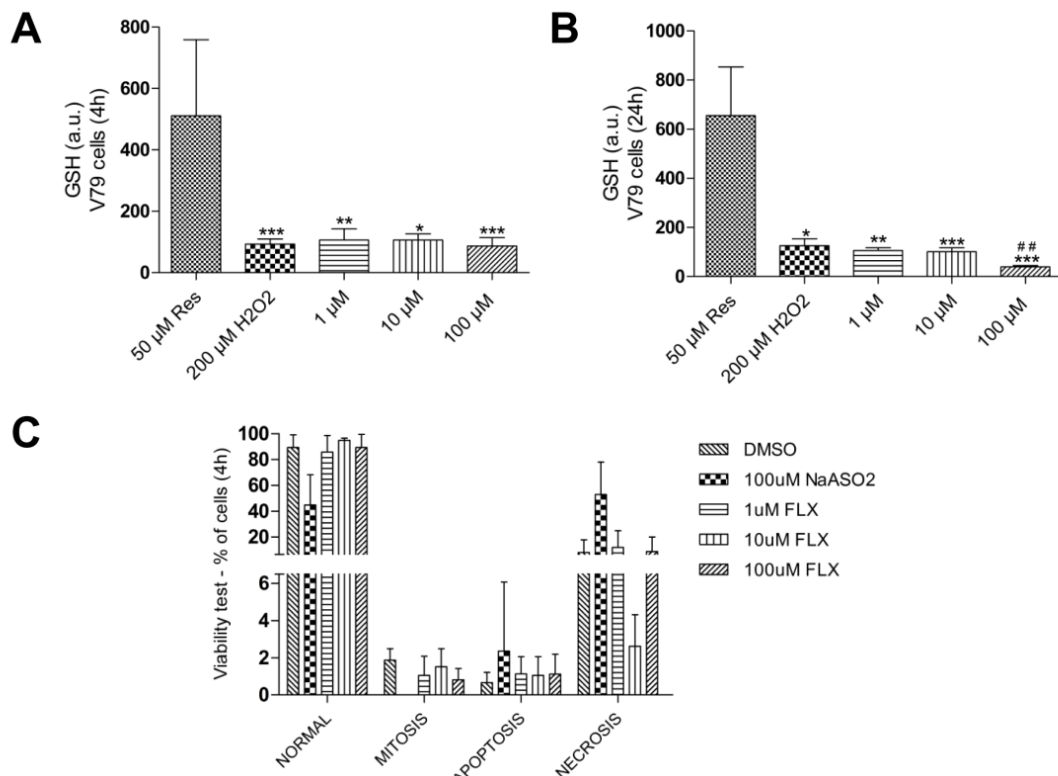
Figure 2 – GSH levels were analyzed by flow cytometry after 30min treatment (A) or 4h treatment (B) with FLX or Resveratrol (Res, positive control) (**A**; *P < 0.05, **P < 0.01, and ***P < 0.001 *vs* 50 µM Res; $^{##}$P < 0.01 *vs* 200 µM H$_2$O$_2$). Cell viability was analyzed by microscopy after exposure to FLX (or NaASO2 as positive control) for 24h (**C**; P > 0.05). DMSO = solvent control ($\leq$ 1% final concentration of DMSO).

Then, we investigated the potential of FLX to induce ROS generation.

Up to 100µM FLX did not induce ROS after 30min or 4h (Figure 3A and 3B).
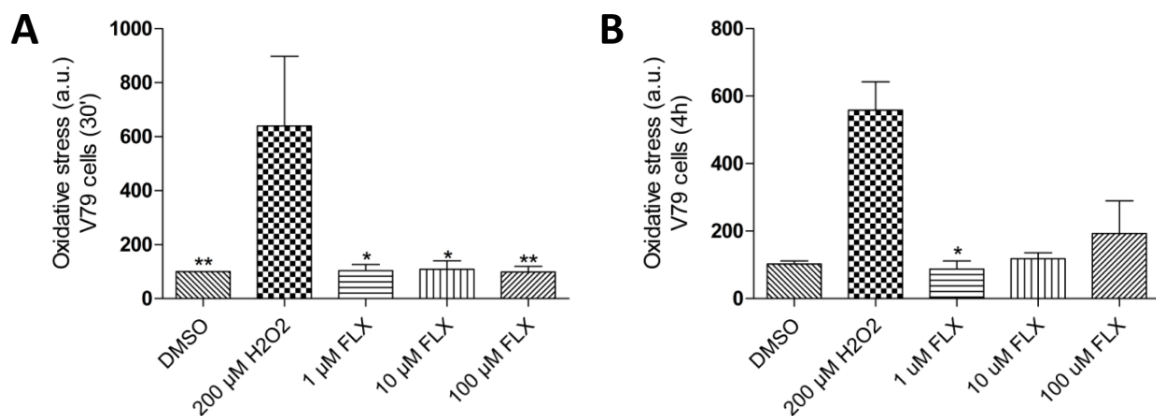
Figure 3 – Oxidative stress assay with V79 cells applying flow cytometry and the dye $H_2DCF-DA$. Experiments were performed for 30min (**A**; *P > 0.05 and **P > 0.01 *vs* 200 µM H_2O_2), and 4h (**B**; *P > 0.05 *vs* 200 µM H_2O_2) with H_2O_2 as positive control. DMSO = solvent control ($\leq$ 1% final concentration of DMSO).

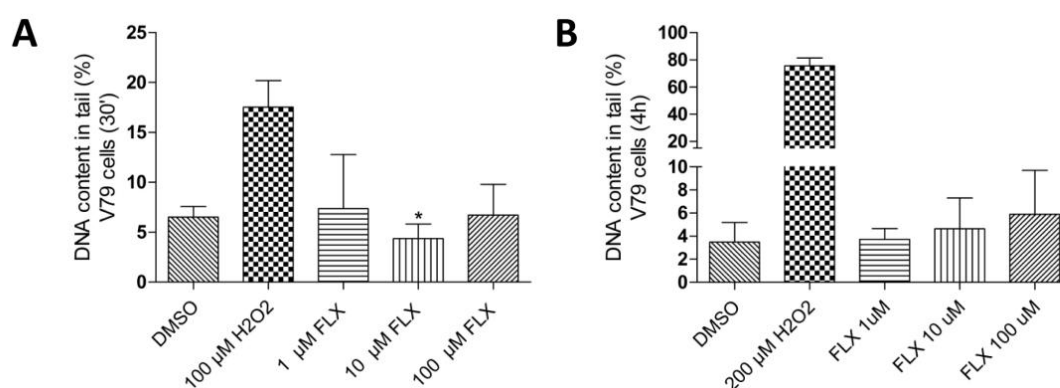By using the comet assay for investigation of DNA-damaging potential it was observed that none of the applied FLX concentrations were able to induce significant DNA-damage after 30min or 4h (Figure 4A and 4B).

Figure 4 – DNA-damage shown as percentage of DNA in the tail region in the comet-assay after exposure to FLX or H_2O_2 (positive control) for 30min (**A**; *P > 0.05 *vs* 200 µM H_2O_2), and 4h (**B**; P < 0.05). DMSO = solvent control ($\leq$ 1% final concentration of DMSO).

4.2 Effects of fluoxetine treatment in Wistar rats

4.2.1 Fluoxetine reduces dysplasia, cryptal proliferation, and preneoplastic angiogenesis in dimethylhydrazine-exposed colon tissue

The chemopreventive potential of FLX was investigated in carcinogen (DMH) -exposed rats. It was found that treating rats with FLX for 6-wks (2-wks before carcinogen-treatment plus 4-wks afterwards) significantly reduced the body weight in comparison with control groups (CTRL, 550.2 $\pm$ 22.08 g, n = 6; DMH, 509 $\pm$ 35.66 g, n = 6; FLX, 375.60 $\pm$ 101.6 g, n = 5; DMH+FLX, 407.5 $\pm$ 29.6 g, n = 6; P < 0.01 between groups without DMH treatment; P < 0.05 between groups with DMH treatment). Also, FLX treatment reduced the development of colon dysplasia (Fig. 5A and 5B) and cryptal proliferation in the

DMH-treated group, while it increased proliferation in the colon tissue of non-carcinogen treated control rats (Fig. 5C and 5D).
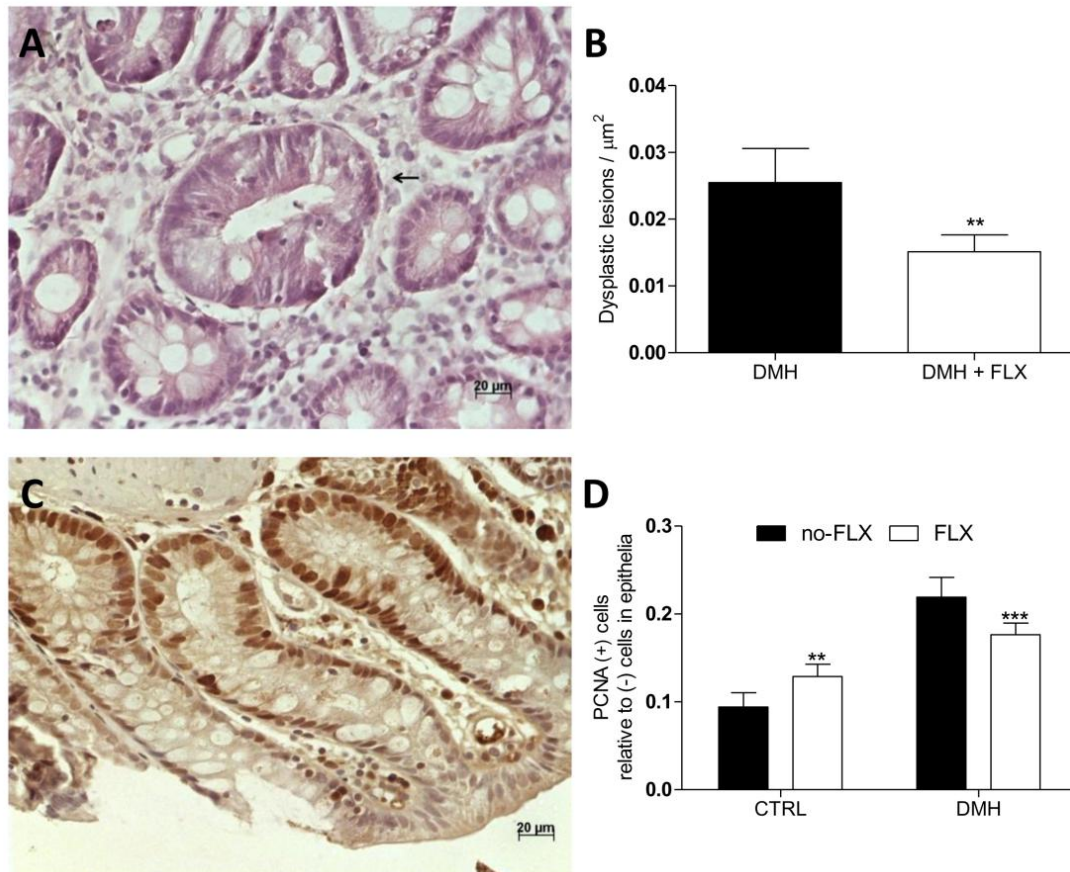
Figure 5 – Dysplastic lesion (arrow) showing elongated cryptal luminal opening, crowded and pseudostratified nuclei, less nuclear polarity, and lower number of globet cells (**A**). Number of dysplastic lesions are shown *per* μm^2 in rats treated with DMH (**B**; **P<0.01 *vs* DMH without FLX, *n= 5*; DMH+FLX, *n= 5*). Representative image of colon section stained with anti-PCNA antibody. All pictures were taken at 400x magnification and scale bars are 20 μm (**C**). Proliferation in colon crypts cells (**D**; **P< 0.01 *vs* CTRL without FLX, *n=6*; FLX, n= 5; ***P< 0.001 *vs* DMH without FLX, *n=5*; DMH + FLX, n= 6).

Angiogenesis was thereafter evaluated in colon tissue. Microvessels (Fig. 6A) were reduced in carcinogen plus FLX-treated rats (Fig. 6B). Besides, FLX treatment decreased VEGF expression within stromal areas (Fig. 6C) in DMH-treated rats (Fig. 6D).
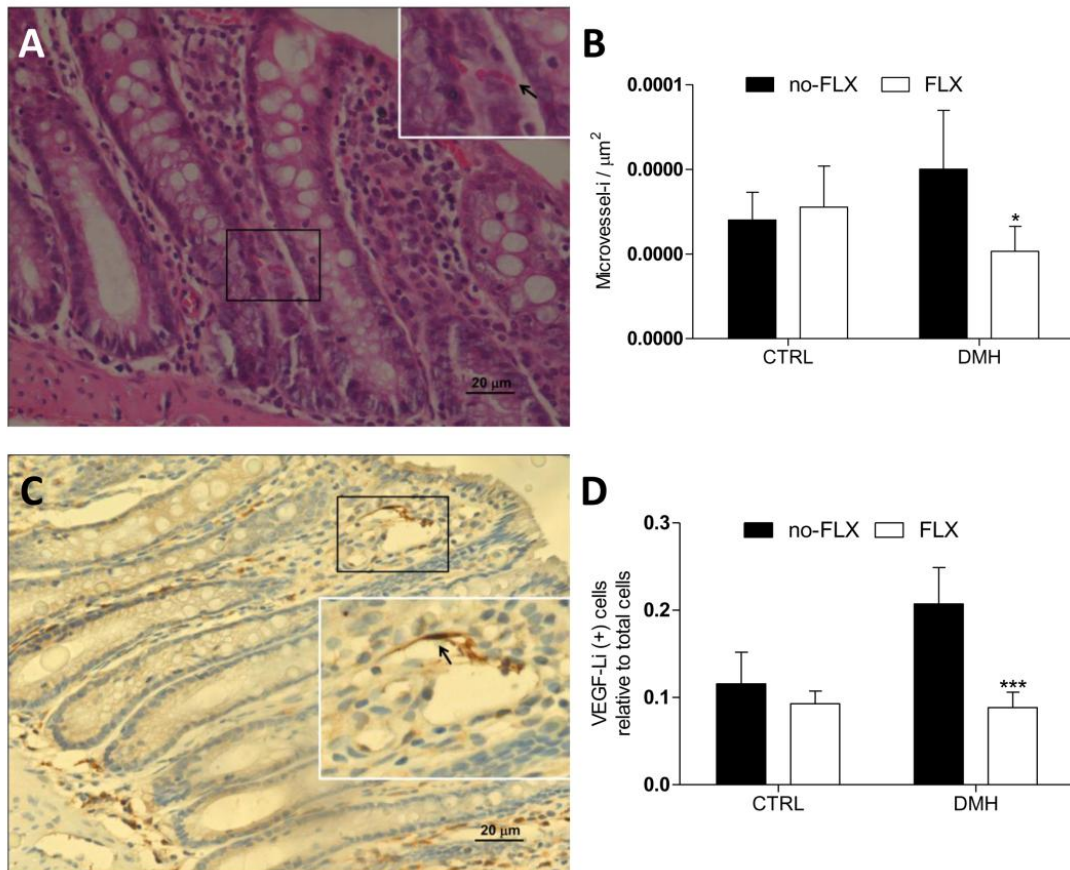
Figure 6 – Representative picture of microvessels within PCCS areas. The picture inset (enlarged from the boxed region) shows a microvessel (arrow) towards crypt. Picture was taken at 400x magnification, scale bars are 20 μm, and inset was magnified 4x (**A**). Microvessel-i (index) is shown *per* μm^2 (**B**; *P < 0.05 *vs* DMH without FLX, *n*= 5; DMH+FLX, *n*= 5). Representative picture shows labeled colon section with anti-VEGF antibody. The picture inset (enlarged from the boxed region) shows a positive cell at microvessel wall (arrow). Picture was taken at 200x magnification, scale bars are 20 μm, and inset was magnified 4x (**C**). VEGF-Li according to labelling index of cells for anti-VEGF antibody (**D**; ***P < 0.001 *vs* DMH without FLX, *n*= 4; DMH+FLX, *n*= 4).

4.3 Effects of fluoxetine treatment in C57BL/6 mice

4.3.1 Fluoxetine decreases dysplasia and preneoplastic angiogenesis in methylnitronitrosoguanidine-exposed colon tissue

Based on the data from the DMH-treated rats, we evaluated next whether FLX treatment could reduce the development of dysplasia in a carcinogen model which is not related to hepatic metabolism. Mice were first exposed to MNNG (local application into the colon) and, then treated with FLX

for 28 days. Although FLX treatment was well tolerated, the body weight of the mice treated with FLX was significantly lower (FLX, 21.0 $\pm$ 1.22 g, n = 5; MNNG+FLX, 19.3 $\pm$ 1.78 g, n = 5; P < 0.001) than in the control groups (CTRL, 25.6 $\pm$ 1.78 g, n = 5; MNNG, 23.6 $\pm$ 0.96 g, n = 5).

Preneoplastic lesions were evaluated by histopathological analysis, and severe MNNG-induced dysplasia was observed in colon sections from mice without FLX treatment (Fig. 7A), which was not observed to such a grade in those from FLX-treated mice (Fig. 7B).
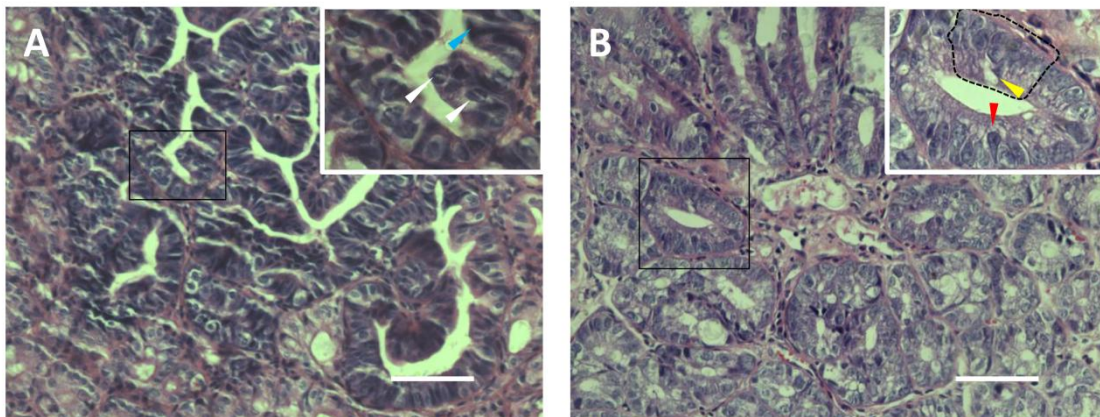
Figure 7 – Representative histological image of a severely dysplastic area (MNNG-exposed mouse). The picture inset (enlarged from the boxed region) shows the characteristic severe dysplastic features; e.g., partial loss of cell polarity, none goblet cells, presence of Paneth cells (blue arrow), and mitosis (white arrows). Pictures were taken at 200x magnification, scale bars represent 20 μm. High-magnification images were taken at 1000x magnification (**A**). Representative image shows a moderate dysplasia (MNNG+FLX treated mouse). The inset shows a compressed cryptal luminal opening, elongated nuclei (red arrow), a crowded and pseudostrafied area (sectioned black line), but with a generally still preserved cell polarity, and a lower number of globet cells (yellow arrow). Magnifications are described above (**B**).

Enumerating dysplastic lesions in MNNG and MNNG+FLX-treated mice showed that FLX reduced dysplasia 5.39-fold (Fig. 8A). FLX treatment significantly reduced the total values of AC *per* mm^2 7.94-fold (Fig. 8B). Microvessels were spread throughout colon stromal areas towards dysplastic

areas (Fig. 8C), where FLX treatment was found to decrease vascularization-related dysplasia 3.13-fold (Fig. 8D).
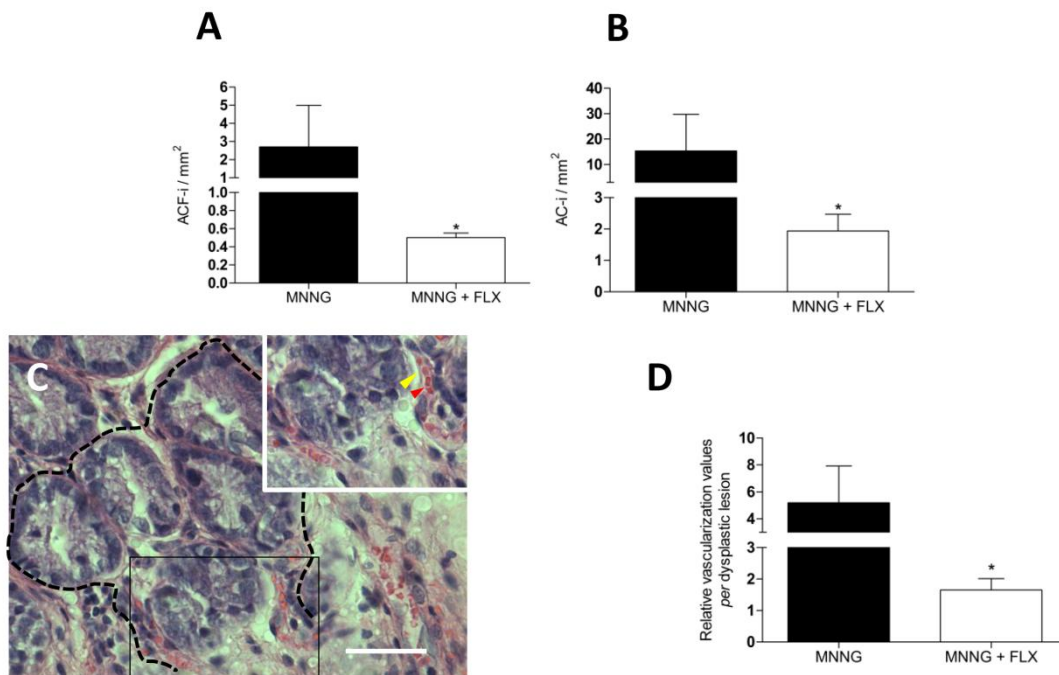
Figure 8 – ACF-i shown as number of dysplastic lesions *per* mm^2 (**A**; *P < 0.05 *vs* MNNG without FLX, *n* = 5; FLX+MNNG, *n* = 4). AC-i shown as number of dysplastic single crypts *per* mm^2 (**B**; *P < 0.05 *vs* MNNG without FLX, *n* = 5; FLX+MNNG, *n* = 4). Representative image of a dysplastic area is shown (sectioned black line) together with its relative vascularization spreading inside. The inset (enlarged from the boxed region) shows two microvessels towards the inner region of the dysplastic area. The yellow arrow points to a microvessel wall, and the red arrow to erythrocytes inside the microvessel walls. Picture was taken at 400x magnification, inset at 1000x magnification, and scale bars represent 20 μm (**C**). Relative dysplastic vascularization, shown as the number of microvessels *per* lesion (**D**; *P < 0.05 *vs* MNNG without FLX, *n* = 5; FLX+MNNG, *n* = 4).

4.3.2 Fluoxetine reduces colon proliferation in epithelia and stromal areas in methylnitronitrosoguanidine-exposed colon tissue

Considering the results above, we investigated whether antiproliferative effects of FLX could take place in epithelia and stromal areas (Fig. 9A.1 and A.2). Labeled sections with anti-Ki67 antibody revealed that FLX attenuated (Fig. 9B) the MNNG-induced increase in proliferation at epithelial and stromal areas (Fig. 9C and D).
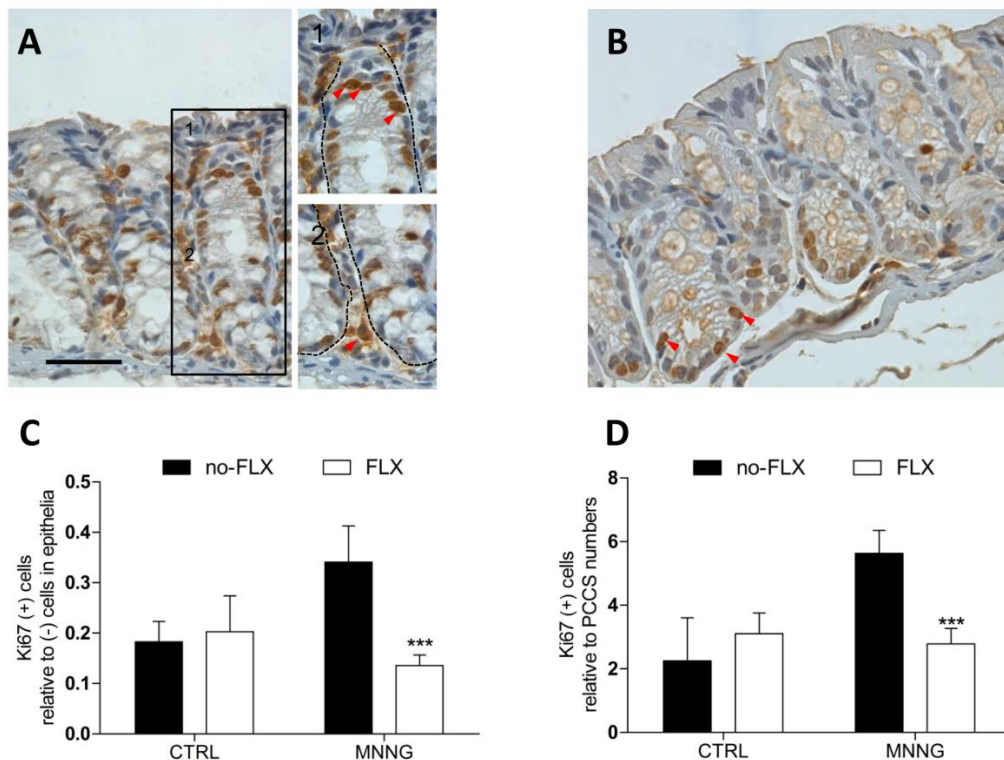
Figure 9 – Proliferating cells detected by staining with anti-Ki67 antibody (MNNG-treated mouse). (1) Red arrows show dark-brown positive cells migrating upward in the epithelial proliferative zone. (2) Stromal positive cells are shown by a red arrow near to the cryptal-bottom (**A**). Proliferating cells (anti-Ki67 antibody; red arrows) in a MNNG+FLX-treated mouse are shown at the cryptal bottom. Pictures were taken at 400x magnification, insets at 1000x magnification, and scale bars represent 20 μm (**B**). Proliferation in epithelial areas shown by labeling with anti-Ki67 antibody (**C**; ***P < 0.001 *vs* MNNG without FLX, *n* = 5; FLX+MNNG, *n* = 4). Proliferation in colon stromal areas by labeling with anti-Ki67 antibody (**D**; ***P < 0.001 *vs* MNNG without FLX, *n* = 5; FLX+MNNG, *n* = 4).

PCNA staining also showed that FLX attenuated the MNNG-induced proliferative activity at both colon areas (Fig. 10A and B).
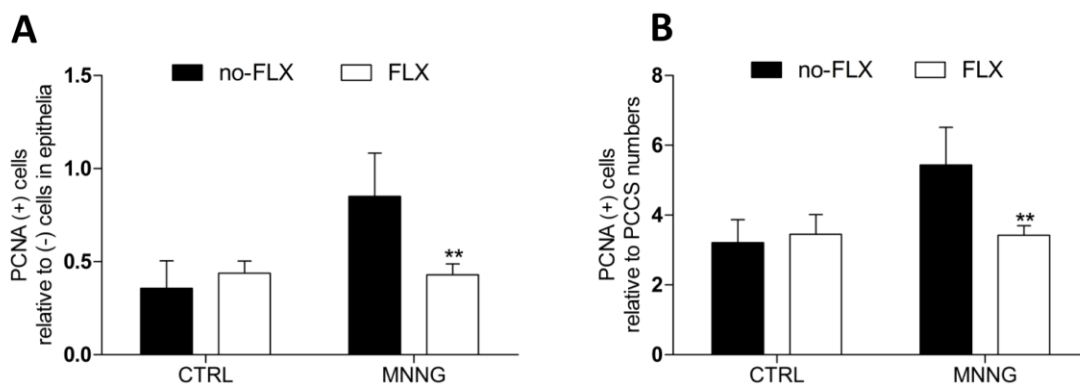
Figure 10 – Proliferation in epithelial areas shown by labeling with anti-PCNA antibody (**A**; **P < 0.01 *vs* MNNG without FLX, *n* = 4; FLX+MNNG, *n* = 4). Proliferation in colon stromal areas shown by labeling with anti-PCNA antibody (**B**; **P < 0.01 *vs* MNNG without FLX, *n* = 4; FLX+MNNG, *n* = 4).

Moreover, a high *c-Myc* expression was found at both colonic areas in MNNG-treated animals, in which FLX-treatment prevented the increase of expression (Fig. 11A and B).
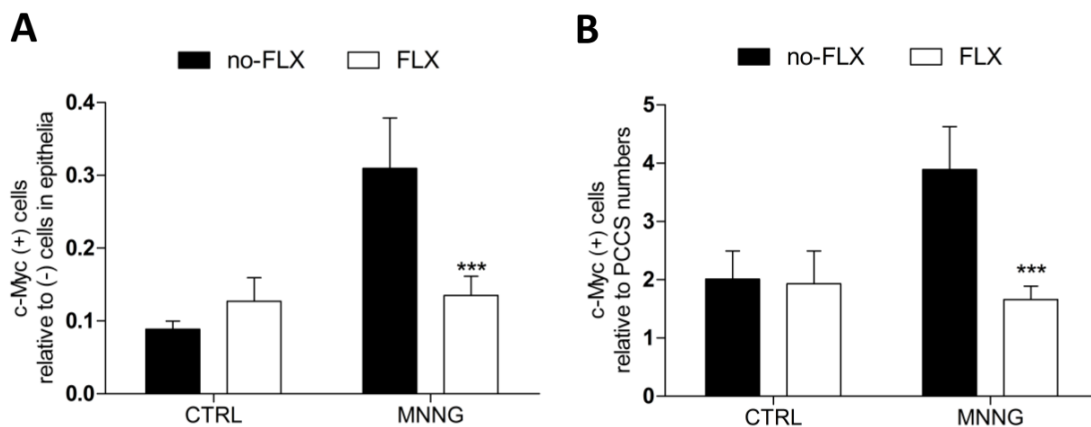
Figure 11 – Expression of *c-Myc* in epithelia of colon tissue (**A**; ***P < 0.001 *vs* MNNG without FLX, *n* = 3; FLX+MNNG, *n* = 4). Expression of *c-Myc* in stromal areas of colon tissue (**B**; ***P < 0.001 *vs* MNNG without FLX, *n* = 3; FLX+MNNG, *n* = 4).

4.3.1 Fluoxetine modulates the expression of NF-κB-signaling elements in methylnitronitrosoguanidine-exposed colon tissue

To understand whether FLX induced effects on colon stromal proliferation are associated with a blockade of transcription factor activities, we evaluated the expression of NF-κB1 (p50) protein in stromal areas (Fig. 12A). As shown in Fig. 12B, FLX-treatment, in MNNG-treated mice, significantly reduced the nuclear presence of NF-κB protein among stromal colonic cells. Although cytoplasmic expression of NF-κB protein remained unaffected in FLX-treated mice (Fig. 12C), its cytoplasm-nucleus transitional ratio was decreased significantly (Fig. 12D).
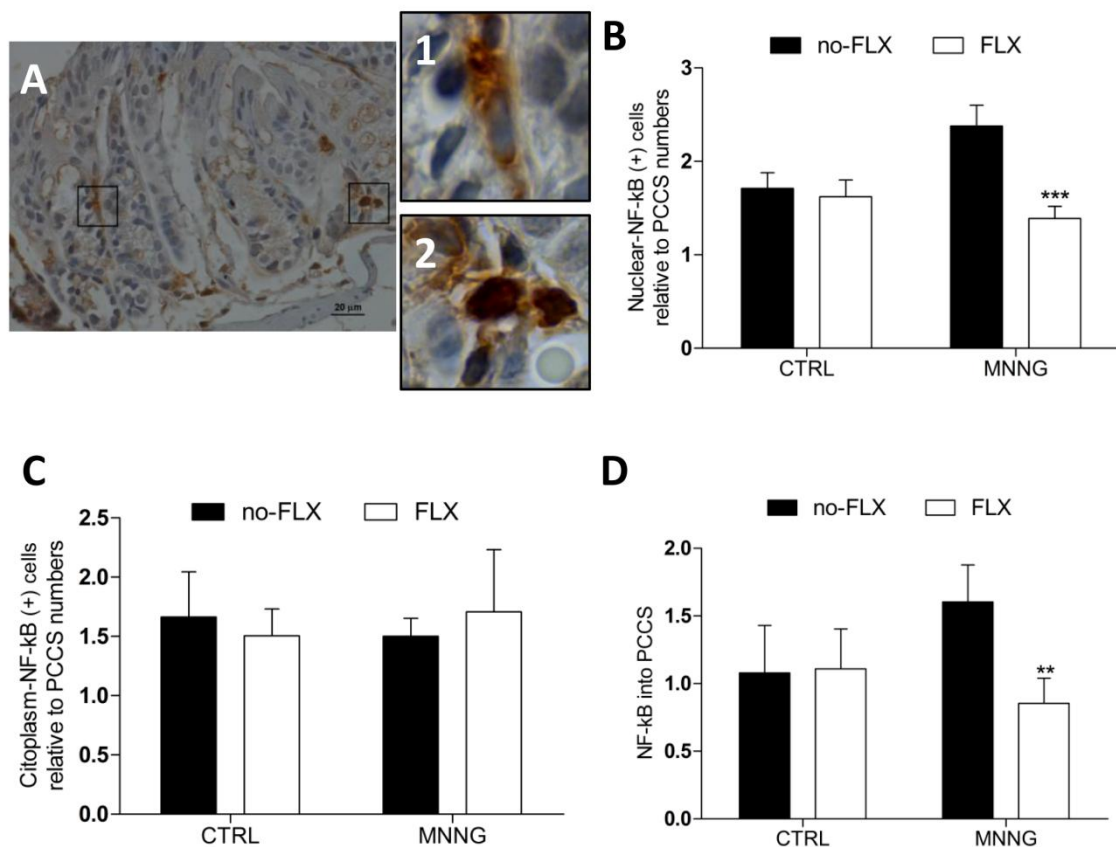
Figure 12 – Representative histological image of a colonic-longitudinal section labeled with anti-NF-κB antibody, picture taken at 400x magnification, and scale bar of 20 μm inserted (**A**). A cytoplasmic anti-NF-κB antibody positively cell detected within cryptal area (**A.1**; 1000x magnification of the boxed region, middle-left). (2) Nuclear-NF-κB protein detected in stromal cells (**A.2**; 1000x magnification of the boxed region, middle-right). Relative number of nuclear-NF-κB positive cells within colon stromal areas (**B**; ***$P < 0.001$ *vs* MNNG without FLX, $n = 4$; FLX+MNNG, $n = 4$). Relative number of citoplasmatic-NF-κB positive cells within PCCS areas (**C**; $P > 0.05$). Nuclear-transitional ratio for NF-κB-protein among stromal cells (**D**; **$P < 0.01$ *vs* MNNG without FLX, $n = 4$; FLX+MNNG, $n = 4$).

To support a presumed FLX-inhibition of the NF-κB signaling pathway, cytoplasmic expression of NF-κB inhibitory proteins was verified within colon stromal areas. It was found that FLX significantly increased cytoplasmic IκB-α and IκB-β expressions in MNNG+FLX-treated mice in comparison with MNNG treatment alone (Fig. 13A and B).
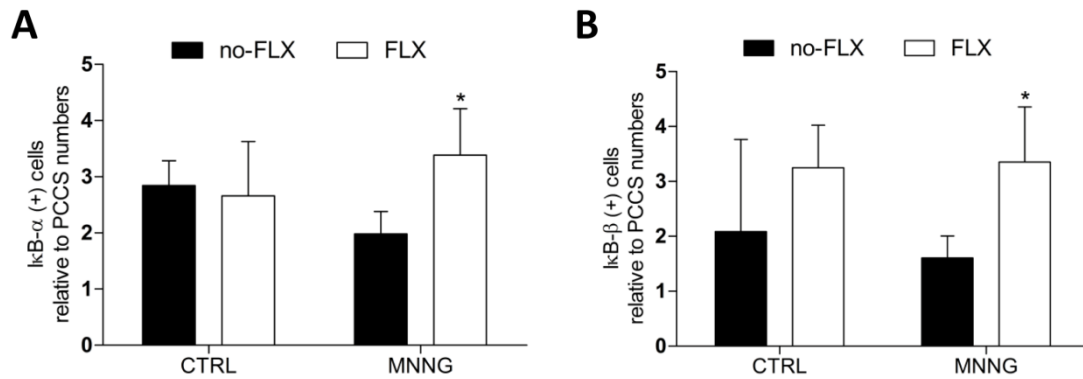
Figure 13 – Relative number of IκB-α positive cells (**A**; *P < 0.05 *vs* MNNG without FLX, $n = 4$; FLX+MNNG, $n = 4$), and IκB-β positive cells within colon stromal areas (**B**; *P < 0.05 *vs* MNNG without FLX, $n = 5$; FLX+MNNG, $n = 4$).

4.3.2 Fluoxetine controls angiogenesis-related markers in methylnitronitrosoguanidine-treated mice

As shown above, FLX treatment might acts against colon preneoplastic proliferation and angiogenesis. Angiogenesis is related to stem cell markers and takes place within stromal areas. Investigating the potential connection between these events, it was observed that FLX treatment decreased the relative number of stromal CD133-positive cells in the carcinogen-exposed group compared to the MNNG group without FLX (MNNG, 3.73 ± 0.44 [$n = 4$] *vs* MNNG+FLX, 1.97 ± 0.14 [$n = 4$]; P < 0.001). Then, CD133-positive cells expressing VEGF were found within stromal areas in mice subjected either to MNNG or MNNG+FLX treatments (Figure 14A). However, stromal cells expressing VEGF were also decreased in MNNG-exposed animals treated with FLX expression (Figure 14B). Intriguingly, CD133 positive cells expressing CD34 glycoprotein were only found among MNNG treated mice (Figure 14C) while FLX treatment significantly decreased the number of stromal CD34-positive cells (Figure 14D).
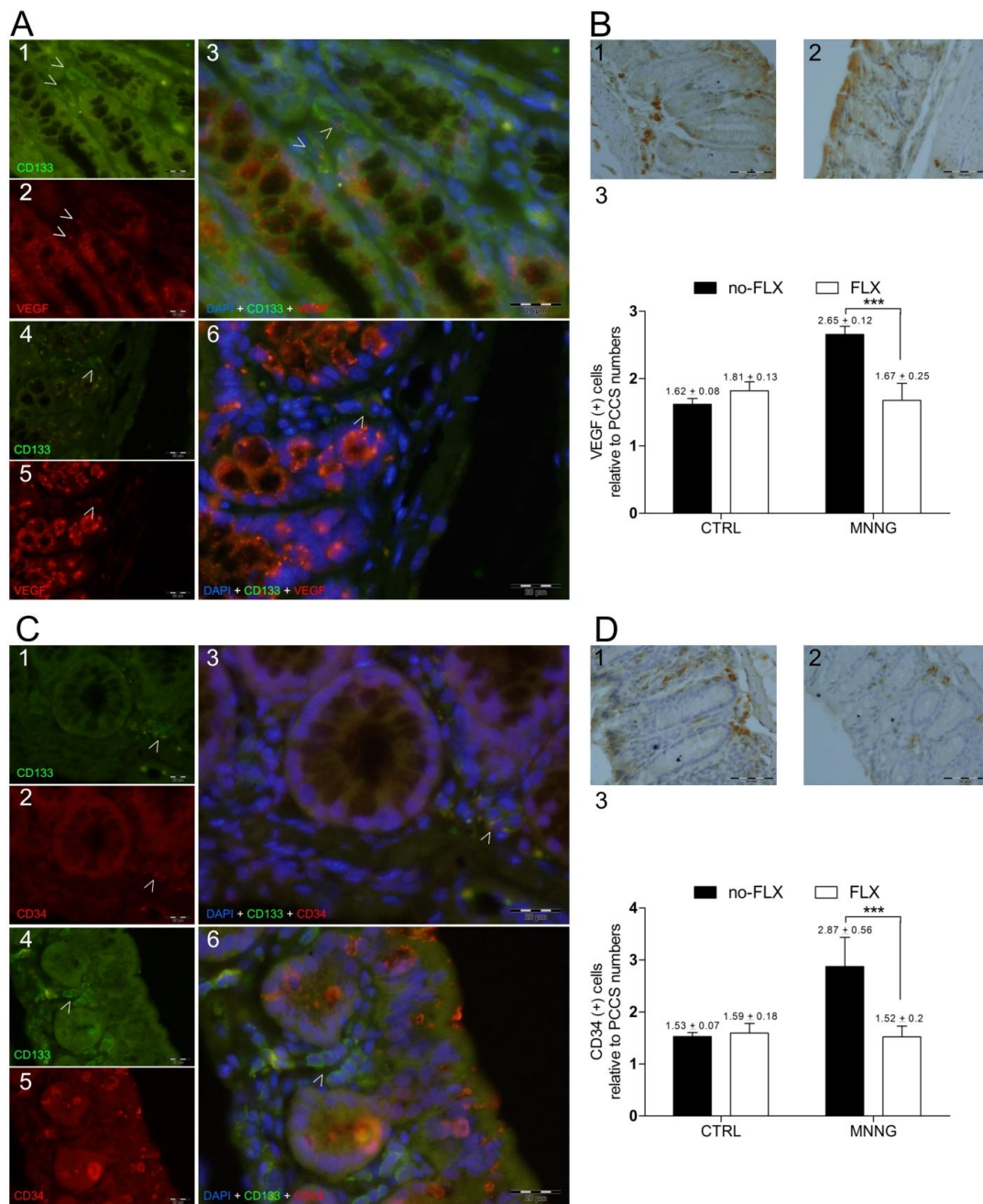
Figure 14 – FLX activity and angiogenesis-related markers. (**A**) Representative images of colon sections labeled with anti-CD133 and anti-VEGF antibodies, and nuclei stained with DAPI. White arrows indicate single-stained and double-stained positive cells in stromal areas in colon sections from (**A1** to **A3**) MNNG without FLX treatment, and (**A4** to **A6**) MNNG+FLX treatment groups. Pictures were taken with FITC (495-521 nm), ultraviolet (358-461 nm), and Texas Red (595-605 nm) filters. All pictures were taken at 600x magnification, scale bars represent 20 μm. (**B**) Representative images of single stained colon sections with anti-VEGF antibody (positive cells are seen with dark-brown cytoplasm) from (**B1**) MNNG without FLX treatment, and (**B2**) MNNG+FLX treatment groups. (**B3**) Relative number of cells expressing VEGF within colon stromal areas (***p<0.001; MNNG without FLX, n = 3; FLX+MNNG, n = 4). All pictures were taken at 400x magnification, scale bars represent 50 μm. (**C**) Representative images of colon sections labeled with anti-CD133 and anti-

CD34 antibodies, and nuclei stained with DAPI. White arrows indicate single-stained and double-stained positive cells in stromal areas in colon sections from (**C1** to **C3**) MNNG without FLX treatment, and (**C4** to **C6**) MNNG+FLX treatment groups. Pictures were taken as described above. (**D**) Representative images of single stained colon sections with anti-CD34 antibody (positive cells are seen with dark-brown cytoplasm) from (**D1**) MNNG without FLX treatment, and (**D2**) MNNG+FLX treatment groups. (**D3**) Relative number of CD34 positive cells in colon stromal areas (***p<0.001; MNNG without FLX, $n = 4$; FLX+MNNG, $n = 4$). All pictures were taken as described above.

Further, the relative total number of CD31-positive cells was enumerated within colon stromal areas, and a significant decrease was found in the MNNG-exposed group under FLX treatment (MNNG, 3.5 ± 0.87 [$n = 4$] *vs* MNNG+FLX, 1.8 ± 0.2 [$n = 4$]; P < 0.01). A comparison between CD34 and CD31-positive cells showed a 1.2-fold increase in CD31-positive cell values among MNNG-exposed mice.

As known, CD31 is an angiogenesis-related marker, and was enhanced during our experiments with MNNG-treatment. Thus, double-staining was performed to understand whether CD133 positive cells were expressing CD31 glycoprotein. In the MNNG and MNNG+FLX groups, CD133 positive cells expressed CD31 in microvessel-like structures within stromal areas (Figure 15A). Potential sites of developing microvessels were detected enumerating CD31-positive cell clusters within colon stromal areas (Figure 15B.1 and B.2). CD31-positive cell clusters were decreased significantly under FLX-treatment in MNNG-exposed mice (Figure 15B.3).
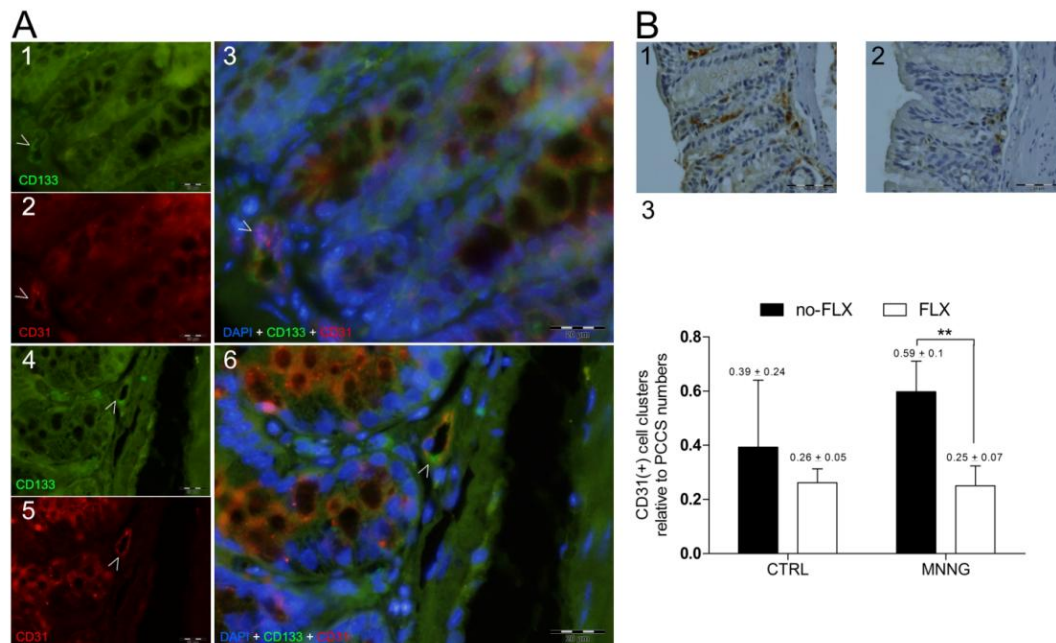
Figure 15 – Fluoxetine activity and angiogenesis-related markers. (**A**) Representative images of colon sections labeled with anti-CD133 and anti-CD31 antibodies, and nuclei stained with DAPI. White arrows indicate single-stained and double-stained positive cells into stromal areas in colon sections from (**A1** to **A3**) MNNG without FLX treatment, and (**A4** to **A6**) MNNG+FLX treatment groups. (A3 and A6) Double-stained positive cells are shown by white arrows in microvessel-like structures nearby cryptal bottoms. Pictures were taken with FITC (495-521 nm), ultraviolet (358-461 nm), and Texas Red (595-605 nm) filters. All pictures were taken at 600x magnification, scale bars represent 20 μm. (**B**) Representative images of single stained colon sections with anti-CD31 antibody (positive cells are seen with dark-brown cytoplasm) from (**B1**) MNNG without FLX treatment, and (**B2**) MNNG+FLX treatment groups. Pictures were taken at 400x magnification, scale bars represent 50 μm. (**B3**) Relative number of CD31 positive cell clusters detected *per* colon stroma area (**p<0.01; MNNG without FLX, *n* = 4; FLX+MNNG, *n* = 4).

4.4 Effects of fluoxetine treatment in colon tumors

4.4.1 First experiment – Caco-2 cell line

4.4.1.1 Fluoxetine reduces reactive oxygen species generation in Caco-2 cells

Taking into account that AntiM blocks the mitochondrial complex III which leads to increasing ROS production, we tested whether FLX could

counteract the AntiM effects. We found that 20 μM FLX was able to control superoxide (O_2^-) generation in Caco-2 adenocarcinoma cells (Fig.16 A and B).
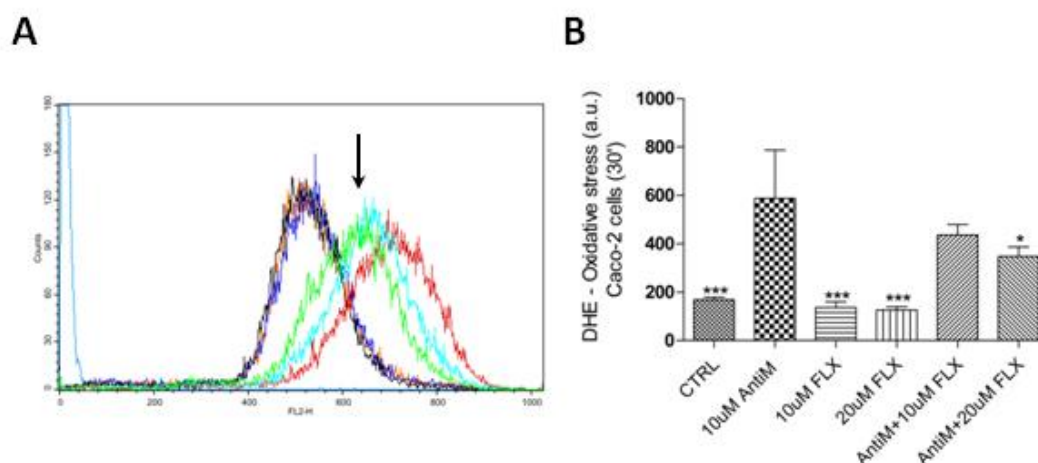
Figure 16 – ROS (O_2^-) generation detected by DHE staining and flow cytometry in Caco-2 cells after 30 min treatment. A black-arrow shows the combined treatment with 10 μM AntiM and 20 μM FLX (**A**; spectral colors are light-blue, DHE-unstained cells; yellow, DHE stained cells (CTRL); purple, 10 μM FLX; black, 20 μM FLX; red, 10 μM AntiM; blue-green, AntiM + 10 μM FLX; green, AntiM + 20 μM FLX). 20 μM FLX reduced ROS generation (**B**; *P < 0.05 and ***P < 0.001 *vs* 10 μM AntiM).

4.4.1.2   Fluoxetine decreases intracellular pH, mitochondrial membrane potential, and superoxide generation in hypoxia-exposed Caco-2 cells

Since FLX is a lipophilic weak base, and seems to have potential effects on mitochondrial activities, a commercial dye marker was used to establish an ipH standard curve for Caco-2 cells by flow cytometry (Fig. 17A).Then, non-hypoxia (normoxia) and hypoxia-exposed Caco-2 cells were treated with 20 μM FLX. This FLX treatment slightly decreased ipH under standard conditions (1-fold), and significantly in hypoxia-exposed cells (Fig.17B; *P < 0.05 *vs* Hypoxia).
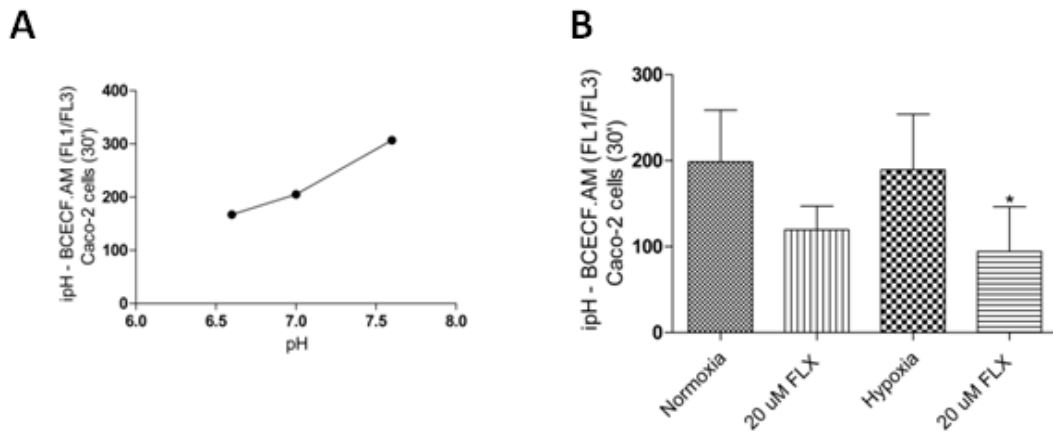
Figure 17 – Intracellular pH (ipH) detected by BCEDCF-AM staining and flow cytometry in Caco-2 cells (**A**). Caco-2 cells underwent normoxic or hypoxic conditions 24h before treatment with 20 μM FLX for 30 min (**B**; *P < 0.05 *vs* hypoxia).

It is known that ipH interferes in $\Delta\Psi$m and ROS generation. Treating Caco-2 cells with 20 μM FLX was found to reduce the $\Delta\Psi$m 1.5-fold and 1.2-fold in cultured cells under standard normoxia or hypoxia conditions, respectively (Fig. 18A). While hypoxia exposure significantly enhanced ROS generation after 24h, the 20 μM FLX treatment decreased O_2^- production in hypoxia-exposed Caco-2 cells (Fig. 18B and C).
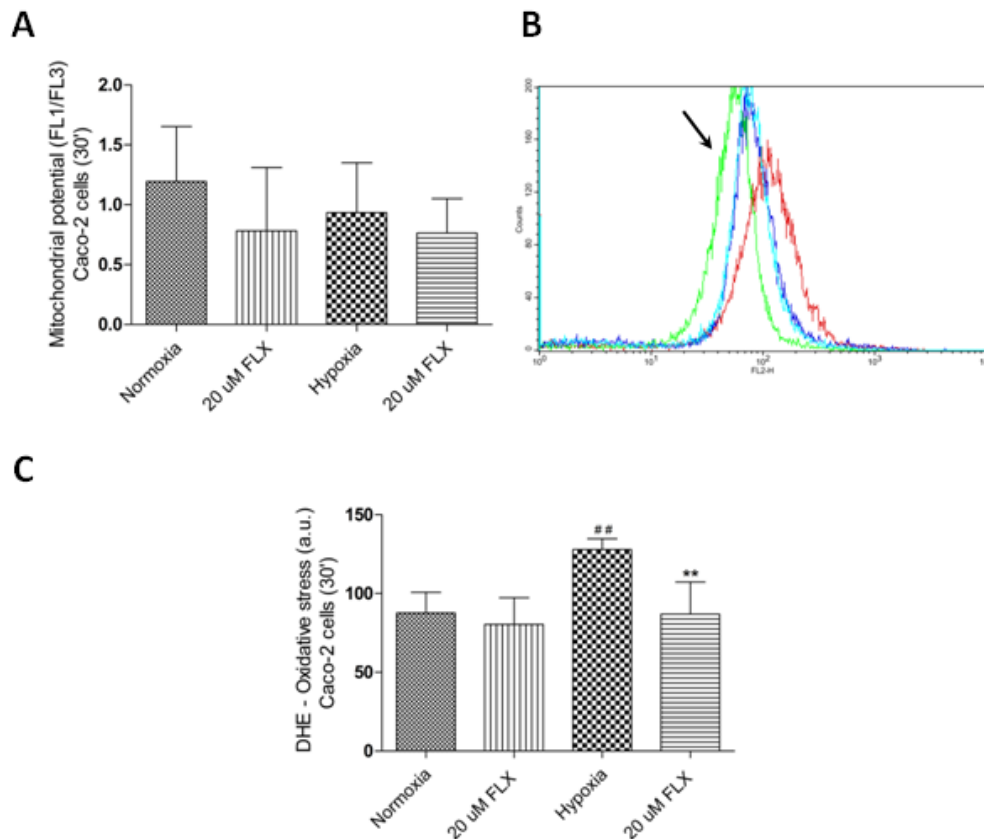
Figure 18 – Mitochondrial membrane potential ($\Delta\Psi m$) was detected by JC-1 staining and flow cytometry. Caco-2 cells underwent normoxia or hypoxia conditions, and then were treated with 20 μM FLX for 30 min (**A**; P > 0.05). O_2^- production detected by DHE staining and flow cytometry in Caco-2 cells after 30 min treatment. A black-arrow shows 20 μM FLX activity in hypoxia-exposed Caco-2 cells (**B**; spectral colors are purple, DHE stained cells (normoxia); light-blue, 20 μM FLX (normoxia); red, hypoxia-exposed cells; green, hypoxia-exposed cells treated with 20 μM FLX). 20 μM FLX reduced OS generation (**C**; $^{\#\#}$P < 0.01 *vs* normoxia; **P < 0.01 *vs* hypoxia).

4.4.1.3   Fluoxetine shrinks Caco-2 xenograft-tumors by reducing proliferation

Since there was a clear effect of FLX on the Caco-2 cell line, NOD-SCID mice bearing Caco-2 xenograft-tumors were treated with FLX for 6 days (Fig. 19A). After 6 days treatment, FLX significantly decreased the tumor volume (Fig. 19B), and tumor growth rates dropped below zero (Fig. 19C).
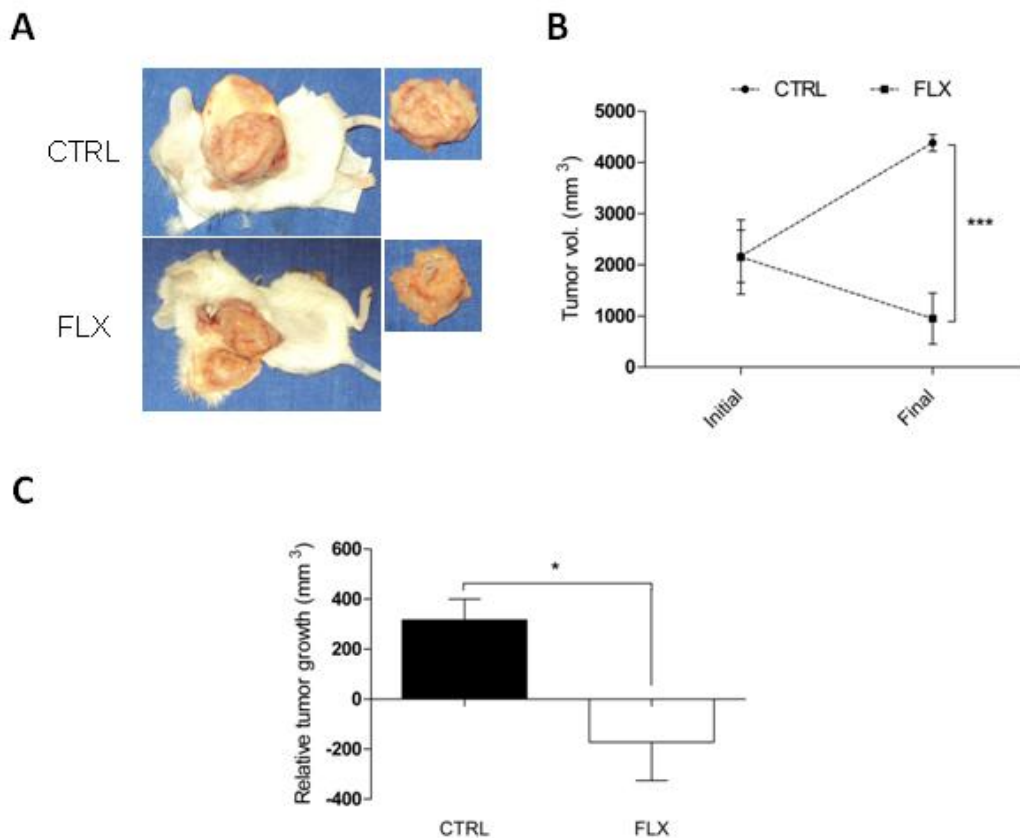
Figure 19 – NOD-SCID mice bearing Caco-2 xenograft-tumors with or without FLX-treatment (**A**). Tumor volume at day zero (Initial) and sixth day (Final) of treatment time (**B**; *P < 0.05 vs CTRL, $n = 5$; FLX, $n = 5$). Relative tumor growth during the six days of FLX-treatment (**C**; **P < 0.01 vs CTRL, $n = 3$; FLX, $n = 4$).

To enumerate proliferating tumor cells, a histopathological analysis was first performed in tissue sections. In general, tumor tissue showed a heterogeneous composition (Fig. 20A) with major areas characterized as TP and necrosis (N). A large number of microvessels spread around N areas was observed. Then, proliferation was evaluated in the three different main tumor areas (IF, PN and TP). Proliferating cells were significantly decreased in mice treated with FLX (Fig. 20B to E). Furthermore, this treatment decreased NF-kB1 protein expression 1.2-fold (Fig. 20F).
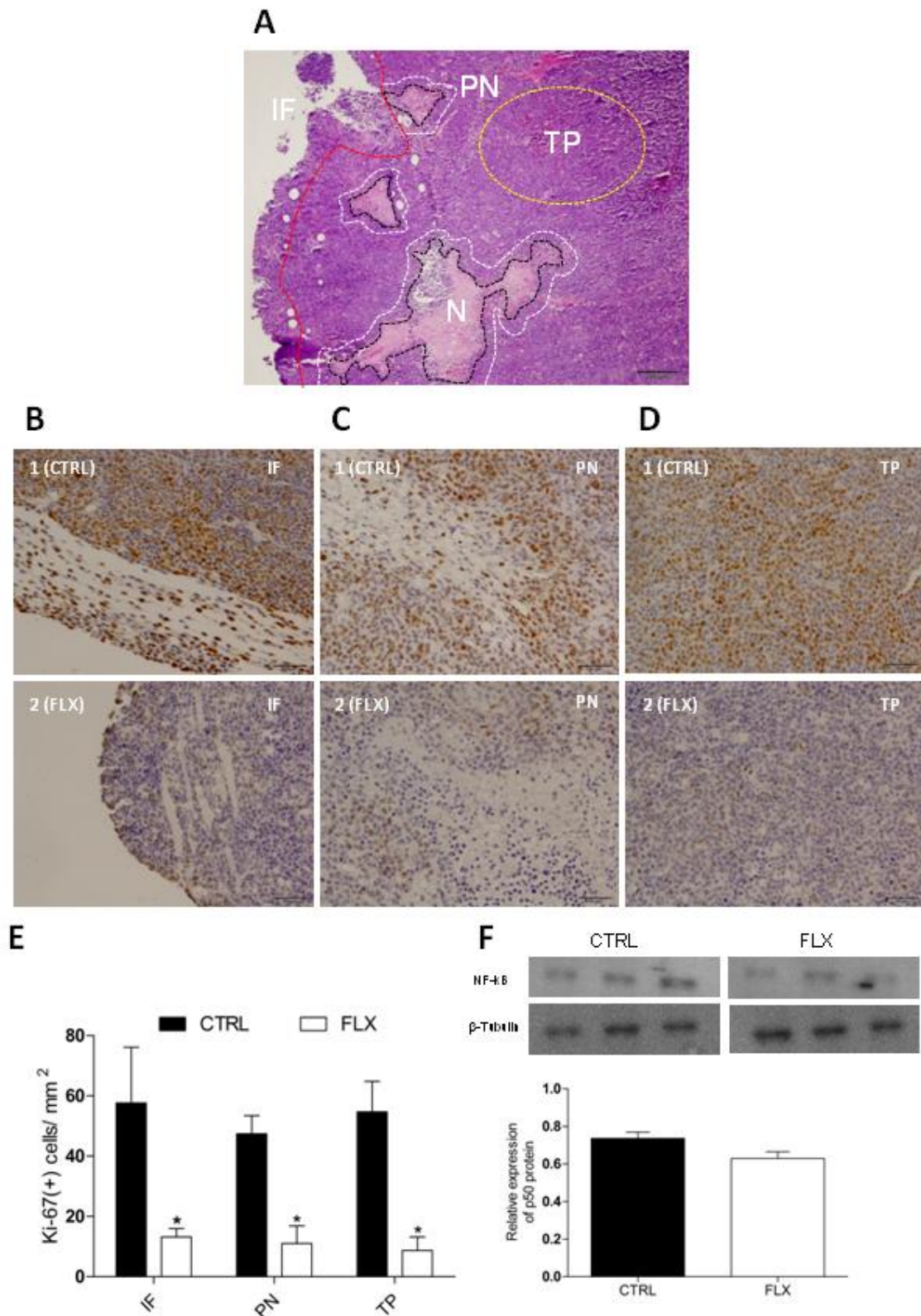
Figure 20 – Representative image of the four different tumor areas, termed invasion front (IF; sectioned red line), tumor parenchyma (TP; sectioned yellow line), peri-necrotic area (PN; sectioned white line), and necrosis areas (N; sectioned black line). Picture was taken at x40 magnification (**A**). Representative images for IF (**B**), PN (**C**), and TP (**D**) areas in tumor sections labeled with anti-Ki67 antibody from CTRL (**1**) and FLX-treated (**2**) groups.

Pictures were taken at *x*200 magnification, scale bars represent 50 μm. Graph shows the proliferative cell values for each tumoral area (**E**; **P < 0.01 *vs* CTRL, *n* = 3; FLX, *n* = *3*). Relative expression of NF-kB protein as determined by western blot (WB) analysis (**F**; P > 0.05).

4.4.2   Second experiment – HT29 cell line

4.4.2.1   Fluoxetine does not induce reactive oxygen species or DNA-damage, but delays HT29 cells at the G_0/G_1 cell-cycle phase

Next, we sought to understand the effects of FLX on HT29 cells. Cell cultures were analyzed for ROS and O_2^- generation, and DNA damage. Cells exposed to 100 µM FLX showed a 2.5-fold increase in ROS levels after 30min treatment, whereas no significant increase was observed with 1 or 10 µM FLX (Fig. 21A). Further experiments showed that the ROS amount in cells exposed to 100 µM FLX was about 2-fold less after 4h than after 30min treatment (Fig. 21B). Comparing the O_2^- generation between DMSO (solvent control, final concentration 1%) and 100 µM FLX exposed cells yielded 2.8-fold increase after 30min (Fig. 21C), whereas a 2-fold enhancement was observed for 4h (Fig. 21D). Moreover, cells exposed to 100 µM FLX showed a 1.4-fold less O_2^- production after 4h treatment than after 30min.
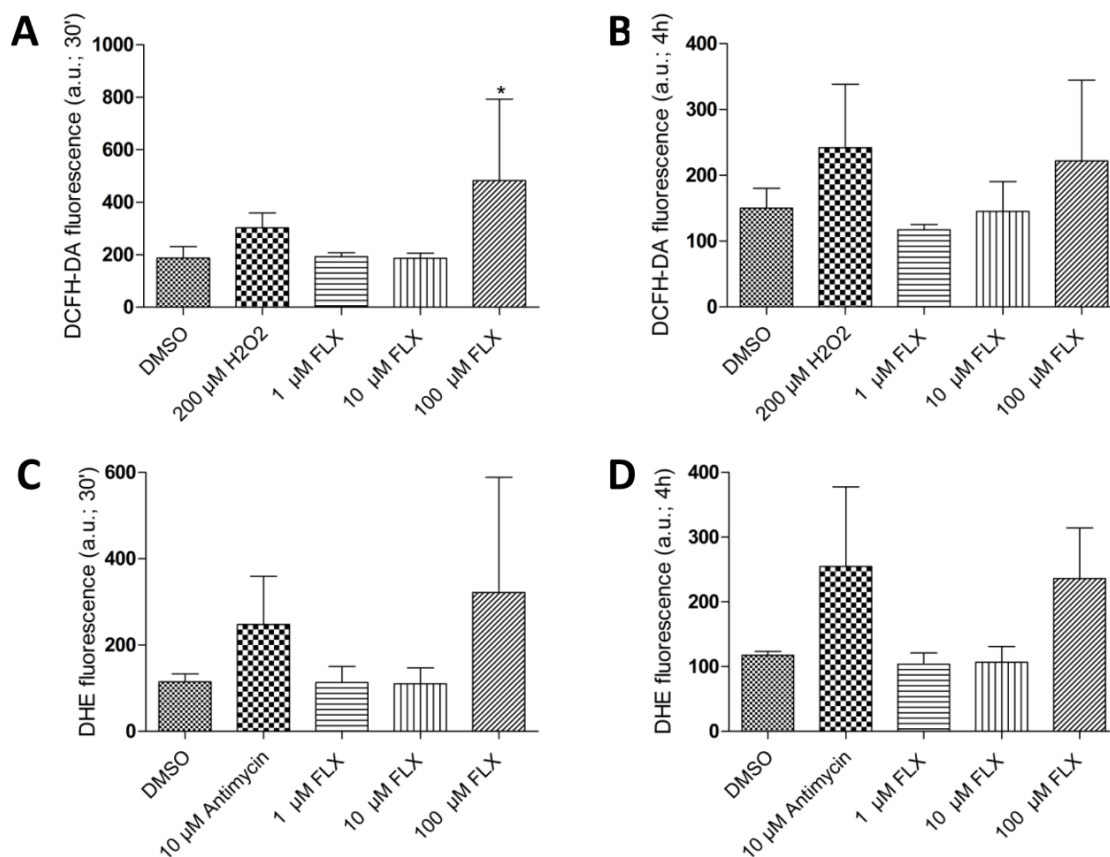
Figure 21 – Reactive oxygen species (ROS) production analyzed by flow cytometry, after exposure to FLX or AntiM for 30min (**A**; *P < 0.05 *vs* DMSO), and 4h (**B**; P > 0.05). O_2^- production for 30min (**C**; P > 0.05 *vs* DMSO), and 4h (**D**; P > 0.05), as detected by DHE staining. DMSO = solvent control ($\leq$ 1% final concentration of DMSO).

All FLX concentrations were unable to induce significant DNA damage in HT29 cells after 30min or 4h treatments (Fig.22A and B).
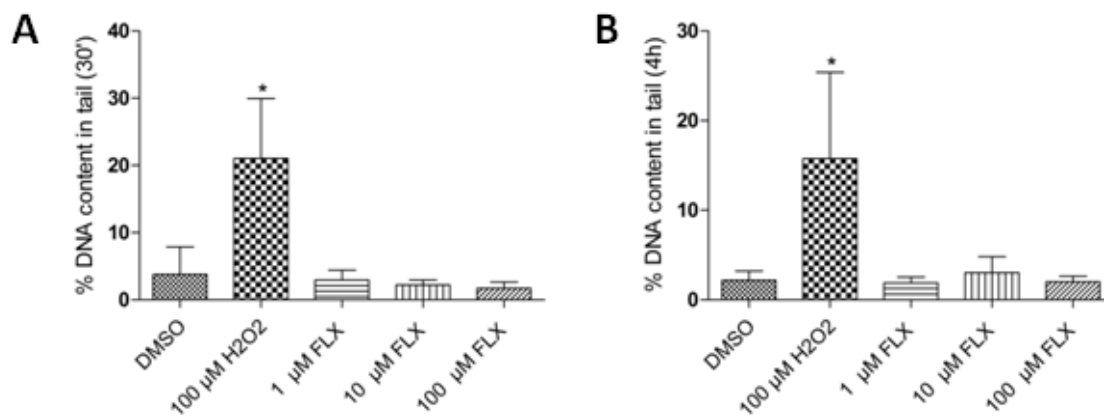
Figure 22 – DNA-damage analyzed by comet assay, after exposure to different FLX concentrations for 30min (**A**; *P < 0.05 *vs* DMSO), and 4h, with % DNA content in tail representing DNA-damage (**B**; *P < 0.05 *vs* DMSO). H_2O_2 was

applied as positive control. DMSO = solvent control ($\leq$ 1% final concentration of DMSO).

A viability and apoptosis test was performed by flow cytometry in HT29 cells exposed to different FLX concentrations. After 24h, 100 µM FLX decreased cell viability significantly and induced apoptosis, although 1 and 10 µM were unable to promote similar effects (Figure 23).
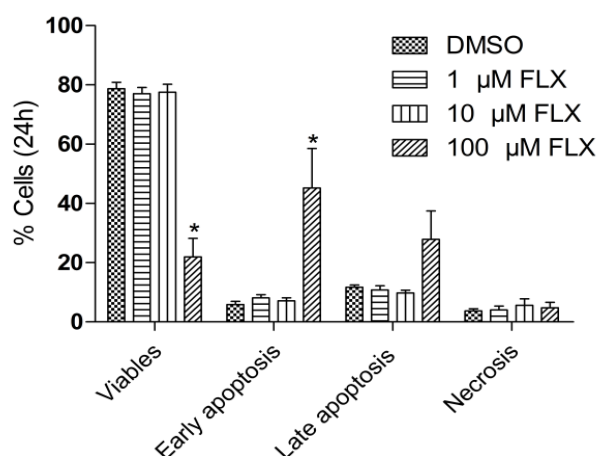
Figure 23 – Viability and apoptosis assay (Annexin V/ PI) performed by flow cytometry, after exposure to different FLX concentrations for 24h (*P<0.05 *vs* DMSO). DMSO = solvent control ($\leq$ 1% final concentration of DMSO). DMSO = solvent control ($\leq$ 1% final concentration of DMSO).

We further investigated whether FLX could act upon the cell-cycle of colon tumor cells. 10 µM FLX caused a significant delay of cells in G_0/G_1 phase after 24h treatment, and a 5.5-fold decrease in G2-M phase (Fig. 24A). When the cell cycle progression related protein p27 was investigated, 10 µM FLX caused a slight upregulation of its expression, while 20 µM FLX increased it 1.3-fold (Fig. 24B).
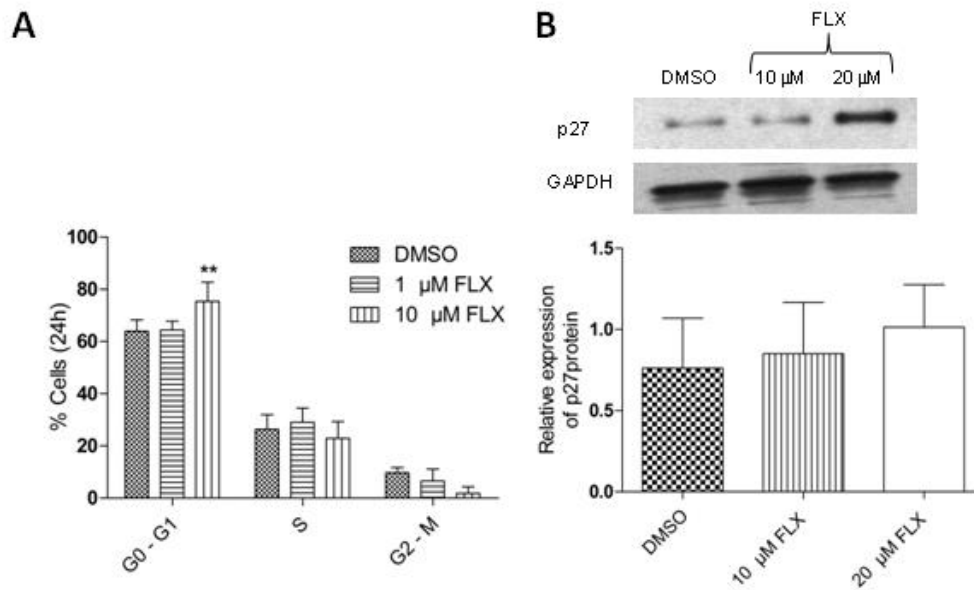
Figure 24 – Distribution of HT29 cells in the cell-cycle phase analyzed by flow cytometry (A) and expression of the cell-cycle related protein p27 (B). In (A), the percentage of cells is shown in G_0/G_1, S, and G_2/M phases are shown, analyzed from cultures with or without a 24h FLX treatment (**A**; **P < 0.01 *vs* DMSO). In (B), the relative expression of p27 protein in HT29 cells, determined by Western Blot analysis is displayed (**B**; P > 0.05).

4.4.2.2 Fluoxetine reduces reactive oxygen species generation in HT29 cells

Having the results from Caco-2 cells in mind, we tested whether FLX could act against AntiM activity in HT29 cells. Once more 20 μM FLX significantly reduced the O_2^- generation induced by AntiM in colon tumor cells (Fig. 25A and B).
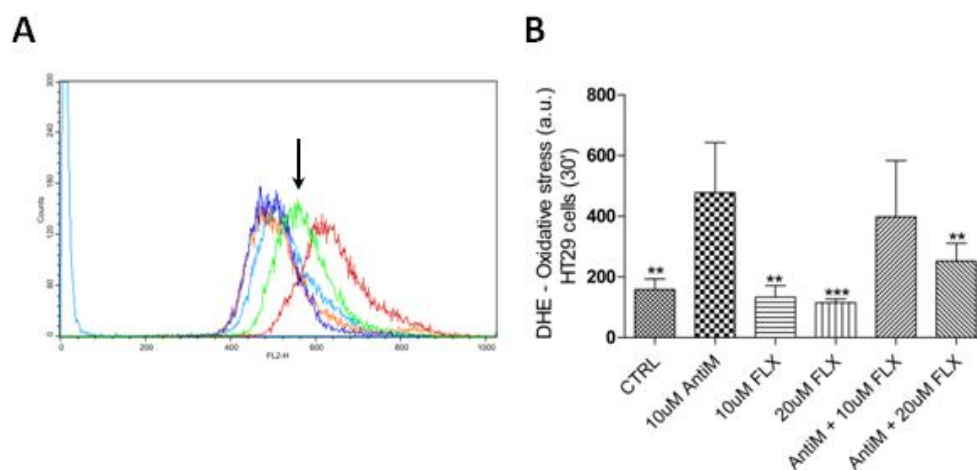
Figure 25 – O_2^- production detected by DHE staining and flow cytometry in Caco-2 cells after 30 min treatment. A black-arrow shows combined treatment with 10 μM AntiM and 20 μM FLX (**A**; spectral colors are extra-light-blue, DHE-unstained cells; light-blue, DHE stained cells (CTRL); yellow, 10 μM FLX; purple, 20 μM FLX; red, 10 μM AntiM; blue-green, AntiM + 10 μM FLX; green, AntiM + 20 μM FLX). 20 μM FLX reduced AntiM dependent ROS generation (**B**; *P < 0.05 and ***P < 0.001 *vs* 10 μM AntiM).

4.4.2.3 Fluoxetine decreases intracellular pH, membrane mitochondrial potential, and superoxide generation arresting hypoxia-exposed HT29 cells at the G0/G1 cell-cycle phase

As found in Caco-2 cells, 20 μM FLX also decreased ipH in hypoxia-exposed HT29 cells (Fig. 26A and B; *P < 0.05 *vs* hypoxia).
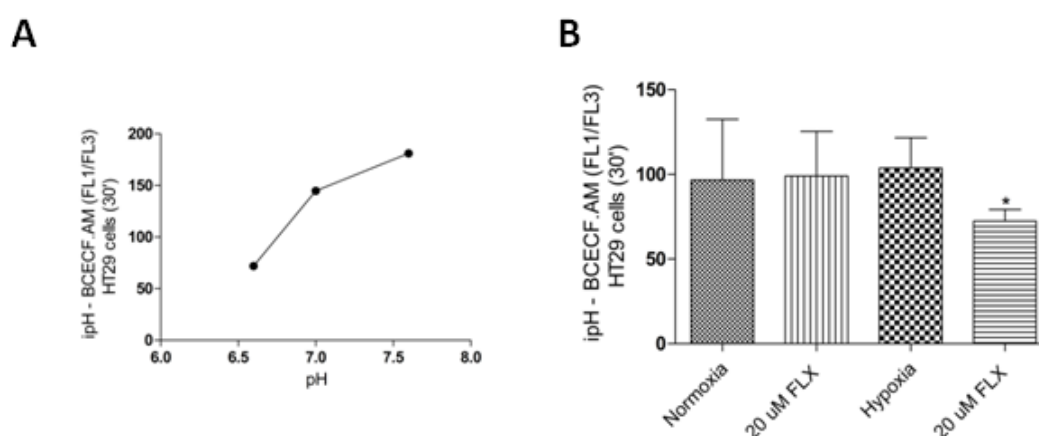
Figure 26 – A standard curve for ipH determined by BCEDCF-AM staining and flow cytometry in HT29 cells (**A**). HT29 cells underwent normoxic or hypoxic conditions 24h before treatment with 20 μM FLX for 30 min (**B**; *P < 0.05 *vs* hypoxia).

In addition, 20 μM FLX treatment significantly decreased $\Delta\Psi$m in hypoxia-exposed HT29 cells (Fig.27A). Under the same experimental conditions, FLX treatment significantly reduced the O_2^- generation (Fig. 27B).
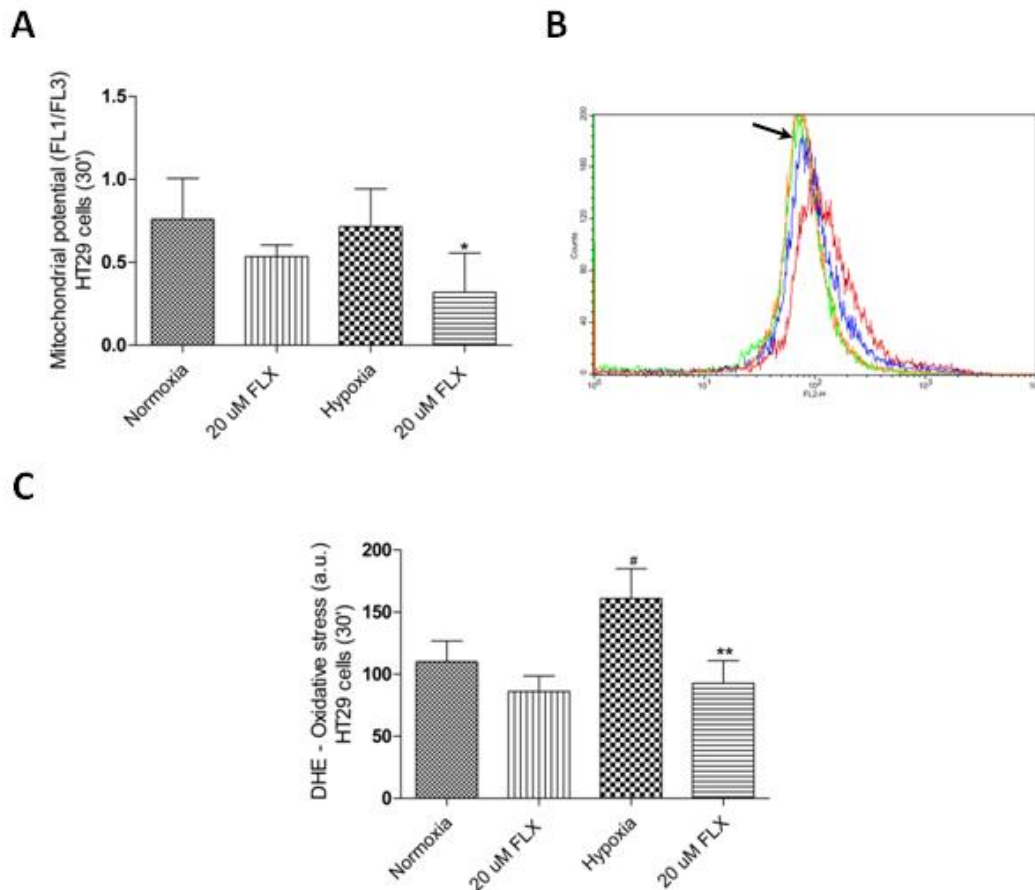
Figure 27 – The mitochondrial membrane potential (ΔΨm) was analyzed in non-hypoxia exposed (normoxia) and hypoxia-exposed HT29 cells. Cell cultures were treated with 20 μM FLX for 30 min (**A**; *P < 0.05 *vs* hypoxia). O_2^- production was detected by DHE staining and flow cytometry in Caco-2 cells after 30 min treatment. A black-arrow shows the activity of 20 μM FLX in hypoxia-exposed Caco-2 cells (**B**; spectral colors are purple, DHE stained cells (normoxia); light-blue, 20 μM FLX (normoxia); red, hypoxia-exposed cells; green, hypoxia-exposed cells treated with 20 μM FLX). 20 μM FLX reduced ROS generation (**C**; ##P < 0.01 *vs* normoxia; **P < 0.01 *vs* hypoxia).

Then, cell-cycle phases were analyzed in non-hypoxia and hypoxia-exposed HT29 cells treated with 20 μM FLX for 24h. FLX induced a G_0/G_1 cell-cycle arrest in HT29 cells under both of two applied experimental conditions, meaning a significant increase of cells in G1-phase, as well as a suppression of S-phase (Fig.28A and B).
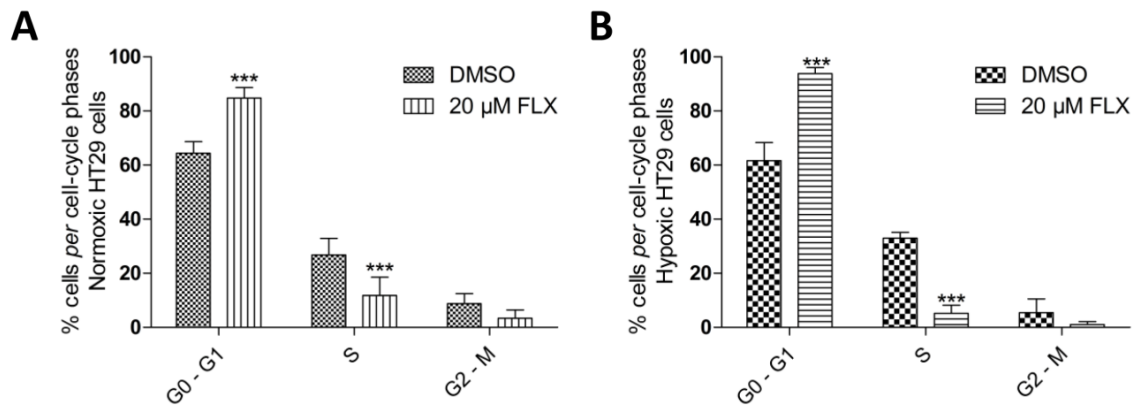
Figure 28 – Flow cytometric cell-cycle analysis in HT29 cells. HT29 cells underwent normoxia or hypoxia 24h before treatment with DMSO (1%) or 20 μM FLX for another 24h. Percentages of normoxic (**A**) and hypoxic HT29 (**B**) cells are shown *per* cell-cycle phase with or without FLX treatment for 24 h (***P < 0.001 *vs* DMSO).

While 20 μM FLX treatments had just slight effects upon p27 protein expression under standard-cell culture conditions after 24h, FLX enhanced its expression in hypoxia-exposed cells 1.3-fold (Fig. 29A and B). However, FLX treatment did not affect the protein expression of cyclin E (Fig. 29A and C).
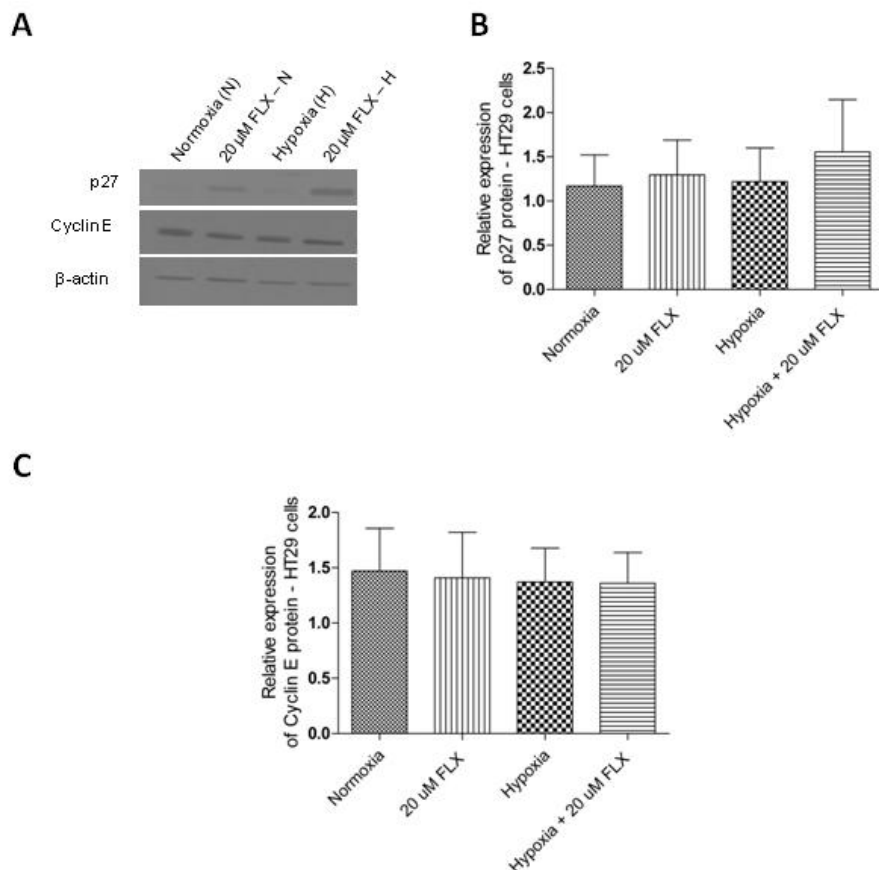
Figure 29 – Western Blot analysis of the expression of p27 and cyclin E. Representative image of a western blot analysis for p27 and cyclin E proteins. The β-actin expression was considered as endogenous control (**A**). Quantification of the relative expression of p27 (**B**) and cyclin E (**C**) proteins in HT29 cells (P > 0.05).

4.4.2.4   Fluoxetine shrinks HT29 xenograft-tumors by reducing proliferation

To verify the effects of FLX in another colon tumor model, NOD/SCID mice bearing HT29 xenograft-tumors were treated with the antidepressant for three days. The body weight of the mice remained unchanged until the end of this treatment (CTRL, 15.4 $\pm$ 2 g, $n = 5$; FLX, 14.4 $\pm$ 2.5 g, $n = 6$). FLX treatment significantly decreased the tumor volume (Fig. 30A), yielding RTG values below zero (Fig. 30B), and reduced tumor weight (2.2-fold) in comparison with the non-treated group (Fig. 30C).
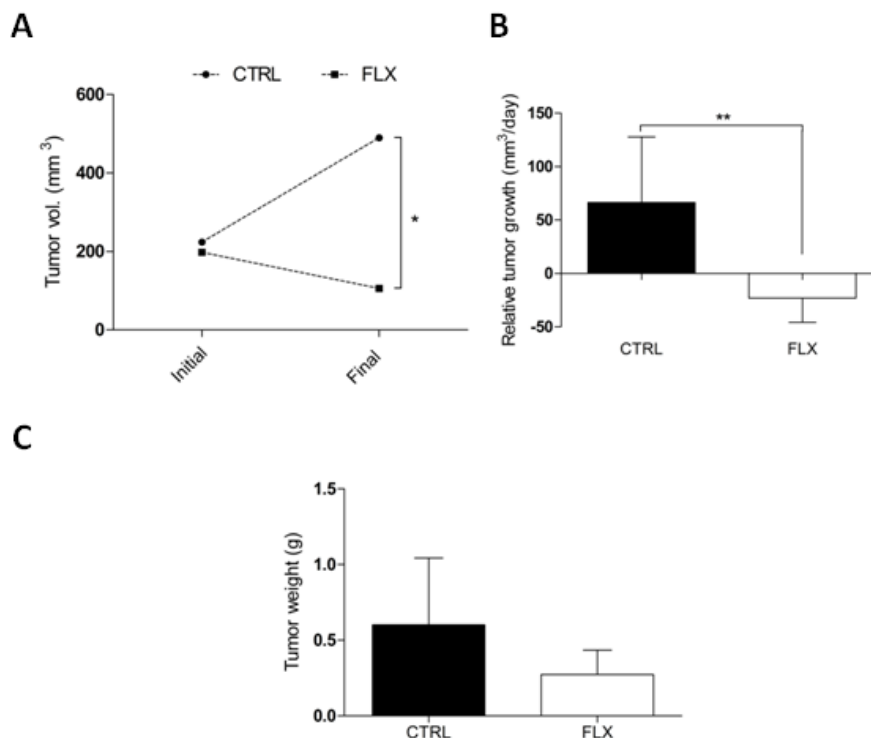
Figure 30 – Tumor volume on the first (Initial) and fourth day (Final) (**A**; *P < 0.05 vs CTRL, $n = 5$; FLX, $n = 5$). Relative tumor growth during the experiment (**B**; **P < 0.01 vs CTRL, $n = 5$; FLX, $n = 5$). Tumor weight at the end (fourth day) after the three days FLX-treatment (**C**; P > 0.05; CTRL, $n = 5$; FLX, $n = 5$).

Proliferation was then evaluated in three different tumor areas (Fig. 31A). In control tumors, proliferation within IF (Fig. 31B.1) and PN (Fig. 31C.1) was found to be significantly higher than in TP areas (Fig. 31D.1; IF, 17.03 $\pm$ 3.38; PN, 13.92 $\pm$ 3.383; TP, 7.9 $\pm$ 2.34; P < 0.01 *vs* TP). FLX-treatment reduced proliferation in IF (Fig. 31B.2) and PN (Fig. 31C.2) areas significantly in comparison with the control samples, whereas proliferative rates in TP (Fig. 31D.2) areas remained unchanged (Fig. 31E).
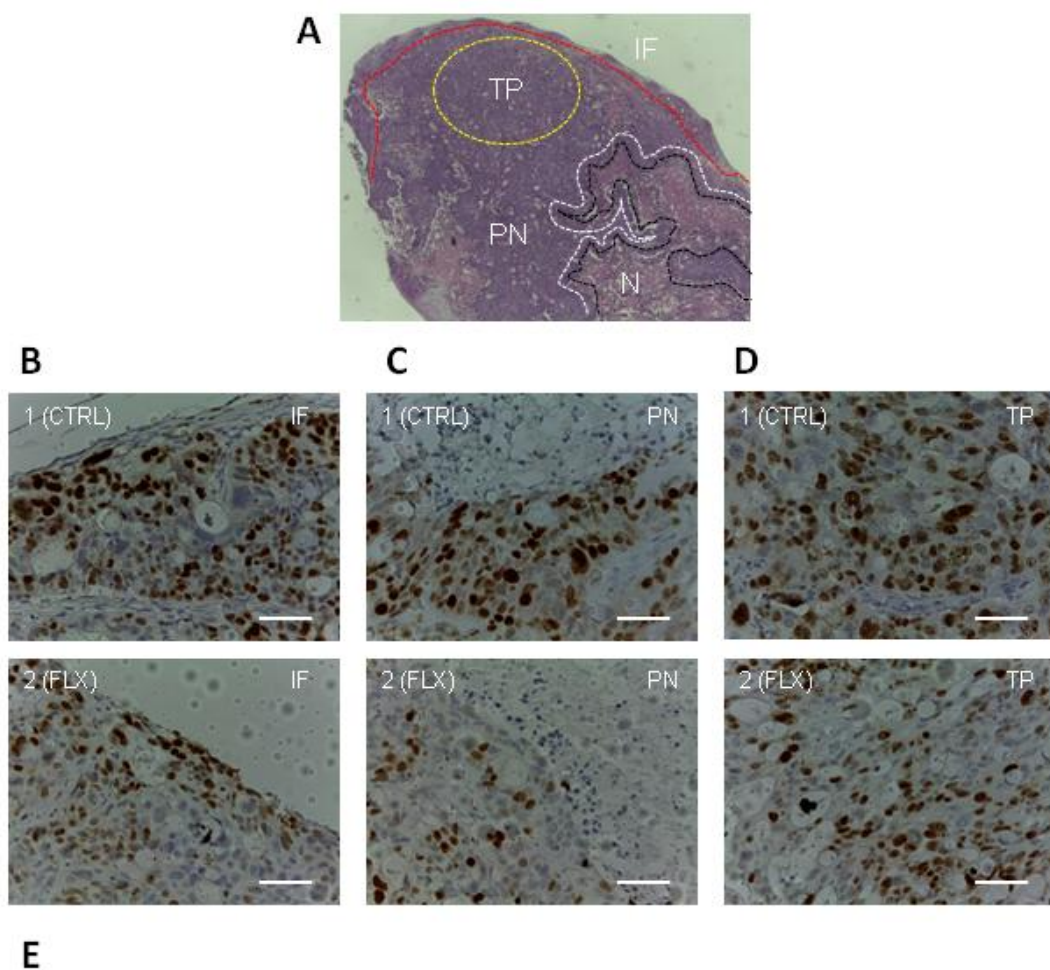
Figure 31 – Representative image indicating the locations of four different tumor areas, termed invasion front (sectioned red line), tumor parenchyma (sectioned yellow line), peri-necrotic area (sectioned white line), and necrotic area (N; sectioned black line). The picture was taken at x100 magnification (**A**). Representative images for IF (**B**), PN (**C**), and TP (**D**) areas in tumor sections labeled with anti-Ki67 antibody from CTRL (**1**) and FLX-treated (**2**) groups. Pictures were taken at 400x magnification, scale bars represent 20 μm. Graph shows the proliferative cell values for each tumoral area (**E**; **P < 0.01 *vs* CTRL, $n = 4$; FLX, $n = 5$). Gene expression for cyclin D1, BIRC5, and NF-kB1 was quantified by qRT=PCR (**F**; *P < 0.05 *vs* CTRL; $n = 3$ [cyclin D1] and 5 [BIRC5] per group).

4.4.3 Third experiment – HT29 tumors

4.4.3.1   Fluoxetine and 5-fluorouracil have similar effects

against HT29 xenograft-tumors

We next aimed to examine whether the FLX induced effects are comparable with those of the known chemotherapeutic agent 5-fluoracil (5-FU). Again, FLX-treatment reduced RTG values to below zero (Fig. 32A). 5-FU also yielded a reduced tumor growth, although not as efficiently as FLX. However, the reduction of the tumor weight compared to the control was similar in both treatments (Fig. 32B).
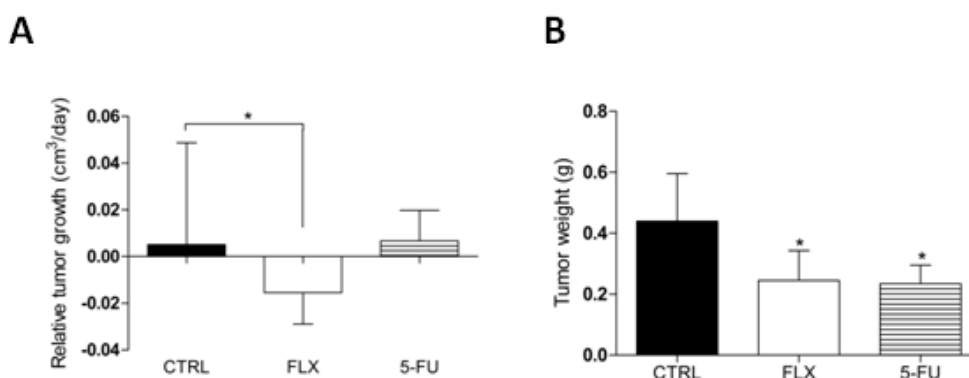
Figure 32 – Tumor growth between the first and fourth days of FLX-treatment (**A**; *P < 0.05 vs CTRL). Tumor weight at the end (fourth day) after the three days FLX-treatment (B; *P < 0.05 *vs* CTRL).

4.4.3.1 Fluoxetine acts against tumor metabolism and molecular signaling

Using a Luminex-based technology, protein expression of mitochondrial complexes was quantified in tumor samples. FLX had no effect on complex I and IV expression, while 5-FU decreased the amounts of both protein almost 1.3-fold. FLX and 5-FU respectively enhanced complex II amount 1.4-fold and 2.2-fold. Moreover, FLX reduced the expression of complex III 1.4-fold and complex V (ATPase) 1.6-fold (Fig. 33A). FLX treatment also decreased a marker of mitochondrial activity (TOMM20) 1.4-fold (Fig. 33B).
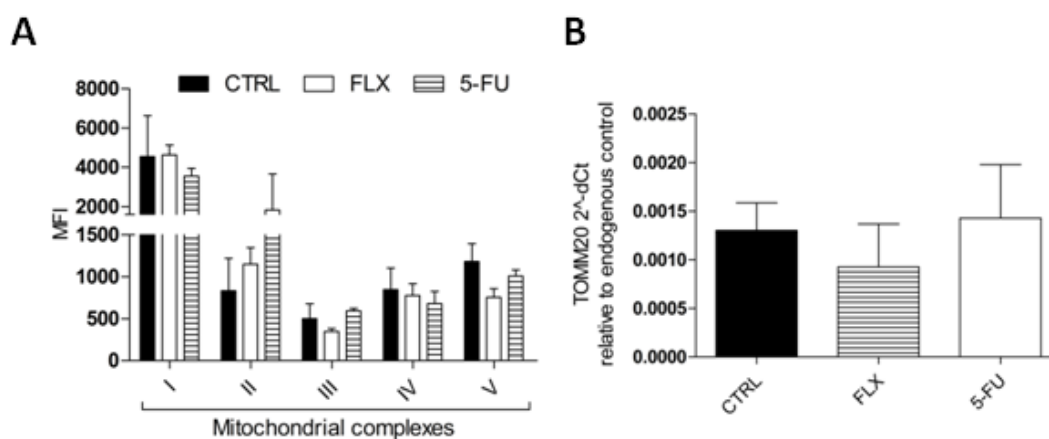
Figure 33 – Tumor lysates were analyzed with a human OXPHOS kit. Median fluorescence intensity (MFI) was acquired with a Luminex® system (**A**; P > 0.05). Gene expression of TOMM20 was analyzed by RT-PCR (**B**; P > 0.05)

FLX and 5-FU treatments enhanced the glucose serum levels in NOD/SCID mice bearing HT29 xenograft-tumors 1.5-fold and 1.8-fold, respectively. This was accompanied by a significant increase in serum lactate levels, whereas no metabolic changes were observed (Fig. 34A). However, 5-FU treatment induced a significant tumor glucose level increase, which FLX enhanced 2.6-fold. Also, FLX and 5-FU increased the tumor lactate levels 1.9-

fold and 1.6-fold, respectively. Calculating the metabolic activity showed that 5-FU significantly enhanced tumor glycolysis [Fig. 34B; CTRL vs FLX (1.42-fold) and 5-FU (2.4-fold)]. Additionally, FLX reduced the gene expression of the glucose transporter (GLUT1) and lactate dehydrogenase (LDHA) 1.3-fold, while the lactate transporter (MCT-4) was significantly downregulated (Fig. 34C).
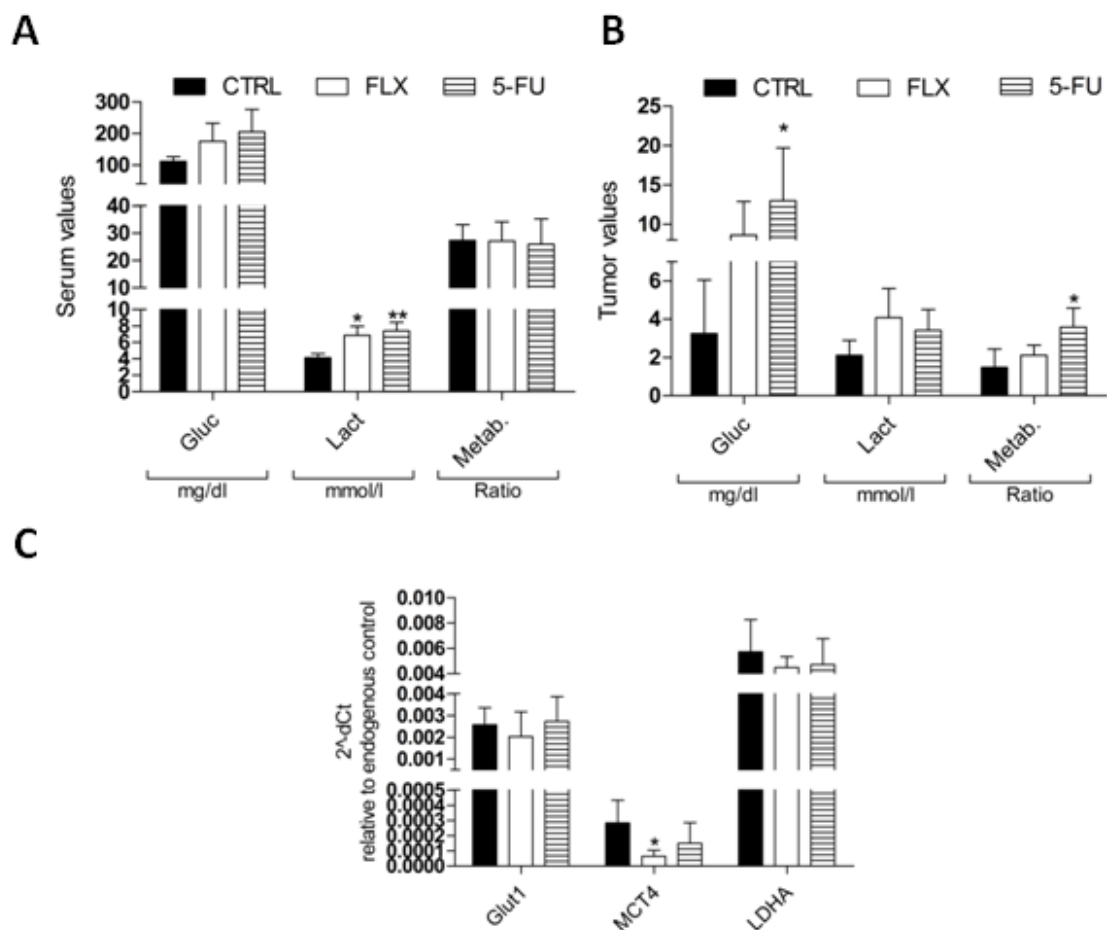
Figure 34 – Glycolytic patterns analyzed in serum samples (**A**) and tumor lysates (B) with biochemical methods (**B**; *P < 0.05 and **P 0.01 *vs* CTRL). Gene expression of Glut1, MCT4 and LDHA analyzed by RT-PCR (**C**; P < 0.05 *vs* CTRL).

FLX and 5-FU treatments downregulated NOX-1 mRNA expression 1.2-fold and 1.9-fold, respectively. While 5-FU enhanced HIF-1 mRNA expression, FLX-treatment downregulated its mRNA expression 2-fold (Fig. 35A). Moreover, FLX

decreased all phosphorylated-proteins from the Akt-mTOR signaling pathway around 1.1-fold (Fig. 35B).
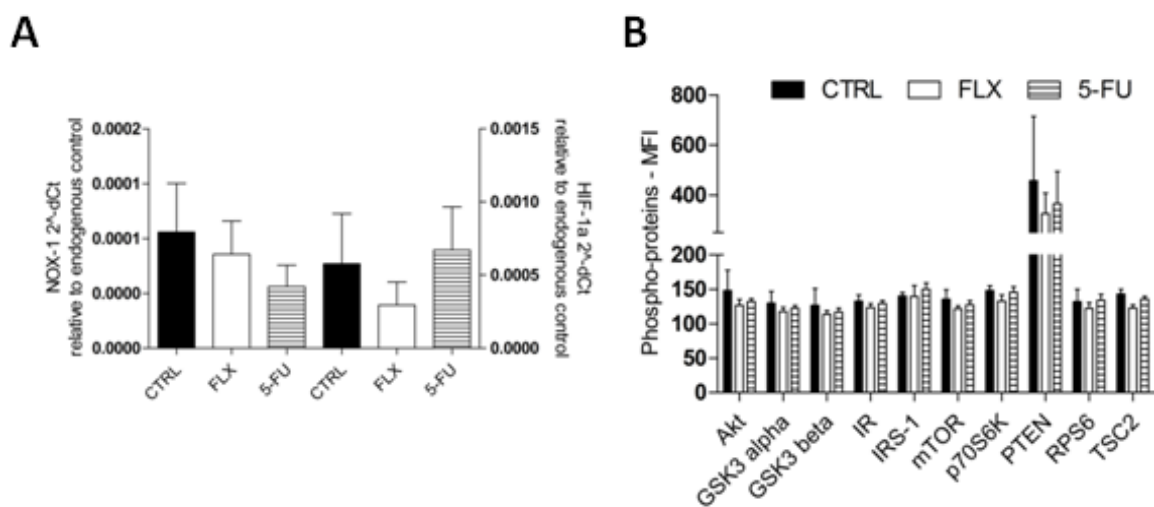
Figure 34 – Gene expression of NOX-1 and HIF-1 as analyzed by RT-PCR (**A**; $P > 0.05$). Tumor lysates (300µg/mL) were analyzed with the Akt/mTOR Phosphoprotein Magnetic Bead Kit according to the assay protocol. MFI was measured with a Luminex® system (**B**; $P > 0.05$).

5   Discussion

5.1   Standard-fluoxetine doses show safety in toxicological in vitro tests

It should first be considered that FLX showed no antioxidant potential in a cell-free assay, as well as it did not induce any pro-oxidant or DNA-damaging events in our cell culture models. Therefore, FLX does not seem to alter non-malignant cellular functions under standard-cell culture conditions to a relevant degree. It was previously reported that normal peripheral blood mononuclear and tonsilar B cells remained highly viable after treatments with 5, 10 or 20µM FLX for 24h, whereas these same drug concentrations induced DNA-fragmentation, loss of ΔΨm, and apoptosis in Burkitt lymphoma cells [17]. Furthermore, experiments with normal rats subjected to FLX-treatment have shown that it protects brain tissue against stress-related damage, mainly up-regulating antioxidant capacity [9-11,81].

Djordjevic and colleagues have analyzed liver tissue from stressed and non-stressed rats and found that FLX just modulated antioxidant mechanisms in those subjected to stressful conditions. They also found that FLX did not prevent DNA fragmentation or apoptosis in stressed rats [82]. Data from spleen samples of mice injected and non-injected with B16F10 melanoma cells showed that FLX reversed pro-oxidant effects of melanoma tumors [14].

On the other hand, FLX promoted DNA fragmentation and apoptosis throughout oxidative stress and mitochondrial-related damage dysfunction in human Burkitt lymphoma and ovarian cancer cells, [16-18]. Furthermore, treating rat PC12, C6 glioma and human SH-SY5Y neuroblastoma cells with FLX was shown to increase DNA-damage, oxidative stress, and mitochondrial

dysfunction reducing cell viability and growth [83-84]. Analyzing blood peripheral cells from stressed mice [12] and brain tissue from tumor-bearing mice [13] further supported the notion that FLX has a pro-oxidant-related activity [12-13],

Taken together, this shows that FLX has a safe standard activity upon fibroblast cell cultures, while divergences about its effects arise due to different experimental designs and conditions.

5.2 Fluoxetine reduces colon dysplasia taking preneoplastic angiogenesis under control

Although FLX showed no antioxidant, pro-oxidant or DNA-damaging potential, previous reports have shown that it might control preneoplastic lesions [5,20]. Our current data support the idea that FLX acts as a chemopreventive agent reducing preneoplastic lesions in the colon. From our first model, we can infer that FLX might have a chemopreventive potential against dysplasia, since treatment was started before the carcinogen application. The second model reinforces this idea of reduction of that carcinogen-related dysplasia, adding the information that FLX could reduce pre-existent colon preneoplastic lesions. Considering the differences between our carcinogenic models together with the similarities found in both of them, it almost ensures that FLX takes the carcinogen-induced preneoplastic changes under control by reducing epithelia proliferation. Thus, proliferation is the first step from where FLX might act in decreasing colon dysplasia.

Previous reports have shown that mutated cells, after DMH or MNNG treatments, can acquire a high proliferation capacity [46,55,85-89]. Treating rats with DMH and FLX, Tutton and Barkla first found that FLX reduces colon cryptal

proliferation [20]. Koh *et al* used a DMH-metabolite (Azoxymethane), in association with oral treatment of dextran sulfate sodium, to induce colitis-associated colon cancer in mice. They found that FLX does not induce colon apoptosis, while decreasing colon dysplasia and tumors [5]. Besides, chemoprevention against the MNNG-induced colon dysplasia was observed in association with decreased proliferation and *c-Myc* expression [87,90].

Interestingly, FLX reduced dysplasia and preneoplastic angiogenesis in both carcinogenic models. From the dataset of the MNNG-induced dysplasia model, we observed that the effects of FLX in reducing preneoplastic angiogenesis were directly related to the decrease of stromal proliferation. Our data further suggest that, by suppressing NF-κB nuclear expression due to increased expression of cytoplasmic IκB-α and IκB-β proteins, FLX reduced *c-Myc* expression and then stromal proliferation. In fact, FLX has been shown to inhibit NF-κB signaling in epithelial carcinogen-induced high cell proliferation [5]. Moreover, high NF-κB-transcriptional activity was closely associated with the transformation from normal to reactive stroma phenotype, since NF-κB promotes the expression of pro-inflammatory molecules and increases the number of periendothelial cells [61-62]. Indeed, inhibiting the proliferation of colon cancer cells has been achieved by suppressing NF-κB-transcriptional activity *in vitro and in vivo*, which reduces the expression of its downstream genes, such as *c-Myc* and VEGF [91-92].

The present findings also reveal that FLX might reduce VEGF expression within the stromal compartment of the colon tissue. This ties the results regarding preneoplastic angiogenesis and stromal proliferation together. However, it should be considered that the activity of FLX on VEGF expression

is a controversial issue, and no study has been published about the relationship between FLX, colon carcinogenesis, and angiogenesis to this day. Concerning VEGF, FLX treatment has been shown to reduce the expression in lung under pathological conditions [93-95]. On the other hand, the effects of FLX on VEGF levels in brain tissue provoke further discussion [96], since there was a large difference between what has been observed in vivo and in vitro [97-100] in comparison with human studies [96,101]. Altogether, VEGF expression has been known to promote angiogenesis and proliferation [102-103], and it has been acknowledged that proliferation plays a key role during angiogenesis [103].

In the MNNG-induced dysplasia model, we further found that FLX might decrease angiogenesis-related cell markers. It encloses the question whether FLX treatment could directly act upon angiogenesis-related cell phenotypes. These current data support the hypothesis that the anti-angiogenic potential of FLX could be related to the control of angiogenesis-related stem cell markers in colon preneoplastic lesions. Intriguingly, this hypothesis was abetted by the discovery of a small subset of stromal spindle cells expressing CD133 and CD34 in angiofibromas. That report suggested that tumors promote stromal cells to transit toward an endothelial phenotype [104]. Other studies reinforced this hypothesis, since endothelial progenitor cells lose the expression of CD133 during their differentiation process into vascular cells, while the expression of CD34 is increased [105-107]. This process has also been related to high proliferation [103], which might mean a downregulation of CD34 expression upon further differentiation [108]. In addition, CD31-positive cells have been designated as a mature endothelial lineage promoting microvessels [109].

Hence, vascular smooth muscle cells increased the expression of CD31 during their differentiation process, whereas a simultaneous decrease of CD133 and CD34 progenitor markers was observed [110].

Taken together, our current data lead to the idea that FLX effectively acts against colon preneoplastic lesions. FLX seems to have a broad and complex activity on epithelia and stromal areas; its anti-angiogenic effect might be the key point for clarification of its activity against carcinogen-induced dysplasia in colon tissue.

5.3   Fluoxetine takes tumor metabolism under control to reduce its growth

Having the data from Caco-2 and HT29 cells in mind, we can observe that FLX reduced ROS production to take control upon tumor proliferation and growth. It is well known that ROS promote tumor growth [71,111]. However, ATP depletion should be also considered as another mechanism driving cancer cells to death [112]. Because FLX is a lipophilic weak base [2] it quickly diffuses into multiple body-sites [113]. Another lipophilic weak base (AU-1421) was reported to uncouple mitochondrial oxidative phosphorylation dissipating the proton motive force during the energized state, which inhibited ATP synthesis [114]. It is known that lipophilic weak bases, such as FLX, show high resonance energy delocalizing positive charges in their protonated form, which reduces mitochondrial respiratory rate and ATP synthesis [114-116]. Thus, a connection between our current findings becomes clear considering that ipH is modulated or can modulate proton currents in cells; besides, these events are close connected with the homeostasis in mitochondrial energy generation machinery and, then, cell proliferation [114-115,117].

From our *in vitro* and *in vivo* data, it is reasonable to conclude that FLX deconstructs the tumoral cellular energy generation machinery, arresting tumor cells in G_0/G_1 cell-cycle phase without a DNA-damaging activity. Reviewing the chemical properties of FLX [2,113] together with previous hypotheses regarding the relationship between lipophilic weak acids and ipH [115,118-119], it sounds reasonable that a non-ionized FLX form passively diffuses across the cell membrane, becomes trapped and accumulates within acidic cellular compartments. Taking into account that the main function of voltage-gated proton channels is to extrude acid from cells FLX was shown to inhibit those [115]; also, it blocked the mitochondrial respiratory chain [116]. This might reinforce the idea that FLX-induced ipH acidification reduces the tumoral strategy of hyperpolarizing $\Delta\Psi m$ as a way to maintain the aerobic glycolysis.

Harguindey *et al* suggested that tumors have alkaline ipH and acidic microenvironment due to acid-base disturbances that completely differentiate them from normal tissues [120]. Specifically, glycolysis increases hydrogen ions enhancing the $\Delta\Psi m$, which allows pyruvate to reenter the redox matrix inducing OXPHOS [76,120]. Activating MCT4 transporters, tumors are not only able to keep their aerobic glycolytic metabolism functional, but also to alkalinize ipH excreting the excessive amount of lactate and hydrogen ions [69-70,72,76]. It was further observed that hypoxic cells increase, in order to gain ATP production, their hypoxia-related aerobic glycolysis through ipH-associated strategies resulting in an uncontrolled cell growth, which in turn enhances the development of new hypoxia microenvironments [71,76,111,121].

The findings of FLX enhancing expression of the cell-cycle checkpoint related protein p27 and the observed G_0/G_1 cell-cycle arrest in hypoxia-exposed

cells uphold our hypothesis. Currently, a growing body of evidences [7,122-123] supports the first description of FLX inhibiting colon tumor proliferation [20]. Furthermore, FLX has been shown to directly bind to the DNA via groove mode and high attraction force [124]. This may further enhance FLX induced delays in cell-cycle progression by inhibiting DNA synthesis [22,125-128]. In breast tumors, FLX was shown to arrest cells at G0/G1 phase by disrupting skp2-CKS1 assembly, which is required to enable cell cycle progression [129]. Recent data have support the idea that FLX acts against tumor proliferating cells reducing *c-Myc* and cyclins (D1, D3, E, B, and A), whereas cell-cycle checkpoints (p15, p16, p21, p27, and p53) are enhanced [7,122,129].

Our current data show that FLX effects are comparable with those of the well established chemotherapeutic agent 5-FU during a short-time treatment. It nevertheless suggests that the mechanism of action differed between both agents, with FLX treatment modulating tumor metabolism and thereby reducing transcription factors and tumor growth. While there is no literature data available comparing the effects of FLX with 5-FU, it is known that FLX prolongs the drug-circulation time and activity of some chemotherapeutic agents reducing multidrug resistance [27-28,130-131]. Besides, it is well known that taking tumor metabolism under control modulates cell signaling mediators and pathways, such as HIF-1 and Akt/mTOR [69-70,72,132]. Up to day, the literature lacks in reports about the ability of FLX to modulate HIF-1 and Akt signaling in tumors. Data from brain and pulmonary tissues have shown that FLX counteracts hypoxia-induced damage, reducing HIF-1 expression and activity [94,133-134]. FLX was also found to reduce monocrotaline-induced pulmonary arterial remodeling by lowering Akt phosphorylation [135]. However,

most of findings regarding the relationship between FLX and Akt signaling were produced in brain tissue, and argue that FLX enhances Akt/PI3K signaling pathway [136-139]. Nevertheless, FLX was shown to have different effects upon normal, stress-exposed, and malignant cells [17,82]. Besides, the large difference between normal and tumor tissues supports, by itself, the contrasting FLX mediated effects on Akt signaling, and suggest that FLX activity might decrease this signaling pathway during colon tumor shrinkage.

6 Conclusion

Our collective data suggest that FLX is a remarkable chemopreventive and oncostatic agent against colon preneoplastic lesions and tumors, acting without DNA-damage or ROS generation. The current findings suggest that FLX might control colon dysplasia, seen for example as reduction of angiogenesis, by its activity on preneoplasia-related reactive colon stroma. Moreover, FLX seems to take the malignant metabolism under control, which contributes to the reduction of the colon tumors. These effects of FLX may lead to new insights into tumor therapy, where depleting energy generation becomes a reasonable strategy to shrink colon tumors.

7 References

1. Fuller RW, Perry KW, Molloy BB (1974) Effect of an uptake inhibitor on serotonin metabolism in rat brain: studies with 3-(p-trifluoromethylphenoxy)-N-methyl-3-phenylpropylamine (Lilly 110140). Life Sci 15: 1161-1171.

2. Kornhuber J, Reichel M, Tripal P, Groemer TW, Henkel AW, et al. (2009) The role of ceramide in major depressive disorder. Eur Arch Psychiatry Clin Neurosci 259 Suppl 2: S199-204.

3. Arimochi H, Morita K (2006) Characterization of cytotoxic actions of tricyclic antidepressants on human HT29 colon carcinoma cells. Eur J Pharmacol 541: 17-23.

4. Bertrand PP, Hu X, Mach J, Bertrand RL (2008) Serotonin (5-HT) release and uptake measured by real-time electrochemical techniques in the rat ileum. Am J Physiol Gastrointest Liver Physiol 295: G1228-1236.

5. Koh SJ, Kim JM, Kim IK, Kim N, Jung HC, et al. (2011) Fluoxetine inhibits NF-kappaB signaling in intestinal epithelial cells and ameliorates experimental colitis and colitis-associated colon cancer in mice. Am J Physiol Gastrointest Liver Physiol 301: G9-19.

6. Coogan PF, Palmer JR, Strom BL, Rosenberg L (2005) Use of selective serotonin reuptake inhibitors and the risk of breast cancer. Am J Epidemiol 162: 835-838.

7. Frick LR, Palumbo ML, Zappia MP, Brocco MA, Cremaschi GA, et al. (2008) Inhibitory effect of fluoxetine on lymphoma growth through the

modulation of antitumor T-cell response by serotonin-dependent and independent mechanisms. Biochem Pharmacol 75: 1817-1826.

8. Khanzode SD, Dakhale GN, Khanzode SS, Saoji A, Palasodkar R (2003) Oxidative damage and major depression: the potential antioxidant action of selective serotonin re-uptake inhibitors. Redox Rep 8: 365-370.

9. Zafir A, Ara A, Banu N (2009) Invivo antioxidant status: a putative target of antidepressant action. Prog Neuropsychopharmacol Biol Psychiatry 33: 220-228.

10. Zafir A, Banu N (2007) Antioxidant potential of fluoxetine in comparison to Curcuma longa in restraint-stressed rats. Eur J Pharmacol 572: 23-31.

11. Chung ES, Chung YC, Bok E, Baik HH, Park ES, et al. (2010) Fluoxetine prevents LPS-induced degeneration of nigral dopaminergic neurons by inhibiting microglia-mediated oxidative stress. Brain Res 1363: 143-150.

12. Novio S, Nunez MJ, Amigo G, Freire-Garabal M (2011) Effects of fluoxetine on the oxidative status of peripheral blood leucocytes of restraint-stressed mice. Basic Clin Pharmacol Toxicol 109: 365-371.

13. Qi H, Ma J, Liu YM, Yang L, Peng L, et al. (2009) Allostatic tumor-burden induces depression-associated changes in hepatoma-bearing mice. J Neurooncol 94: 367-372.

14. Kirkova M, Tzvetanova E, Vircheva S, Zamfirova R, Grygier B, et al. (2010) Antioxidant activity of fluoxetine: studies in mice melanoma model. Cell Biochem Funct 28: 497-502.

15. Kim HJ, Choi JS, Lee YM, Shim EY, Hong SH, et al. (2005) Fluoxetine inhibits ATP-induced [Ca(2+)](i) increase in PC12 cells by inhibiting both

extracellular Ca(2+) influx and Ca(2+) release from intracellular stores. Neuropharmacology 49: 265-274.

16. Serafeim A, Grafton G, Chamba A, Gregory CD, Blakely RD, et al. (2002) 5-Hydroxytryptamine drives apoptosis in biopsylike Burkitt lymphoma cells: reversal by selective serotonin reuptake inhibitors. Blood 99: 2545-2553.

17. Serafeim A, Holder MJ, Grafton G, Chamba A, Drayson MT, et al. (2003) Selective serotonin reuptake inhibitors directly signal for apoptosis in biopsy-like Burkitt lymphoma cells. Blood 101: 3212-3219.

18. Lee CS, Kim YJ, Jang ER, Kim W, Myung SC (2010) Fluoxetine induces apoptosis in ovarian carcinoma cell line OVCAR-3 through reactive oxygen species-dependent activation of nuclear factor-kappaB. Basic Clin Pharmacol Toxicol 106: 446-453.

19. Levkovitz Y, Gil-Ad I, Zeldich E, Dayag M, Weizman A (2005) Differential induction of apoptosis by antidepressants in glioma and neuroblastoma cell lines: evidence for p-c-Jun, cytochrome c, and caspase-3 involvement. J Mol Neurosci 27: 29-42.

20. Tutton PJ, Barkla DH (1982) Influence of inhibitors of serotonin uptake on intestinal epithelium and colorectal carcinomas. Br J Cancer 46: 260-265.

21. Brandes LJ, Arron RJ, Bogdanovic RP, Tong J, Zaborniak CL, et al. (1992) Stimulation of malignant growth in rodents by antidepressant drugs at clinically relevant doses. Cancer Res 52: 3796-3800.

22. Volpe DA, Ellison CD, Parchment RE, Grieshaber CK, Faustino PJ (2003) Effects of amitriptyline and fluoxetine upon the in vitro proliferation of tumor cell lines. J Exp Ther Oncol 3: 169-184.

23. Jia L, Shang YY, Li YY (2008) Effect of antidepressants on body weight, ethology and tumor growth of human pancreatic carcinoma xenografts in nude mice. World J Gastroenterol 14: 4377-4382.

24. Coogan PF, Strom BL, Rosenberg L (2009) Antidepressant use and colorectal cancer risk. Pharmacoepidemiol Drug Saf 18: 1111-1114.

25. Chubak J, Boudreau DM, Rulyak SJ, Mandelson MT (2011) Colorectal cancer risk in relation to antidepressant medication use. Int J Cancer 128: 227-232.

26. Tutton PJ, Barkla DH (1986) Serotonin receptors influencing cell proliferation in the jejunal crypt epithelium and in colonic adenocarcinomas. Anticancer Res 6: 1123-1126.

27. Peer D, Dekel Y, Melikhov D, Margalit R (2004) Fluoxetine inhibits multidrug resistance extrusion pumps and enhances responses to chemotherapy in syngeneic and in human xenograft mouse tumor models. Cancer Res 64: 7562-7569.

28. Argov M, Kashi R, Peer D, Margalit R (2009) Treatment of resistant human colon cancer xenografts by a fluoxetine-doxorubicin combination enhances therapeutic responses comparable to an aggressive bevacizumab regimen. Cancer Lett 274: 118-125.

29. Jemal A, Siegel R, Xu J, Ward E (2010) Cancer statistics, 2010. CA Cancer J Clin 60: 277-300.

30. Lea A, Allingham-Hawkins D, Levine S (2010) BRAF p.Val600Glu (V600E) Testing for Assessment of Treatment Options in Metastatic Colorectal Cancer. PLoS Curr 2: RRN1187.

31. Siegel R, DeSantis C, Virgo K, Stein K, Mariotto A, et al. (2012) Cancer treatment and survivorship statistics, 2012. CA Cancer J Clin 62: 220-241.

32. Jemal A, Center MM, DeSantis C, Ward EM (2010) Global patterns of cancer incidence and mortality rates and trends. Cancer Epidemiol Biomarkers Prev 19: 1893-1907.

33. Dehal AN, Newton CC, Jacobs EJ, Patel AV, Gapstur SM, et al. (2012) Impact of diabetes mellitus and insulin use on survival after colorectal cancer diagnosis: the Cancer Prevention Study-II Nutrition Cohort. J Clin Oncol 30: 53-59.

34. Chibaudel B, Tournigand C, Andre T, de Gramont A (2012) Therapeutic strategy in unresectable metastatic colorectal cancer. Ther Adv Med Oncol 4: 75-89.

35. Cunningham D, Atkin W, Lenz HJ, Lynch HT, Minsky B, et al. (2010) Colorectal cancer. Lancet 375: 1030-1047.

36. Fearon ER, Vogelstein B (1990) A genetic model for colorectal tumorigenesis. Cell 61: 759-767.

37. Foulds L (1958) The natural history of cancer. J Chronic Dis 8: 2-37.

38. Khare S, Verma M (2012) Epigenetics of colon cancer. Methods Mol Biol 863: 177-185.

39. Migheli F, Migliore L (2012) Epigenetics of colorectal cancer. Clin Genet 81: 312-318.

40. Luebeck EG, Hazelton WD (2002) Multistage carcinogenesis and radiation. J Radiol Prot 22: A43-49.

41. Meza R, Jeon J, Moolgavkar SH, Luebeck EG (2008) Age-specific incidence of cancer: Phases, transitions, and biological implications. Proc Natl Acad Sci U S A 105: 16284-16289.

42. Waldner MJ, Neurath MF (2010) The molecular therapy of colorectal cancer. Mol Aspects Med 31: 171-178.

43. Paulsen JE, Loberg EM, Olstorn HB, Knutsen H, Steffensen IL, et al. (2005) Flat dysplastic aberrant crypt foci are related to tumorigenesis in the colon of azoxymethane-treated rat. Cancer Res 65: 121-129.

44. Paulsen JE, Namork E, Steffensen IL, Eide TJ, Alexander J (2000) Identification and quantification of aberrant crypt foci in the colon of Min mice--a murine model of familial adenomatous polyposis. Scand J Gastroenterol 35: 534-539.

45. Bird RP (1987) Observation and quantification of aberrant crypts in the murine colon treated with a colon carcinogen: preliminary findings. Cancer Lett 37: 147-151.

46. Maurin N, Forgue-Lafitte ME, Levy P, Zimber A, Bara J (2007) Progression of tumors arising from large ACF is associated with the MUC5AC expression during rat colon MNNG carcinogenis. Int J Cancer 120: 477-483.

47. Bird RP (1995) Role of aberrant crypt foci in understanding the pathogenesis of colon cancer. Cancer Lett 93: 55-71.

48. Bird RP, Good CK (2000) The significance of aberrant crypt foci in understanding the pathogenesis of colon cancer. Toxicol Lett 112-113: 395-402.

49. McLellan EA, Medline A, Bird RP (1991) Sequential analyses of the growth and morphological characteristics of aberrant crypt foci: putative preneoplastic lesions. Cancer Res 51: 5270-5274.

50. Paulsen JE, Knutsen H, Olstorn HB, Loberg EM, Alexander J (2006) Identification of flat dysplastic aberrant crypt foci in the colon of azoxymethane-treated A/J mice. Int J Cancer 118: 540-546.

51. Zeilstra J, Joosten SP, Wensveen FM, Dessing MC, Schutze DM, et al. (2011) WNT signaling controls expression of pro-apoptotic BOK and BAX in intestinal cancer. Biochem Biophys Res Commun 406: 1-6.

52. Cohen G, Mustafi R, Chumsangsri A, Little N, Nathanson J, et al. (2006) Epidermal growth factor receptor signaling is up-regulated in human colonic aberrant crypt foci. Cancer Res 66: 5656-5664.

53. Wong WM, Mandir N, Goodlad RA, Wong BC, Garcia SB, et al. (2002) Histogenesis of human colorectal adenomas and hyperplastic polyps: the role of cell proliferation and crypt fission. Gut 50: 212-217.

54. Wong WM, Garcia SB, Wright NA (1999) Origins and morphogenesis of colorectal neoplasms. APMIS 107: 535-544.

55. Garcia SB, Park HS, Novelli M, Wright NA (1999) Field cancerization, clonality, and epithelial stem cells: the spread of mutated clones in epithelial sheets. J Pathol 187: 61-81.

56. Waldner MJ, Wirtz S, Jefremow A, Warntjen M, Neufert C, et al. (2010) VEGF receptor signaling links inflammation and tumorigenesis in colitis-associated cancer. J Exp Med 207: 2855-2868.

57. Pretlow TP, Barrow BJ, Ashton WS, O'Riordan MA, Pretlow TG, et al. (1991) Aberrant crypts: putative preneoplastic foci in human colonic mucosa. Cancer Res 51: 1564-1567.

58. TIsty TD, Hein PW (2001) Know thy neighbor: stromal cells can contribute oncogenic signals. Curr Opin Genet Dev 11: 54-59.

59. Hu B, Castillo E, Harewood L, Ostano P, Reymond A, et al. (2012) Multifocal epithelial tumors and field cancerization from loss of mesenchymal CSL signaling. Cell 149: 1207-1220.

60. Coussens LM, Raymond WW, Bergers G, Laig-Webster M, Behrendtsen O, et al. (1999) Inflammatory mast cells up-regulate angiogenesis during squamous epithelial carcinogenesis. Genes Dev 13: 1382-1397.

61. Vandoros GP, Konstantinopoulos PA, Sotiropoulou-Bonikou G, Kominea A, Papachristou GI, et al. (2006) PPAR-gamma is expressed and NF-kB pathway is activated and correlates positively with COX-2 expression in stromal myofibroblasts surrounding colon adenocarcinomas. J Cancer Res Clin Oncol 132: 76-84.

62. Hardwick JC, van den Brink GR, Offerhaus GJ, van Deventer SJ, Peppelenbosch MP (2001) NF-kappaB, p38 MAPK and JNK are highly expressed and active in the stroma of human colonic adenomatous polyps. Oncogene 20: 819-827.

63. Shinagawa K, Kitadai Y, Tanaka M, Sumida T, Kodama M, et al. (2010) Mesenchymal stem cells enhance growth and metastasis of colon cancer. Int J Cancer 127: 2323-2333.

64. Kitadai Y, Sasaki T, Kuwai T, Nakamura T, Bucana CD, et al. (2006) Targeting the expression of platelet-derived growth factor receptor by

reactive stroma inhibits growth and metastasis of human colon carcinoma. Am J Pathol 169: 2054-2065.

65. Vermeulen L, De Sousa EMF, van der Heijden M, Cameron K, de Jong JH, et al. (2010) Wnt activity defines colon cancer stem cells and is regulated by the microenvironment. Nat Cell Biol 12: 468-476.

66. Glaire MA, El-Omar EM, Wang TC, Worthley DL (2012) The mesenchyme in malignancy: A partner in the initiation, progression and dissemination of cancer. Pharmacol Ther 136: 131-141.

67. Tetsu O, McCormick F (1999) Beta-catenin regulates expression of cyclin D1 in colon carcinoma cells. Nature 398: 422-426.

68. Firestein R, Bass AJ, Kim SY, Dunn IF, Silver SJ, et al. (2008) CDK8 is a colorectal cancer oncogene that regulates beta-catenin activity. Nature 455: 547-551.

69. Jones NP, Schulze A (2012) Targeting cancer metabolism--aiming at a tumour's sweet-spot. Drug Discov Today 17: 232-241.

70. Cairns RA, Harris IS, Mak TW (2011) Regulation of cancer cell metabolism. Nat Rev Cancer 11: 85-95.

71. Brahimi-Horn C, Pouyssegur J (2006) The role of the hypoxia-inducible factor in tumor metabolism growth and invasion. Bull Cancer 93: E73-80.

72. Swietach P, Vaughan-Jones RD, Harris AL (2007) Regulation of tumor pH and the role of carbonic anhydrase 9. Cancer Metastasis Rev 26: 299-310.

73. Nys K, Maes H, Dudek AM, Agostinis P (2011) Uncovering the role of hypoxia inducible factor-1alpha in skin carcinogenesis. Biochim Biophys Acta 1816: 1-12.

74. Pouyssegur J, Dayan F, Mazure NM (2006) Hypoxia signalling in cancer and approaches to enforce tumour regression. Nature 441: 437-443.

75. Barrow H, Rhodes JM, Yu LG (2011) The role of galectins in colorectal cancer progression. Int J Cancer 129: 1-8.

76. Cardone RA, Casavola V, Reshkin SJ (2005) The role of disturbed pH dynamics and the Na+/H+ exchanger in metastasis. Nat Rev Cancer 5: 786-795.

77. Abraham SK, Eckhardt A, Oli RG, Stopper H (2012) Analysis of in vitro chemoprevention of genotoxic damage by phytochemicals, as single agents or as combinations. Mutat Res 744: 117-124.

78. Meurette O, Lefeuvre-Orfila L, Rebillard A, Lagadic-Gossmann D, Dimanche-Boitrel MT (2005) Role of intracellular glutathione in cell sensitivity to the apoptosis induced by tumor necrosis factor {alpha}-related apoptosis-inducing ligand/anticancer drug combinations. Clin Cancer Res 11: 3075-3083.

79. Kannen V, Marini T, Turatti A, Carvalho MC, Brandao ML, et al. (2011) Fluoxetine induces preventive and complex effects against colon cancer development in epithelial and stromal areas in rats. Toxicol Lett 204: 134-140.

80. Kannen V, Hintzsche H, Zanette DL, Silva WA, Jr., Garcia SB, et al. (2012) Antiproliferative effects of fluoxetine on colon cancer cells and in a colonic carcinogen mouse model. PLoS One 7: e50043.

81. Zhu BG, Sun Y, Sun ZQ, Yang G, Zhou CH, et al. (2012) Optimal dosages of fluoxetine in the treatment of hypoxic brain injury induced by 3-

nitropropionic acid: implications for the adjunctive treatment of patients after acute ischemic stroke. CNS Neurosci Ther 18: 530-535.

82. Djordjevic J, Djordjevic A, Adzic M, Elakovic I, Matic G, et al. (2011) Fluoxetine affects antioxidant system and promotes apoptotic signaling in Wistar rat liver. Eur J Pharmacol.

83. Han YS, Lee CS (2009) Antidepressants reveal differential effect against 1-methyl-4-phenylpyridinium toxicity in differentiated PC12 cells. Eur J Pharmacol 604: 36-44.

84. Slamon ND, Ward TH, Butler J, Pentreath VW (2001) Assessment of DNA damage in C6 glioma cells after antidepressant treatment using an alkaline comet assay. Arch Toxicol 75: 243-250.

85. Zhang B, Wang X, Wang Y (2009) Altered gene expression and miRNA expression associated with cancerous IEC-6 cell transformed by MNNG. J Exp Clin Cancer Res 28: 56.

86. Garcia SB, Barros LT, Turatti A, Martinello F, Modiano P, et al. (2006) The anti-obesity agent Orlistat is associated to increase in colonic preneoplastic markers in rats treated with a chemical carcinogen. Cancer Lett 240: 221-224.

87. Cardoso JF, Cohen C, Jordao AA, Jr., Vannucchi H, Garcia SB, et al. (2011) Light and moderate doses of ethanol in chemical carcinogenesis of the colon in rats. Nutr Cancer 63: 1029-1035.

88. Reshef R, Rozen P, Fireman Z, Fine N, Barzilai M, et al. (1990) Effect of a calcium-enriched diet on the colonic epithelial hyperproliferation induced by N-methyl-N'-nitro-N-nitrosoguanidine in rats on a low calcium and fat diet. Cancer Res 50: 1764-1767.

89. Demarzo MM, Martins LV, Fernandes CR, Herrero FA, Perez SE, et al. (2008) Exercise reduces inflammation and cell proliferation in rat colon carcinogenesis. Med Sci Sports Exerc 40: 618-621.

90. Jiang XY, Qian LP, Zheng XJ, Xia YY, Jiang YB, et al. (2009) Interventional effect of Ginkgo biloba extract on the progression of gastric precancerous lesions in rats. J Dig Dis 10: 293-299.

91. Yang Z, Li C, Wang X, Zhai C, Yi Z, et al. (2010) Dauricine induces apoptosis, inhibits proliferation and invasion through inhibiting NF-kappaB signaling pathway in colon cancer cells. J Cell Physiol 225: 266-275.

92. Paul S, DeCastro AJ, Lee HJ, Smolarek AK, So JY, et al. (2010) Dietary intake of pterostilbene, a constituent of blueberries, inhibits the beta-catenin/p65 downstream signaling pathway and colon carcinogenesis in rats. Carcinogenesis 31: 1272-1278.

93. Porzionato A, Zaramella P, Macchi V, Grisafi D, Salmaso R, et al. (2012) Fluoxetine may worsen hyperoxia-induced lung damage in neonatal rats. Histol Histopathol 27: 1599-1610.

94. Han DD, Wang Y, Zhang XH, Liu JR, Wang HL (2012) Fluoxetine protects against monocrotaline-induced pulmonary arterial remodeling by inhibition of hypoxia-inducible factor-1alpha and vascular endothelial growth factor. Can J Physiol Pharmacol 90: 445-454.

95. Riksen EA, Stunes AK, Kalvik A, Gustafsson BI, Snead ML, et al. (2010) Serotonin and fluoxetine receptors are expressed in enamel organs and LS8 cells and modulate gene expression in LS8 cells. Eur J Oral Sci 118: 566-573.

96. Gaillard R, Mir O (2011) Fluoxetine and motor recovery after ischaemic stroke. Lancet Neurol 10: 499; author reply 500-491.

97. Allaman I, Fiumelli H, Magistretti PJ, Martin JL (2011) Fluoxetine regulates the expression of neurotrophic/growth factors and glucose metabolism in astrocytes. Psychopharmacology (Berl) 216: 75-84.

98. Fournier NM, Lee B, Banasr M, Elsayed M, Duman RS (2012) Vascular endothelial growth factor regulates adult hippocampal cell proliferation through MEK/ERK- and PI3K/Akt-dependent signaling. Neuropharmacology 63: 642-652.

99. Lesemann A, Reinel C, Huhnchen P, Pilhatsch M, Hellweg R, et al. (2012) MPTP-induced hippocampal effects on serotonin, dopamine, neurotrophins, adult neurogenesis and depression-like behavior are partially influenced by fluoxetine in adult mice. Brain Res 1457: 51-69.

100. Greene J, Banasr M, Lee B, Warner-Schmidt J, Duman RS (2009) Vascular endothelial growth factor signaling is required for the behavioral actions of antidepressant treatment: pharmacological and cellular characterization. Neuropsychopharmacology 34: 2459-2468.

101. Tsai SJ, Hong CJ, Liou YJ, Chen TJ, Chen ML, et al. (2009) Haplotype analysis of single nucleotide polymorphisms in the vascular endothelial growth factor (VEGFA) gene and antidepressant treatment response in major depressive disorder. Psychiatry Res 169: 113-117.

102. Garrido-Urbani S, Jemelin S, Deffert C, Carnesecchi S, Basset O, et al. (2011) Targeting vascular NADPH oxidase 1 blocks tumor angiogenesis through a PPARalpha mediated mechanism. PLoS One 6: e14665.

103. Tammali R, Reddy AB, Srivastava SK, Ramana KV (2011) Inhibition of aldose reductase prevents angiogenesis in vitro and in vivo. Angiogenesis 14: 209-221.

104. Ngan BY, Forte V, Campisi P (2008) Molecular angiogenic signaling in angiofibromas after embolization: implications for therapy. Arch Otolaryngol Head Neck Surg 134: 1170-1176.

105. Hristov M, Erl W, Weber PC (2003) Endothelial progenitor cells: mobilization, differentiation, and homing. Arterioscler Thromb Vasc Biol 23: 1185-1189.

106. Sovalat H, Scrofani M, Eidenschenk A, Pasquet S, Rimelen V, et al. (2011) Identification and isolation from either adult human bone marrow or G-CSF-mobilized peripheral blood of CD34(+)/CD133(+)/CXCR4(+)/ Lin(-)CD45(-) cells, featuring morphological, molecular, and phenotypic characteristics of very small embryonic-like (VSEL) stem cells. Exp Hematol 39: 495-505.

107. Meregalli M, Farini A, Belicchi M, Torrente Y (2010) CD133(+) cells isolated from various sources and their role in future clinical perspectives. Expert Opin Biol Ther 10: 1521-1528.

108. Krause DS, Fackler MJ, Civin CI, May WS (1996) CD34: structure, biology, and clinical utility. Blood 87: 1-13.

109. Li H, Zimmerlin L, Marra KG, Donnenberg VS, Donnenberg AD, et al. (2011) Adipogenic potential of adipose stem cell subpopulations. Plast Reconstr Surg 128: 663-672.

110. Ye C, Bai L, Yan ZQ, Wang YH, Jiang ZL (2008) Shear stress and vascular smooth muscle cells promote endothelial differentiation of

endothelial progenitor cells via activation of Akt. Clin Biomech (Bristol, Avon) 23 Suppl 1: S118-124.

111. Beasley NJ, Wykoff CC, Watson PH, Leek R, Turley H, et al. (2001) Carbonic anhydrase IX, an endogenous hypoxia marker, expression in head and neck squamous cell carcinoma and its relationship to hypoxia, necrosis, and microvessel density. Cancer Res 61: 5262-5267.

112. Verrax J, Beck R, Dejeans N, Glorieux C, Sid B, et al. (2011) Redox-active quinones and ascorbate: an innovative cancer therapy that exploits the vulnerability of cancer cells to oxidative stress. Anticancer Agents Med Chem 11: 213-221.

113. Lefebvre M, Marchand M, Horowitz JM, Torres G (1999) Detection of fluoxetine in brain, blood, liver and hair of rats using gas chromatography-mass spectrometry. Life Sci 64: 805-811.

114. Nagamune H, Fukushima Y, Takada J, Yoshida K, Unami A, et al. (1993) The lipophilic weak base (Z)-5-methyl-2-[2-(1-naphthyl)ethenyl]-4-piperidinopyridine (AU-1421) is a potent protonophore type cationic uncoupler of oxidative phosphorylation in mitochondria. Biochim Biophys Acta 1141: 231-237.

115. Song JH, Marszalec W, Kai L, Yeh JZ, Narahashi T (2012) Antidepressants inhibit proton currents and tumor necrosis factor-alpha production in BV2 microglial cells. Brain Res 1435: 15-23.

116. Hroudova J, Fisar Z (2012) In vitro inhibition of mitochondrial respiratory rate by antidepressants. Toxicol Lett 213: 345-352.

117. Narahashi T, Frazier T, Yamada M (1970) The site of action and active form of local anesthetics. I. Theory and pH experiments with tertiary compounds. J Pharmacol Exp Ther 171: 32-44.

118. Kozin SV, Gerweck LE (1998) Cytotoxicity of weak electrolytes after the adaptation of cells to low pH: role of the transmembrane pH gradient. Br J Cancer 77: 1580-1585.

119. Gerweck LE, Seetharaman K (1996) Cellular pH gradient in tumor versus normal tissue: potential exploitation for the treatment of cancer. Cancer Res 56: 1194-1198.

120. Harguindey S, Orive G, Luis Pedraz J, Paradiso A, Reshkin SJ (2005) The role of pH dynamics and the Na+/H+ antiporter in the etiopathogenesis and treatment of cancer. Two faces of the same coin--one single nature. Biochim Biophys Acta 1756: 1-24.

121. Silva AS, Yunes JA, Gillies RJ, Gatenby RA (2009) The potential role of systemic buffers in reducing intratumoral extracellular pH and acid-mediated invasion. Cancer Res 69: 2677-2684.

122. Stepulak A, Rzeski W, Sifringer M, Brocke K, Gratopp A, et al. (2008) Fluoxetine inhibits the extracellular signal regulated kinase pathway and suppresses growth of cancer cells. Cancer Biol Ther 7: 1685-1693.

123. Yue CT, Liu YL (2005) Fluoxetine increases extracellular levels of 3-methoxy-4-hydroxyphenylglycol in cultured COLO320 DM cells. Cell Biochem Funct 23: 109-114.

124. Kashanian S, Javanmardi S, Chitsazan A, Omidfar K, Paknejad M (2012) DNA-binding studies of fluoxetine antidepressant. DNA Cell Biol 31: 1349-1355.

125. Hoose SA, Duran C, Malik I, Eslamfam S, Shasserre SC, et al. (2012) Systematic analysis of cell cycle effects of common drugs leads to the discovery of a suppressive interaction between gemfibrozil and fluoxetine. PLoS One 7: e36503.

126. Eddahibi S, Fabre V, Boni C, Martres MP, Raffestin B, et al. (1999) Induction of serotonin transporter by hypoxia in pulmonary vascular smooth muscle cells. Relationship with the mitogenic action of serotonin. Circ Res 84: 329-336.

127. Pitt BR, Weng W, Steve AR, Blakely RD, Reynolds I, et al. (1994) Serotonin increases DNA synthesis in rat proximal and distal pulmonary vascular smooth muscle cells in culture. Am J Physiol 266: L178-186.

128. Lee SL, Wang WW, Lanzillo JJ, Fanburg BL (1994) Regulation of serotonin-induced DNA synthesis of bovine pulmonary artery smooth muscle cells. Am J Physiol 266: L53-60.

129. Krishnan A, Hariharan R, Nair SA, Pillai MR (2008) Fluoxetine mediates G0/G1 arrest by inducing functional inhibition of cyclin dependent kinase subunit (CKS)1. Biochem Pharmacol 75: 1924-1934.

130. Peer D, Margalit R (2006) Fluoxetine and reversal of multidrug resistance. Cancer Lett 237: 180-187.

131. Ong JC, Sun F, Chan E (2011) Development of stealth liposome coencapsulating doxorubicin and fluoxetine. J Liposome Res 21: 261-271.

132. Foster R, Griffin S, Grooby S, Feltell R, Christopherson C, et al. (2012) Multiple metabolic alterations exist in mutant PI3K cancers, but only glucose is essential as a nutrient source. PLoS One 7: e45061.

133. Dai F, Mao Z, Xia J, Zhu S, Wu Z (2012) Fluoxetine protects against big endothelin-1 induced anti-apoptosis by rescuing Kv1.5 channels in human pulmonary arterial smooth muscle cells. Yonsei Med J 53: 842-848.

134. Shin TK, Kang MS, Lee HY, Seo MS, Kim SG, et al. (2009) Fluoxetine and sertraline attenuate postischemic brain injury in mice. Korean J Physiol Pharmacol 13: 257-263.

135. Wang HM, Wang Y, Liu M, Bai Y, Zhang XH, et al. (2012) Fluoxetine inhibits monocrotaline-induced pulmonary arterial remodeling involved in inhibition of RhoA-Rho kinase and Akt signalling pathways in rats. Can J Physiol Pharmacol 90: 1506-1515.

136. Huang W, Zhao Y, Zhu X, Cai Z, Wang S, et al. (2012) Fluoxetine Upregulates Phosphorylated-AKT and Phosphorylated-ERK1/2 Proteins in Neural Stem Cells: Evidence for a Crosstalk between AKT and ERK1/2 Pathways. J Mol Neurosci. [Epub ahead of print]

137. Reus GZ, Abelaira HM, Agostinho FR, Ribeiro KF, Vitto MF, et al. (2012) The administration of olanzapine and fluoxetine has synergistic effects on intracellular survival pathways in the rat brain. J Psychiatr Res 46: 1029-1035.

138. Sutton LP, Rushlow WJ (2011) The effects of neuropsychiatric drugs on glycogen synthase kinase-3 signaling. Neuroscience 199: 116-124.

139. Polter AM, Yang S, Jope RS, Li X (2012) Functional significance of glycogen synthase kinase-3 regulation by serotonin. Cell Signal 24: 265-271.

8 Acknowledgement

I thank God for my life, well being, guidance, and wisdom. I would have achieved nothing without His mercy and love for me.

I thank my family for the support, patience, and advices in all moments of my life. You are the most precious gift that I have and ever will.

I thank my first advisor Prof. Dr. Helga Stopper for including me in her working group, as well as for the kindness, patience, and advices through these years.

I thank my second advisor Prof. Dr. Sergio Britto Garcia for the friendship, support, patience, and advices since my master degree.

I thank the supervisory board committee, Prof. Dr. Ana Maria Waaga-Gasser for her great support, friendship, and advices; and, Prof. Dr. Ricardo Benavente for the suggestions and collaboration during this project.

I acknowledge the Deutscher Akademischer Austausch Dienst (DAAD) for the scholarship supporting my PhD program at the Graduate School of Life Sciences, University of Wuerzburg.

9   Curriculum Vitae

Msc. Vinicius Kannen Cardoso

Institute adress:

Institute of Pharmacology
and Toxicology
University of Würzburg
Versbacher Str. 9
D-97078 Wuerzburg/ Germany

Department of Surgery I,
Molecular Oncology and
Immunology
University of Würzburg
Oberduerrbacher Str. 6
D-97080 Wuerzburg/ Germany

Personal Information

Full name	Vinicius Kannen Cardoso
Birth	02/12/1983 - Porto Alege/RS - Brazil
Passport	CZ510525 – DPF/POR/SP
Email	vinicius.cardoso@uni-wuerzburg.de

Languages

German	Understanding well , Speaking well, Writing Basic, Reading Basic
English	Understanding well , Speaking well, Writing well, Reading Fluent
Portuguese	Native speaker.

Formal Education

Scholarships:
Deutscher Akademischer Austauschdienst – 2010/2013

CAPES - Coordenação de Aperfeiçoamento de Pessoal de
Nível Superior – 2009/2010

PhD degree

Tittle: The role of Fluoxetine against preneoplastic lesions and
tumors in colon tissue.

Julius-Maximilians – Universität Würzburg/ Germany
Institute of Pharmacology and Toxicology
Advisor: Prof. Dr. Helga Stopper

University of São Paulo/ Brazil
Department of Pathology
Advisor: Prof. Dr. Sergio Britto Garcia

Master degree in Medical Sciences – Experimental Pathology

2007 - 2009

Scholarship:
CNPQ – Conselho Nacional de Desenvolvimento Científico e Tecnológico – 2007/2009
Title: The colon carcinogenesis and its relationship with melatonin in rats under constant-light conditions.

University of São Paulo/ Brazil
Department of Pathology
Advisor: Prof. Dr. Sergio Britto Garcia

2003 - 2006

Bachelor degree – Physiotherapy.
University Herminio Ometto/ Brazil

Complementary Education

2012

Scientific Writing
University of Wuerzburg/ Germany

2012

Grundkurs Tierschutz und Versuchstierkunde
"Basic course animal welfare and laboratory animal science"
University of Wuerzburg/ Germany

2011-2012

English for academic purpose
University of Wuerzburg/ Germany

2011

Special FACS workshop – about cell cycle analysis (BrDU-Pi)
University of Wuerzburg/ Germany

2011

Microarray analysis
University of Wuerzburg/ Germany

2011

Management Skills
University of Wuerzburg/ Germany

2006

3rd Winter Pathology Course
University of São Paulo/ Brazil

2006

Anatomical techniques in humans and animals.
University Center Herminio Ometto/ Brazil

Book chapter

1. Sergio Garcia, V.K.a.L.N., 2011. The Role of Stem Cells in the Glioma Growth. In: Ghosh, A. (Ed.) Glioma – Exploring Its Biology and Practical Relevance. InTech, Rijeka, pp. 189-200.

Published articles

1. Kannen, V., Hintzsche, H., Zanette, D.L., Silva, W.A., Jr., Garcia, S.B., Waaga-Gasser, A.M., Stopper, H., 2012. Antiproliferative effects of fluoxetine on colon cancer cells and in a colonic carcinogen mouse model. PLoS One 7, e50043.
2. Kannen, V., Zanette, D.L., Fernandes, C.R., Ferreira, F.R., Marini, T., Carvalho, M.C., Brandao, M.L., Junior, J.E., Mauad, F.M., Silva, W.A., Jr., Stopper, H., Garcia, S.B., 2012. High-fat diet causes an imbalance in the colonic serotonergic system promoting adipose tissue enlargement and dysplasia in rats. Toxicol Lett 213, 135-141.
3. Kannen, V., Marini, T., Turatti, A., Carvalho, M.C., Brandao, M.L., Jabor, V.A., Bonato, P.S., Ferreira, F.R., Zanette, D.L., Silva, W.A., Jr., Garcia, S.B., 2011. Fluoxetine induces preventive and complex effects against colon cancer development in epithelial and stromal areas in rats. Toxicol Lett 204, 134-140.
4. Kannen, V., Marini, T., Zanette, D.L., Frajacomo, F.T., Silva, G.E., Silva, W.A., Jr., Garcia, S.B., 2011. The melatonin action on stromal stem cells within pericryptal area in colon cancer model under constant light. Biochem Biophys Res Commun 405, 593-598.

Articles under review

1. Kannen, V., Marini, T., Garcia, S.B., Waaga-Gasser, A.M., Glucagon-like peptides 2 in colon carcinogenesis: possible target for anti-cancer therapy? Pharmacology & Therapeutics (review article; since November/2012).
2. Kannen, V., Fernandes, C.R., Zanette, D.L., Ferreira, F.R., Frajacomo, F.T., Carvalho, M.C., Brandão, M.L., Elias Junior, J., Jordão Junior, A.A., Uyemura, S.A., Waaga-Gasser, A.M., Garcia, S.B. Short-term dietary restriction does not reduce carcinogen-induced dysplastic lesions in the colon tissue of rats. Molecular Carcinogenesis (original article; since January/2013).

Summary published in annals of events (summary)

1. OKUBO, R.; FERNANDES, C. R.; FRAJACOMO, F. T.; FARNESI, A. P.; KANNEN, V; FALCAI, M.J.; MARINI, T; FAZAN, V.P.; SHIMANO, A.C.; VOLPON, J.B.; GARCIA, SB. Effects of swimming exercise and diet tibias of rats: a biomechanical study In: Experimental biology, 2010, Anaheim. The FASEB Journal. , 2010. v.5. p.637.4

2. OLIVEIRA, E. C.; MENEZES,J.G; Kannen, V; LUQUETTI, A. O.; NETO, S. G.; GARCIA, SB. The Relationship between megacolon and

constipation in Chagas' disease In: Neurogatroenterology and motility, 2009, Chicago. NEUROGASTROENTEROL MOTIL 2009. London, UK: Neurogastroenterology & Motility, 2009. v.21. p.1 - 98

3.   FRAJACOMO, F. T.; FERNANDES, C. R.; FARNESI, A. P.; MARINI, T; DEMARZO, M. M. P.; KANNEN, V; JORDAO JUNIOR, A. A.; GARCIA, SB. Continuous light reverts physical exercise effects on colon carcinogenesis induced by 1,2-dimethyl-hydrazine in rats. In: I International Meeting in Exercise Physiology, 2008, São Carlos. Proceedings of the I INTERNATIONAL MEETING IN EXERCISE PHYSIOLOGY. Digital Commons, 2008. v.1. p.s89 - s89

4.   MARINI, T; FERNANDES, C. R.; FRAJACOMO, F. T.; DEMARZO, M. M. P.; BACHUR, J. A.; KANNEN, V; GARCIA, SB. Effects of single weekly bout of exercise on cell proliferation during the rat colon carcinogenesis In: I International Meeting in Exercise Physiology, 2008, São Carlos. Proceedings of the I INTERNATIONAL MEETING IN EXERCISE PHYSIOLOGY.   Digital   Commons,2008.v.1.p.s93-293

Participation in events

1.   Poster Presentation at 6th International Symposium "Bio Bang", University of Wuerzburg, 2011. Fluoxetine induced colon tumor shrinkage by modulating multiple oncogenic signaling pathways.

1.   Poster Presentation at Symposium of Experimental Pathology, University of São Paulo, 2010. Fluoxetine treatment in colon of carcinogenic animals.

2.   Poster Presentation at 78th European Atherosclerosis Society, 2010. HIgh-fat, high-fat-protein and exercise: distinct adaptations in the thoracic aorta and lipid profile.

3.   Poster Presentation at 78th European Atherosclerosis Society, 2010. Influence of body fat distribution, diet and exercise on the formation of nitrotyrosine in the heart of rats.

4.   Poster Presentation at 9th Congress of the Brazilian Society of Mutagenesis, Carcinogenesis and Environmental Teratogenesis, 2009. Fluoxetine treatment in colon of carcinogenic animals.

5.   Poster Presentation at 9th Symposium Exercise Immunology - Emerging relevance in clinical medicine, 2009. Influence of frequency and intensity of swimming on rat colon carcinogenesis.

6.   Poster Presentation at 1st International Meeting in Exercise Physiology, 2008. Continuous light reverts physycal exercise effects on colon carcinogenesis induced 1,2-dimethyl-hydrazine in rats.

7.   Poster Presentation at 1st International Meeting in Exercise Physiology, 2008. Effects of single weekly bouts of exercise on cell proliferation during the rat colon carcinogenesis.

Würzburg, January 1st, 2012

_____
Vinicius Kannen Cardoso

10 Affidavit

I hereby declare that my thesis entitled "The role of Fluoxetine against preneoplastic lesions and tumors in colon tissue" is the result of my own work. I did not receive any help or support from commercial consultants. All sources and/or materials applied are listed and specified in the thesis.

The data presented here were partially published in two separate articles:

1. Kannen V, Hintzsche H, Zanette DL, Silva WA, Jr., Garcia SB, et al. (2012) Antiproliferative effects of fluoxetine on colon cancer cells and in a colonic carcinogen mouse model. PLoS One 7: e50043.

2. Kannen V, Marini T, Turatti A, Carvalho MC, Brandao ML, et al. (2011) Fluoxetine induces preventive and complex effects against colon cancer development in epithelial and stromal areas in rats. Toxicol Lett 204: 134-140.

Furthermore, I verify that this thesis has not yet been submitted as part of another examination process neither in identical nor in similar form.

Würzburg, January 1st, 2012

_____
Vinicius Kannen Cardoso